Regulation pathways of c-MYC under glutamine-starving conditions in colon carcinoma cells

Regulierungsmechanismen von c-MYC in Darmkrebszellen unter Glutaminmangelbedingungen

Dissertation zur Erlangung des

naturwissenschaftlichen Doktorgrades

der Julius-Maximilians-Universität Würzburg

vorgelegt von

Kevin Heimberger

aus Karlburg

Würzburg, 2024

Eingereicht am: ……..……..

<u>Mitglieder der Promotionskommission:</u>

Vorsitzender: ……..

Gutachter: Prof. Dr. Thomas Dandekar

Gutachter: Prof. Dr. Martin Eilers

Gutachter: Prof. Dr. Susanne Kramer

Tag des Promotionskolloquiums: ……..…

Doktorurkunde ausgehändigt am: …….

Table of contents

Table of contents

Table of contents

Table of contents

Summary

Colon carcinomas (CRC) are statistically among the most fatal cancer types and hence one of the top reasons for premature mortality in the developed world. CRC cells are characterized by high proliferation rates caused by deregulation of gene transcription of proto-oncogenes and general chromosomal instability. On macroscopic level, CRC cells show a strongly altered nutrient and energy metabolism.

This work presents research to understand general links between the metabolism and transcription alteration. Mainly focussing on glutamine dependency, shown in colon carcinoma cells and expression pathways of the pro-proliferation protein c-MYC.

Previous studies showed that a depletion of glutamine in the cultivation medium of colon carcinoma cell lines caused a proliferation arrest and a strong decrease of overall c-MYC levels. Re-addition of glutamine quickly replenished c-MYC levels through an unknown mechanism. Several proteins altering this regulation mechanism were identified and proposed as possible starting point for further in detail studies to unveil the precise biochemical pathway controlling c-MYC translation repression and reactivation in a rapid manner.

On a transcriptional level the formation of RNA:DNA hybrids, so called R-loops, was observed under glutamine depleted conditions. The introduction and overexpression of RNaseH1, a R-loop degrading enzyme, in combination with an ectopically expressed c-MYC variant, independent of cellular regulation mechanisms by deleting the regulatory 3'-UTR of the *c-MYC* gene, lead to a high rate of apoptotic cells in culture. Expression of a functionally inactive variant of RNaseH1 abolished this effect. This indicates a regulatory function of R-loops formed during glutamine starvation in the presence of c-MYC protein in a cell. Degradation of R-loops and high c-MYC levels in this stress condition had no imminent effect on the cell cycle progression is CRC cells but disturbed the nucleotide metabolism. Nucleotide triphosphates were strongly reduced in comparison to starving cells without R-loop degradation and proliferating cells.

This study proposes a model of a terminal cycle of transcription termination, unregulated initiation and elongation of transcription leading to a depletion of energy resources of cells. This could finally lead to high apoptosis of the cells. Sequencing experiments to determine a coinciding of termination sites and R-loop formation sides failed so far but show a starting point for further studies in this essential survival mechanism involving R-loop formation and c-MYC downregulation.

Zusammenfassung

Darmkrebs gehört statistisch zu den Krebsarten mit den höchsten Sterblichkeitsraten und zählen somit zu den häufigsten Todesursachen der entwickelten Länder. Darmkrebszellen zeichnen sich durch chromosomale Instabilität und hohe Proliferationsraten aus, die durch eine Deregulierung der Expression verschiedener Proto-Onkogene zustande kommen. Generell besitzen diese Krebszellen einen stark veränderten Nährstoff- und Energiestoffwechsel im Vergleich zu gesunden somatischen Zellen.

Diese Arbeit strebt ein besseres Verständnis der Verbindung zwischen dem Metabolismus und der Gen-Expression an. Das Hauptaugenmerk liegt hierbei auf dem Mechanismus der Expression des proliferationsfördernden Proteins c-MYC und der Abhängigkeit von Glutamin, die Darmkrebszellen charakterisiert.

Frühere Studien haben gezeigt, dass der Entzug von Glutamin aus dem Kulturmedium von Darmkrebszelllinien eine Arretierung des Zellzyklus bewirkt sowie die Konzentration des Proteins c-MYC reduziert. Erneute Zugabe von Glutamin zum Medium stellt die MYC-Konzentration schnell wieder her. Die Hintergründe dieses Mechanismus sind bislang aber kaum verstanden. Einige Proteine wurden hier als potenzielle Kandidaten identifiziert, die einen Einfluss auf den biochemischen Prozess haben könnten, der die schnelle Wiederaufnahme der c-MYC Translation gewährleistet.

Auf Translationsebene wurden RNA:DNA-Hybriden, sogenannte R-loops, gefunden, die sich unter anderem unter Glutamin-Mangelbedingungen im Genom bilden können. Ein gezielter Abbau dieser R-loops mithilfe des Enzyms RNaseH1, in Kombination mit der ektopischen Expression einer c-MYC-Variante, die unempfindlich gegenüber der zelleigenen Regulationsmechanismen ist, führte zu einer erhöhten Anzahl an apoptotischen Zellen in Kultur. Exprimiert man eine funktionell inaktive Variante der RNaseH1, statt der funktionellen, so kann dieser Apoptose-fördernde Prozess nicht beobachtet werden. Dies bestärkt die Hypothese, dass die R-loops, die sich während eines Glutamin-Mangels und hoher c-MYC-Konzentration bilden, eine regulatorische Funktion innehaben. Als Ursache für die Apoptose konnte ein Effekt der veränderten Expression auf das Fortschreiten des Zellzyklus ausgeschlossen werden. Jedoch zeigte sich eine Veränderung im Nukleotid-Metabolismus. Betroffene Zellen zeigten deutlich reduzierte Nuklotidtriphosphat-Konzentrationen im Vergleich zu Zellen unter Glutaminmangelbedingungen ohne R-loop-Abbau.

In dieser Arbeit wurde ein Modell entwickelt, das einen sich selbst negativ verstärkenden Zyklus vorschlägt, der die Zellen zur Apoptose führt. Transkriptionstermination und eine unkontrollierte Initiation der Transkription im Wechsel führt zu einem Verbrauch der lebensnotwendigen Energieressourcen der Zellen. Sequenzierungsexperimente zur Lokalisierung der R-loops und Terminationsstellen sind bislang fehlgeschlagen, bieten jedoch Ansätze für künftige Forschung.

1 Introduction

1.1 Role of glutamine in cancer metabolism

Cancer is statistically the top reason for premature mortality in the developed world. The incidences of different forms of this very heterogeneous disease vary strongly between mortality and world region. The most common and most fatal cancer types are lung cancer, breast and prostate cancer and colorectal cancer (Bray, et al., 2018). Although they are all classified as 'cancer', the different variants show a wide range of development, progression, and treatability.

In colorectal cancer (CRC) or colon carcinoma a main driver of tumour progression is chromosomal instability, which can cause significant changes in copy number and structure of oncogenes and proto-oncogenes. Loss of a wild-type allele of the tumour-suppressor gene *APC* is the most common mutation in colorectal cancers as a loss of this protein can cause transcriptional alteration and expression of proto-oncogenes (Markowitz, Bertagnolli, 2009). Other mutations in this so called "Wnt signalling pathway" are also common in CRC. Any deregulation, that leads to stabilization and reduced degradation of Catenin beta-1 (β-Cat) poses a risk for normal cell functionality as β-Cat can enter the nucleus and bind to the transcription factor TCF to transcribe proto-oncogenes like *c-MYC* (Habas, Dawid, 2005).

1.1.1 Energy metabolism in colon carcinoma

The highly proliferative nature of colon carcinoma cells requires them to sustain specific adaptations in metabolism like in other aggressive cancer cells. These adaptations distinguish CRC cells from healthy highly proliferative cells. Healthy cells usually generate a major part of their energy in form of adenosine triphosphate (ATP) through oxidative phosphorylation of glucose in the mitochondria of the cells. In tumour cells another energy providing pathway is performed, the so called "Warburg effect". This pathway relies on glycolysis as the primary energy source even under aerobic conditions. Aerobic glycolysis is much more inefficient than oxidative phosphorylation and uses high amounts of glucose in the process, which is why most cancer cells rely on a high intake of glucose to survive (Vander Heiden, et al. 2009).

To satisfy the high glucose demand, glucose transporters (GLUT-proteins) are strongly overexpressed in tumour cells. These proteins perform the active intake of glucose through the cellular membranes. Glucose processing enzymes like hexokinase (HK) and glyceraldehyde-3-phosphate dehydrogenase (GAPDH), which are involved in the first steps of glycolysis, are essential for high glycolysis rates as well (Fang, Fang, 2013). High glycolysis rates provide another critical effect for the tumour cell: the overproduction of lactate. Lactate is created as a side product of glycolysis to regenerate nicotinamide adenosine diphosphate (NAD^+) to keep up the glycolysis without NAD^+ generation through mitochondric respiration. The lactate is secreted by the tumour cells to their surroundings, where it

diminishes the immune response through reduced cytokine production and impairment of the function of cytotoxic T lymphocytes (Fischer, et al.,2007; Swietach et al., 2007).

The reason for all these adaptations to the energy metabolism is not yet fully understood. Besides the immune response evasion, switching to high glycolysis rates may also be significant to reduce oxidative stress during high proliferation phases. Reducing mitochondric activity prevents the accumulation of reactive oxygen species (ROS). ROS pose a significant risk of DNA damage during DNA synthesis (Brand, Hermfisse, 1997). Also, the oxygen supply for rapidly growing tumours by the surrounding blood vessels could be insufficient. It is necessary to switch to anaerobic energy production to keep up the supply of the high energy demand of the tumour cell (Cerella, et al., 2013).

1.1.2 Glutamine dependent nucleotide synthesis

Glutamine is relevant in biosynthesis pathways of many essential molecules in the cellular metabolism. It is the main source of nitrogen for *de novo* biosynthesis of nucleotides. Purine synthesis consists of three independent enzymatic reactions, all vitally depending on glutamine as obligate nitrogen donor (Wise, et al, 2010).

Inosine 5'-monophosphate (IMP) is the final precursor molecule for the purine nucleotides adenosine and guanosine. IMP can be converted into adenosine monophosphate (AMP) and guanosine monophosphate (GMP). As a starting point for IMP synthesis 5-phosphoribosylpyrophosphate (PRPP) is formed from activated ribose. PRPP reacts catalysed by PurF with glutamine as a nitrogen donor and a few enzymatic steps later FGAR reacts in an energy dependent reaction catalysed by PurL again with glutamine as nitrogen donor to FGAM (Figure 1.1). The whole reaction from PRPP to IMP consumes glutamine in two different steps, as well as aspartic acid, glycine, and ATP (Zhang, et al., 2008).

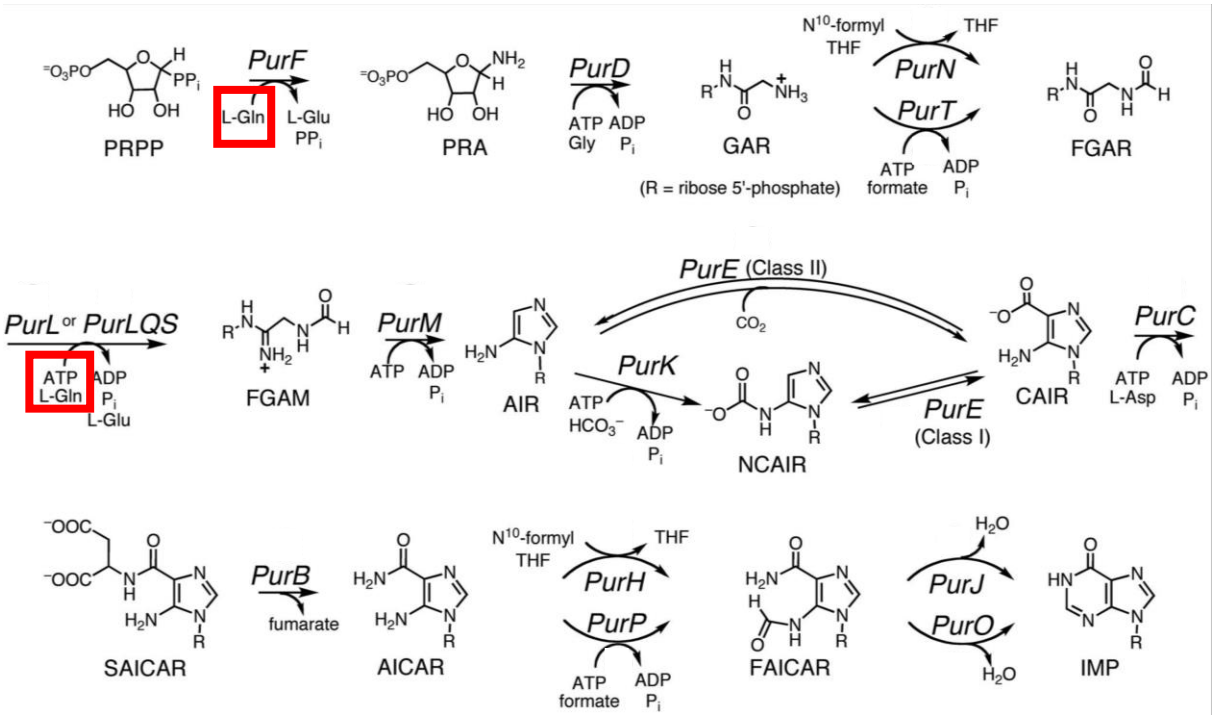

Figure 1.1: **De novo *Synthesis pathway of inosine 5'-monophosphate (IMP) from 5-phosphoribosylpyrophosphate (PRPP).*** *Glutamine acts as nitrogen donor in two different steps (red markings). Adapted from Zhang, et al., 2008.*

Two independent enzymatic reactions are necessary to synthesize pyrimidines *de novo* under involvement of glutamine as nitrogen donor (Wise, et al, 2010). The CAD enzyme catalyses bicarbonate, ATP, and glutamine to dihydrooretate, which is further processed in the inner mitochondrial membrane. The final two cytoplasmatic steps synthesize uridine monophosphate (UMP) for further processing into all other pyrimidine nucleotides (Huang, Graves, 2003).

As a secondary source of nucleotides, cells can recycle nucleotides from DNA and RNA in salvaging pathways. The salvaging of nucleotides plays only a small role in cancer nucleotide metabolism, as the *de novo* synthesis pathways are usually strongly upregulated in cancer cells (Natsumeda, et al., 1984). Therefore, glutamine is essential for the upkeep of the nucleotide pool in rapidly proliferating cancer cells to satisfy the high demand of nucleotides in cancer metabolism.

1.1.3 Glutamine addiction and the effect of glutamine starvation

1.1.3.1 Glutamine addiction in cancer cells

Glucose itself is not sufficient as an energy source for transformed cancer cells. Many cancer cells rely on high conversion rates of glutamine as a secondary, but essential energy source. This necessity is often referred to as "glutamine addiction" (Bhutia, et al., 2015). The amino acid glutamine is taken up via specific active transporter proteins and transferred to the mitochondria. Here glutamine is converted into glutamate, which is used in the TCA cycle to create α-ketoglutarate. This substrate can be used in the progressing TCA cycle or be transferred to the cytosol, where it functions as a substrate for anaplerotic reactions to synthesize other amino acids, nucleotides, or several lipids (Cerella, et al., 2013). In cancer cells though, this is not the only value of glutamine. It is also used to generate reductive molecules like NADPH through glutaminolysis, the conversion of glutamine to lactate. This conversion supports the high rates of glycolysis, when the mitochondrial pyruvate metabolism is diminished (DeBerardinis, et al., 2007).

During metabolic reprogramming of cancer cells to maintain high proliferation rates, large quantities of glutamine and glucose are also used to maintain basic anabolic synthesis pathways. Activation of the PI3K/AKT/mTOR-pathway induces the accumulation of NRF2 in the nucleus, which promotes redirection of glutamine and glucose to the anabolic pathways to support stable cell proliferation (Mitsuishi, et al., 2012).

1.1.3.2 The effect of glutamine starvation in cancer cells

Glutamine deprivation plays an important role in early tumorigenesis. Tumour growth quickly exceeds the usual supply of nutrients, especially glutamine in early growth stages. This environmental glutamine restriction leads to an intracellular shortage of α-ketoglutarate. α-ketoglutarate can promote hypomethylation of DNA and histones to induce an overexpression of differentiation-associated genes. Early glutamine starvation leads to accelerated tumour progression and evolution (Tran, et al., 2020).

In cell culture glutamine is one of the most used up amino acids, although it is a non-essential amino acid (Kosuke, et al., 2016). Glutamine starvation in colorectal cancer cells can induce a reversible cell cycle arrest, which can be reversed by re-supplementing the cells with glutamine. This arrest might be caused by a coordinated decrease of c-MYC levels and mTOR activity. c-MYC levels are strongly decreased in glutamine deprived colon carcinoma cells, which allows these cells to enter a quiescent state through not fully understood metabolic adaptations. These dormant cells, although glutamine addicted, can survive long periods without external supply of glutamine and quickly restart proliferation after re-addition of glutamine (Dejure, et al., 2017).

1.2 The global transcription amplifier c-MYC

The MYC protein family involves three main members, c-MYC, n-MYC, and l-MYC. These proteins are oncogenic transcription factors with a major role in regulation of proliferation gene expression. The focus in this study will be on c-MYC. It is formed by a basic helix-loop-helix structure combined with a leucine zipper motif. The latter allows binding to its main interaction partner protein MAX to form its active heterodimeric form, while the helix-loop-helix structure can bind to E-boxes in the genome, special consensus sequences that consist of the base sequence CACGTG (Adhikary, Eilers, 2005; Rahl, Young, 2014).

1.2.1 c-MYC dependent gene transcription regulation

c-MYC generally occurs in cells as single protein or as a homodimer. In these forms MYC is unable to bind DNA to regulate gene expression. The main interaction partner of c-MYC is the protein MAX. This protein binds to the helix-loop-helix structure at c-MYC's C-terminal region to allow DNA-binding at the E-boxes as a MYC-MAX heterodimer complex (Blackwell, et al., 1993). This complex serves as an activator to gene expression since it recruits RNA polymerase II (RNAPII) to open promoters. It binds to WD40-repeat protein (WDR5) binding sites across the genome using WDR5 as a guiding protein (Thomas et al., 2015). For transcription activation MYC interacts with several co-activators to open the chromatin for active transcription by modifying histones H3 and H4 (Frank, et al., 2003). After the chromatin is prepared for transcription and RNAPII is recruited to the gene, MYC also plays an important role in pause release of RNAPII and in promoting active elongation by recruiting the elongation factor P-TEFb (Rahl and Young, 2014). P-TEFb phosphorylates the NELF and DSIF complexes bound to RNAPII to initiate the promoter-proximal pause release (Rahl, et al.,2010). There are also a few transcriptional repressing mechanisms involving c-MYC. High levels of c-MYC lead to an increased MYC/MIZ1 complexation, which decreases transcription of MIZ1 target genes (Walz et al., 2014).

1.2.2 post-translational regulation of c-MYC protein levels

c-MYC expression is highly regulated among quiescent and proliferating cells. While quiescent and highly differentiated cells express only low levels of c-MYC, proliferating cells, hence also tumour cells, can contain between 10 and 40 times the amount of *c-MYC* mRNA (Kelly et al., 1983). *c-MYC* mRNA has a high turnover rate with only a short half-life time. The main regulation takes place at its 3'-UTR. It contains several structural elements determining the stability of mRNA, the so-called adenosine-uridine rich elements or AREs (Audic and Hartley, 2004). The AREs are targets for several mRNA stability regulating proteins like Human antigen R (HuR), TIA-1 related protein (TIAR) or ARE/poly(U)-binding/degradation factor 1 (AUF-1). Shortening of the 3'-UTR of *c-MYC* mRNA and

removing the AREs abolishes translational regulation and increases MYC protein levels (Dejure et al., 2017, Figure 1.2).

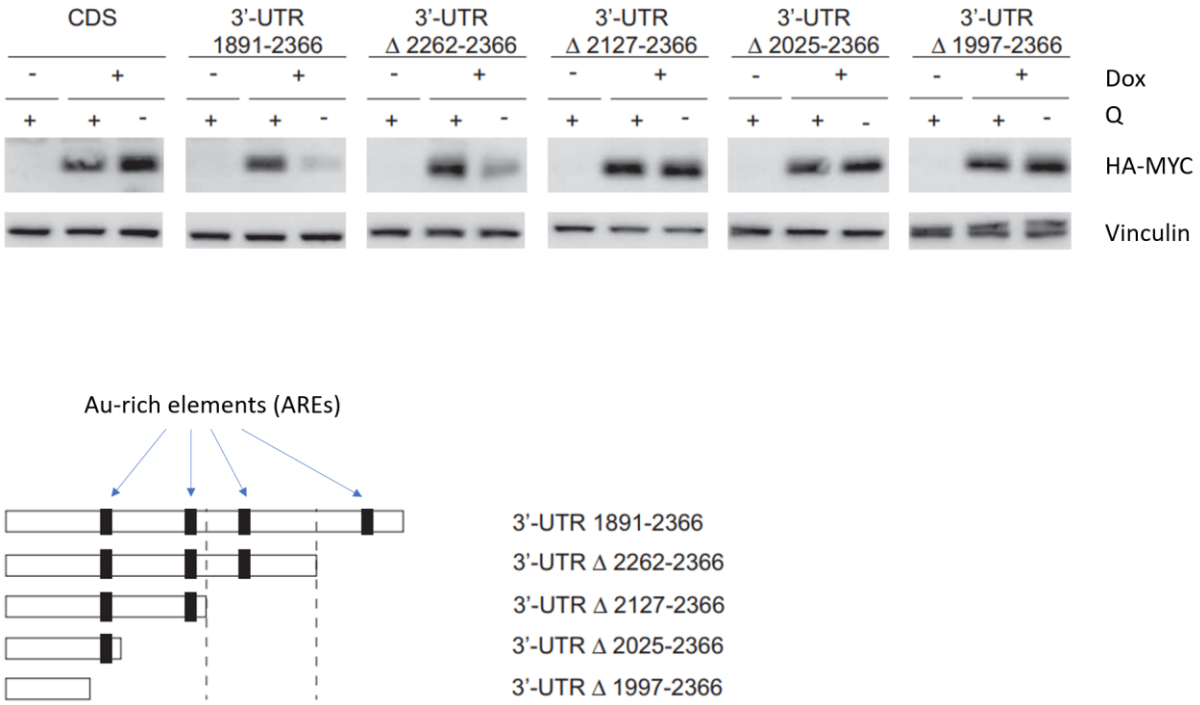

Figure 1.2 Deletion of AREs reduces translational MYC regulation. *Immunostaining showed an increased c-MYC levels during glutamine starvation when shortening* c-MYC *mRNA's 3'-UTR. Deleting the posterior AREs abolishes nearly all translational regulation. Adapted from Dejure, et al., 2017.*

Another way of regulating c-MYC translation via the 3'-UTR are micro RNAs (miRNAs). miRNAs like miR-34 family miRNAs are short non-coding RNAs, that can bind to specialized complementary sequences in mRNAs to sterically block translation of its target mRNAs. Groups of miRNAs like the miR-34 family can targets several targets and play an important role in specifying the expression patterns of cells for example by targeting proliferation protein translation (Bartel et al., 2009).

Therefore, introducing transgenes of c-MYC, which lack its 3'-UTR is a viable approach to circumvent overall translational regulation as well as glutamine dependent translational regulation.

c-MYC protein also has a very limited life span in the cell and is rapidly depleted. These high turnover rates depend on a few phosphorylation cascades, which induce a ubiquitin-dependent proteasomal turnover of c-MYC (Jaenicke et al., 2016). To reach high levels of c-MYC protein, for example in a tumour cell, a constant resupply by expression must be maintained to match the high degradation and turnover rates, which tightly regulate c-MYC levels in the cell.

1.3 DNA:RNA-hybrids: Transcriptional regulator and pathological symptom

During transcription, the double stranded DNA strand are unwound and denatured. This open structure is necessary for the RNA-polymerases to form nascent RNA using the template DNA strand. Under some circumstances, the freshly synthesized RNA can align to the template DNA strand and form a strong bond. This DNA:RNA-hybrid structure is called R-loop (Aguilera, et al., 2012).

1.3.1 Formation and function of DNA:RNA-hybrids in normal cells

DNA:RNA-hybrid structures are common in normal cell functionality. For example, the Okazaki fragments, small RNA-primers used during DNA replication are well understood and essential for this process. RNA polymerases themselves also contain small RNA pieces in their active site to provide proper binding abilities to the DNA (Costantino, Koshland, 2015).

R-loops form by longer RNA-fragments than the Okazaki fragments or the ones contained in RNA polymerases. Usually, the complementary DNA strand to the nascent RNA is occupied by its own non-coding DNA strand. During transcription, the DNA strands are separated from each other and are negatively supercoiled in this process. This can allow nascent RNA to bind to its template DNA strand (Liu, Wang, 1987). Prolonged elongation, RNAPII-stalling or disrupted termination of transcription causes a proximity of the nascent RNA and the template DNA, which promotes the formation of R-loops. Also, unmasking the RNA by splicing defects or a lack of the involved proteins can increase the binding potential of RNA to the DNA (Wahba, et al., 2013).

R-loops are not negative events in any case. They play an important role in the human immune system. Immunoglobulin class switch is necessary in activated B-cells to change the type of antibody the cells are producing. This process is promoted by a provoked R-loop formation. The depending regions in the genome for class switch contain long sequences of guanosine repeats (G-rich regions), which favour R-loop formation to present different sites of single stranded DNA to the activation-induced cytidine deaminase (AID), which mutates the B-cells to provide different antibodies (Roy, et al., 2008).

R-loops are also involved in transcription regulation. The DNA:RNA-hybrids can influence epigenetic reprogramming of cells. They are known to form at transcriptionally active CpG islands close to promoter regions, which are usually targets for methylation by methyltransferases. These methylated CpG islands silence the genes to which they are associated. Existing R-loops in these sites can protect the promoters from this form of gene silencing (Ginno, et al., 2012). Furthermore, R-loops might also influence chromatin structure. It was shown in drosophila and mice, that R-loop accumulation can cause histone phosphorylation and therefore packaging of chromatin (Proudfoot, et al., 2011).

R-loops can also form on specific G-rich sites near transcription termination sites. This event can cause an RNAPII pausing and promote the formation of R-loops and prevent termination (Skourti-Stathaki, et al., 2011). Several other functions of R-loops are known, but poorly understood to this day. They might

even play roles in cell senescence (Balk, et al., 2013) or DNA double strand break repair (Keskin, et al., 2014).

1.3.2 Pathological R-loops in human diseases

Unwanted R-loop formation can cause serious damage to cells and potentially to the whole organism. R-loop formation and persistence is linked to DNA damage in various ways. While the DNA:RNA-hybrid is existent, the complementary DNA strand is single stranded. This exposed DNA strand is vulnerable to mutations and DNA damage due to its reduced chemical stability. This leads to the binding of deaminases like AID and repair enzymes. These proteins can induce DNA lesions and nicks, which can in turn lead to DNA recombination and double strand breaks by transcription-replication conflicts (Skourti-Stathaki, Proudfoot, 2014).

Several human diseases are linked to uncontrolled R-loop formation. The fragile X syndrome (FraX), one of the most common forms of genetics related mental retardation, is caused by an expansion of short repetitive G-rich DNA sequences located on the X-chromosome. R-loop formation in this region combined with insufficient DNA damage repair could be one reason for this repeat expansion (Lopez Castel, et al., 2010). Ataxia and ALS4 are also linked to R-loop formation. Different mutations in RNA/DNA helicases cause R-loop formation and induce defects in transcriptional termination (Skourti-Stathaki, et al., 2011). A lack of R-loop resolution ability is the hallmark of Aicardi-Goutieres-Syndrome, a neurological inflammatory disorder. Mutations in RNase H2 inhibit its ability to resolve RNA/DNA hybrids created by incorporation of single RNAs into DNA, which leads to genome instability (Reijns et al., 2012).

In cancer cells, which are known for their genome instability, R-loops may play an important role, too. Since decreased resolution of R-loops or promoted formation of these leads to genome instability, R-loops might drive tumour development. Tight control of R-loop levels is therefore essential for tumour prevention. Mutations in genes involved in these control mechanisms like cleavage and polyadenylation factor FIP1L1 are often found in tumours and promote chromatin instability (Stirling et al., 2012).

1.3.3 Resolution of R-loops

There are several ways to prevent the formation of R-loops or dissolve those, which are already in place. Proper function of the transcription-export complex (TREX) involves elongation stimulation, packaging of nascent mRNA and export of processed RNA and prevent the formation of DNA:RNA-hybrids. Defects in this protein can cause R-loop formation by insufficient processing of nascent mRNA and prolonged proximity of RNA and single stranded DNA (Huertas, Aguilera, 2003). Enzymes like DNA topoisomerase 1 (TOP1) involved in relaxing and resolving negative DNA supercoiling also prevent formation of R-loops (El Hage et al., 2010).

Most importantly the two proteins RNase H1 and RNase H2 are responsible for dissolution of persisting R-loops. They can specifically degrade different forms of RNA:DNA-hybrids. Both can dissolve R-loops, but RNase H2 can also remove Okazaki-fragments after DNA replication and single RNAs incorporated during the replication process (Qiu et al., 1999). Endogenous RNase H1 can resolve R-loops in the nucleus and in the mitochondria. It is also necessary for mitochondrial replication. RNase H1 is highly conserved among organisms and contains a hybrid binding domain at its N-terminus allowing high affinity binding to RNA:DNA-hybrids (Cerritelli, 2008; Nowotny et al., 2008). RNase H1 can introduce strand breaks in the nascent RNA bound to DNA. These breaks can be used to induce transcription termination and RNAPII release by XRN2 binding and termination described in the "torpedo-model" (Villarreal et al., 2020). Other mechanism to resolve R-loops for example via RNA/DNA helicases like Senataxin (SETX) play a minor role in resolution of R-loops, but a lack of their activity can cause defects and diseases none the less (Skourti-Stathaki, Proudfoot, 2014).

1.4 Aim of this thesis

It is known that c-MYC levels are strongly deregulated in cancer cells during metabolic reprogramming. Its translation and the actual protein levels are strictly linked to glutamine availability in colon carcinoma cells. This study aims to find proteins involved in this translational regulation pathway, which could pose further targets to address in cancer therapy since c-MYC itself cannot be targeted directly. Furthermore, it was shown by Dejure et al., 2017 that glutamine starvation and ectopically expressed c-MYC could drive colon carcinoma cells into apoptosis. A link between the apoptotic pathway and a measured accumulation of DNA:RNA hybrids (R-loops) could be assumed. The following study should shed light on this proposed link and check for possibilities to use R-loop degradation to uncover the apoptotic mechanism.

2 Results

2.1 siRNA screen to detect proteins involved in glutamine dependent MYC translation regulation

In advance to all following experiments the group of Stefan Kempa in Berlin performed an *in vitro* pull-down to identify proteins, which can bind to *c-MYC* mRNA. They artificially created labelled 3'-UTR of the *c-MYC* mRNA and mixed them with whole cell lysate of HCT116 cells. One cell culture was grown in the presence of glutamine and another one in the absence of glutamine. A pull-down of the mRNA and all bound proteins was performed, and the adhesive proteins analysed via mass spectrometry. A total of 78 proteins were identified as RNA-binding proteins to the 3'-UTR of *c-MYC* (Table 2.1).

***Table 2.1: Results of* in vitro *pull-down of 3'-UTR binding proteins in presence and absence of glutamine* performed by Stefan Kempa's group in Berlin.**

Proteins binding 3'-UTR of MYC mRNA in absence of		Proteins binding 3'-UTR of MYC mRNA in presence of glutamine			
Annexin A2;Putative annexin A2-like protein	ANXA2;ANXA2P2	Cell division cycle protein 16 homolog	CDC16	H/ACA ribonucleoprotein complex subunit 2	NHP2
Amphiregulin	AREG	Coilin	COIL	Nucleolar protein 11	NOL11
ATP synthase subunit alpha, mitochondrial	ATP5A1	Probable ATP-dependent RNA helicase DDX20	DDX20	H/ACA ribonucleoprotein complex subunit 3	NOP10
Calmodulin-like protein 5	CALML5	Microprocessor complex subunit DGCR8	DGCR8	Endonuclease III-like protein 1	NTHL1
Cofilin-1	CFL1	Probable dimethyladenosine transferase	DIMT1	DNA-directed RNA polymerases I and III subunit RPAC1	POLR1C
Caseinolytic peptidase B protein homolog	CLPB	H/ACA ribonucleoprotein complex subunit 4	DKC1	DNA-directed RNA polymerase II subunit RPB2	POLR2B
Eukaryotic translation initiation factor 6	EIF6	DnaJ homolog subfamily C member 13	DNAJC13	DNA-directed RNA polymerases I, II, and III subunit RPABC3	POLR2H
Alpha-enolase	ENO1	Dynein light chain 1, cytoplasmic	DYNLL1	DNA-directed RNA polymerases I, II, and III subunit RPABC5	POLR2L
Heat shock protein beta-1	HSPB1	Epithelial splicing regulatory protein 2	ESRP2	DNA-directed RNA polymerase III subunit RPC1	POLR3A
60 kDa heat shock protein, mitochondrial	HSPD1	Gem-associated protein 4	GEMIN4	DNA-directed RNA polymerase, mitochondrial	POLRMT
10 kDa heat shock protein, mitochondrial	HSPE1	Nucleolar GTP-binding protein 2	GNL2	Serine/threonine-protein phosphatase PP1-gamma	PPP1CC
Protein LSM12 homolog	LSM12	GTP-binding protein 1	GTPBP1	Replication factor C subunit 1	RFC1
Malate dehydrogenase, mitochondrial	MDH2	Peroxisomal multifunctional enzyme type 2;(3R)-	HSD17B4	Ribonuclease H2 subunit C	RNASEH2C
Pyruvate kinase PKM	PKM	Protein Red	IK	TATA-binding protein-associated factor 2N	TAF15
Protein arginine N-methyltransferase 5	PRMT5	Inosine-5-monophosphate dehydrogenase 1	IMPDH1	RISC-loading complex subunit TARBP2	TARBP2
60S ribosomal protein L15	RPL15	Kinesin-like protein KIF14	KIF14	Dimethyladenosine transferase 2, mitochondrial	TFB2M
60S ribosomal protein L19	RPL19	Importin subunit alpha-1	KPNA2	Tubulin gamma-2 chain;Tubulin gamma-1 chain	TUBG1
60S ribosomal protein L30	RPL30	Importin subunit beta-1	KPNB1	Tubulin gamma-2 chain;Tubulin gamma-1 chain	TUBG2
40S ribosomal protein S28	RPS28	MAGUK p55 subfamily member 7	MPP7	E3 ubiquitin-protein ligase UHRF1	UHRF1
Small nuclear ribonucleoprotein F	SNRPF	39S ribosomal protein L53, mitochondrial	MRPL53	U3 small nucleolar RNA-associated protein 15 homolog	UTP15
Translocon-associated protein subunit delta	SSR4	28S ribosomal protein S2, mitochondrial	MRPS2	pre-mRNA 3 end processing protein WDR33	WDR33
Spermatid perinuclear RNA-binding protein	STRBP	28S ribosomal protein S27, mitochondrial	MRPS27	WD repeat-containing protein 43	WDR43
Triosephosphate isomerase	TPI1	28S ribosomal protein S28, mitochondrial	MRPS28	WD repeat-containing protein 6	WDR6
RING finger protein unkempt homolog	UNK	C-1-tetrahydrofolate synthase	MTHFD1	Pre-mRNA-splicing regulator WTAP	WTAP
Valine--tRNA ligase	VARS	H/ACA ribonucleoprotein complex non-core subunit NAF1	NAF1	Zinc finger CCHC domain-containing protein 8	ZCCHC8
		Nuclear receptor coactivator 5	NCOA5	Zinc finger protein 385A	ZNF385A
				Zinc finger protein 706	ZNF706

2.1.1 Glutamine starvation reduces c-MYC protein levels in HCT116 by over 60% via translational regulation

As described earlier, the glutamine level has important effects on c-MYC expression. To determine the scale of c-MYC protein levels in the newly created HCT116 cell line, a first siRNA experiment was performed. 3500 cells per well in a 96-well plate were seeded in triplicates in glutamine-containing medium or glutamine-deprived medium (Figure 2.1). To ensure that the cells cannot utilize any supplements in the FCS of the growing medium, dialyzed FCS which was cleansed of all molecules larger than 10 kDa, was used. 48 h before fixation the siRNA treatment was applied to the cells. One group of cultures was treated with a specific siRNA against c-MYC and the other one was treated with

unspecific scrambled RNA as a negative control. 24 h before fixation, the growing medium (+Q) was replaced by glutamine-deprived medium for the cultures labelled as glutamine starvation (-Q) and glutamine starvation with 2 h recovery in glutamine containing medium (-Q/2h+Q). After fixation and permeabilization the cells were stained with DAPI (nucleus) and a primary antibody against c-MYC (Y96) with a fluorescent secondary antibody (Alexa488).

The fluorescence intensity was measured using the Operetta High Throughput Imaging System at a 20-fold magnification. The DAPI fluorescence signal was used to count every single cell nucleus by automated cell counting. The Alexa488 signal determined the relative distribution of c-MYC in the fixated cells. The signal threshold was normalized to the fluorescence intensity of the wells treated with the siRNA against c-MYC.

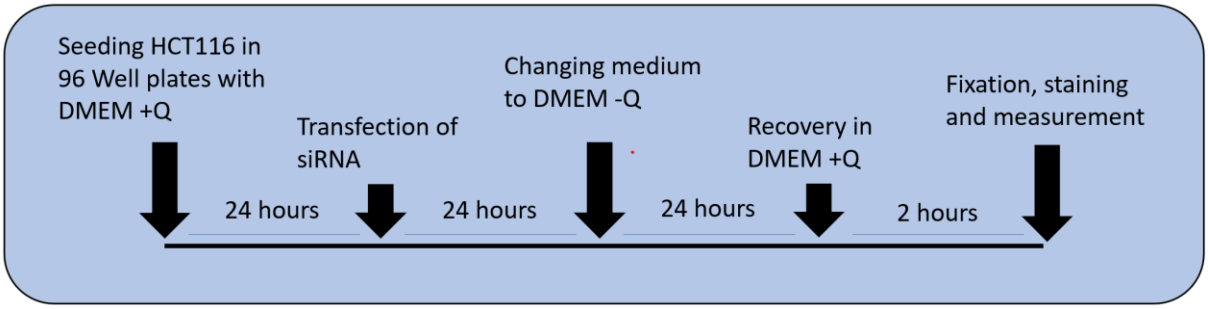

Figure 2.1: Workflow of the glutamine starvation experiment with incubation times and specific conditions.

All measurements were normalized to the mean fluorescence intensity of the +Q wells for better comparison. As described in Dejure, et al.,2017, the fluorescence intensity representative for the c-MYC protein level drops significantly when the cells were starved for glutamine. The intensity drops under glutamine starvation in average by 68% when treated with scrambled siRNA (Figure 2.2, red bar). When glutamine starved cells were transferred to glutamine rich medium 2 h prior fixation, the fluorescence intensity was reduced by less than 10% compared to the +Q condition. This indicates a rapid recovery of c-MYC levels after starvation (Figure 2.2, cyan bar). The speed of replenishment of c-MYC protein suggests a regulation by glutamine on the translational level of c-MYC expression. As shown in Dejure, et al., the *c-MYC* mRNA levels were increased during glutamine starvation. The cells treated with a siRNA against c-MYC showed altogether a relative fluorescence intensity of about 25% of the +Q control cells (Figure 2.2, right bar group). Since the RNA interference mechanism regulates on the translational pathway as well, the similar fluorescence intensities of glutamine starvation and the siRNA against c-MYC support the hypothesis that the glutamine dependent c-MYC regulation takes place on the translational level.

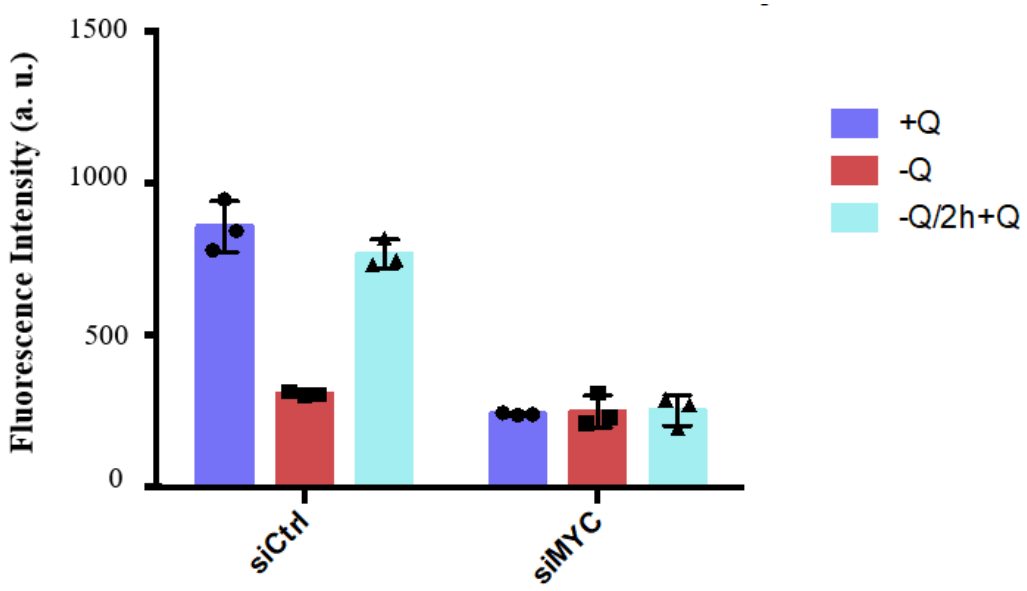

Figure 2.2: Glutamine starvation decreased c-MYC protein levels comparable to specific siRNAs. *After cells were grown and prepared as described in Figure 4.1, the fluorescence intensity measurement using the Operetta high-throughput microscopy system showed a strong decrease in fluorescence intensity of the c-MYC probe. When recovered with glutamine supplement, the fluorescence signal normalized rapidly. The experiment was performed 3 times with measurements in 3 wells of a 96-well plate. Each symbol represents the mean nuclear fluorescence intensity of the three wells.*

2.1.2 Knockdown of importin subunit beta-1 (KPNB) and heat shock protein E1 (HSPE1) alters glutamine dependent c-MYC expression regulation

In the following experiments both scrambled siRNA and siMYC were also performed as controls on each 96-well plate to ensure a consistence during all measurements and to normalize the fluorescence signal threshold. All 78 proteins described in table 2.1 were knocked down with specific siRNAs and measured in the same way as described in 2.1.1. The relative fluorescence intensities were in all 78 cases normalized to the mean intensity of the +Q condition of the siRNA treated group. 74 of these siRNAs showed no significant effect on the fluorescence intensity and hence no effect on glutamine dependent c-MYC regulation. The relative fluorescence intensities of +Q, -Q and -Q/2h+Q showed the same pattern as the control cells treated with scrambled siRNA. However, siRNAs against KPNB and HSPE1 showed a strong effect on glutamine dependent c-MYC expression regulation (Figure 2.3). The relative fluorescence intensity decrease during glutamine starvation was in cells with siRNA treatment against these two proteins insignificantly low. The intensity decreased to about 80% of the +Q condition in both cases.

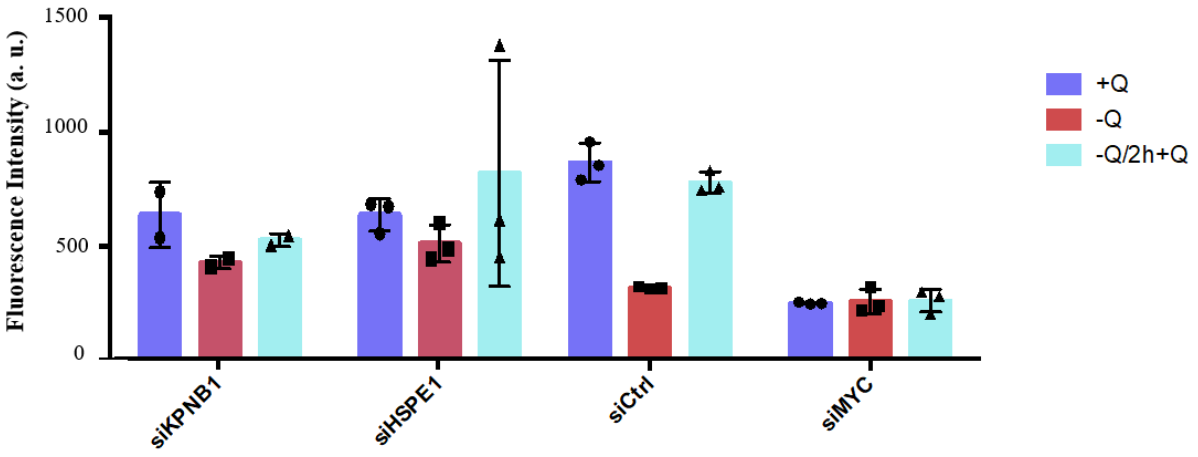

Figure 2.3: Knockdown of the proteins KPNB1 and HSPE1 decreased the effect of glutamine starvation on MYC levels. *The cells were treated with specific siRNAs against the importin subunit beta-1 (KPNB) and the heat shock protein E1 (HSPE1). Knockdown of these proteins decreases the c-MYC protein deprivation during glutamine starvation, keeping an almost constant level of c-MYC protein in these cells. The experiment was performed 3 times with measurements in 3 wells of a 96-well plate with the siHSPE1 and 2 times with the siKPNB1. Each symbol represents the mean nuclear fluorescence intensity of the three wells.*

2.1.3 Knockdown of RNA-polymerase subunits increases c-MYC protein levels during glutamine starvation

When knocking down the Polymerase III subunit A protein expression (POLR3A) and the Polymerase II, I and III subunit L (POLR2L) the pattern of fluorescence intensities alters drastically in these cell cultures. Instead of decreasing during glutamine starvation, the intensity increases (Figure 2.4, red bars). This indicates the c-MYC protein levels were higher during glutamine starvation and afterwards during recovery (Figure 2.4, cyan bars).

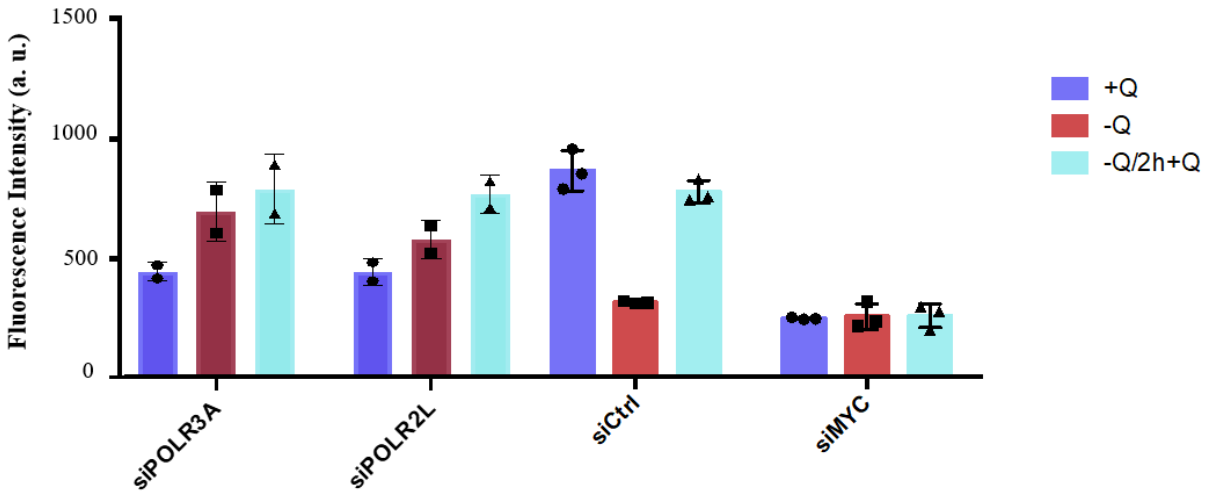

Figure 2.4: Knockdown of POLR3A and POLR2L increased c-MYC protein levels. *HCT116 cells were treated with siRNAs against the Polymerase III subunit A (POLR3A) and the Polymerase II, I and III subunit L (POLR2L). The knockdown of the two essential subunits of polymerase activity deregulated MYC protein expression. Even during glutamine starvation, the c-MYC protein levels were like the control condition or even increased. The experiment was performed 2 times with measurements in 3 wells of a 96-well plate. Each symbol represents the mean nuclear fluorescence intensity of the three wells.*

The changes in fluorescence intensity were also clearly visible when comparing digital images of each condition. The fluorescence threshold was again normalized to the +Q cells treated with scrambled siRNA (Figure 2.5, top left panel). The quenching of fluorescence during glutamine starvation could only be seen in with scrambled siRNA, which also showed high fluorescence intensity after recovery. Cells treated with siRNA against c-MYC show only weak fluorescence overall (Figure 2.5, second column). The siRNA against HSPE1 caused the cells to shine brightly either with or without glutamine and after recovery (Figure 2.5, third column). No quenching of fluorescence signal could be observed with the naked eye after glutamine starvation. Cells treated with the siRNAs against the polymerase subunits showed a weaker fluorescence signal then the control cells (Figure 2.5, fourth column).

The fluorescence images supported the results of the relative fluorescence intensity measurement further. These combined results suggested a link between KPNB1 and HSPE1 and the glutamine dependent c-MYC translation regulation pathway. Furthermore, the knockdown of RNA polymerase subunits deregulates the pathway. As described in Dejure, et al., c-MYC translation is strongly dependent on the availability of adenosine. This dependency could explain the deregulation after knockdown of the subunits as RNA polymerases are also strongly dependent on the availability of nucleosides.

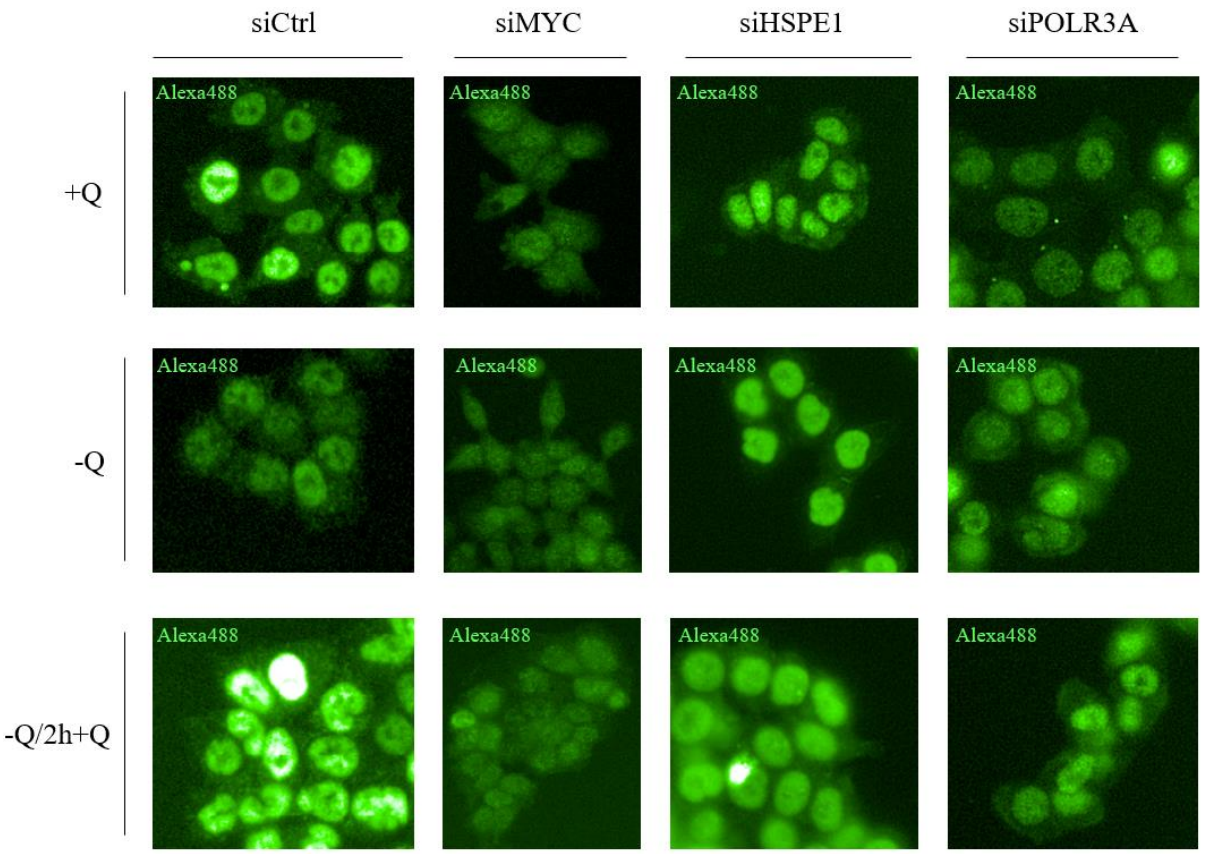

Figure 2.5 Fluorescence microscopic view on the change of intensity of c-MYC probe in the nucleus of treated cells (Figures 2.2 and 2.3). *Glutamine starved cells show a similar decrease of fluorescence intensity to cells treated with a specific siRNA against c-MYC. Nuclear fluorescence intensity stayed constant regardless of glutamine availability during knockdown of HSPE1 and POLR3A.*

2.2 RaPID-Assay to detect protein interaction partners of c-MYC 3'-UTR

As a counterpart to the siRNA screen which was based on an *in vitro* approach to find interaction partners of the c-MYC 3'-UTR, we also went for an in vivo method. In contrast to the afore mentioned pull down, the RNA-Protein Interaction Detection Assay (RaPID) uses a biotin ligase enzyme expressed in live cells to biotinylate proteins in close proximity. The enzyme is guided by a specific RNA structure, the BoxB-stem loop. To establish the method, the U1 spliceosomal snRNA was chosen as it is an RNA with very well documented protein interaction partners. The U1 snRNA interacts closely with the Sm-ring which forms the core unit of the RNA spliceosome (Nagai, et al., 2001). This ring consists of seven proteins smB/B', smD1, smD2, smD3, smE, smF and smG (Will, Lührmann, 2011). BoxB-stem loops were cloned to both sides of the U1 snRNA to direct the biotin ligase *in vivo* to its target. The expression of the U1 snRNA with the BoxB-stem loops had to be detected indirectly, as the stem loops form strong secondary structures and due to their small size, it was not possible to target them directly by a primer

for qPCR. Instead, a 4-fold increase of U1 snRNA could be measured in cells expressing U1 snRNA with stem loops (Figure 2.6), which indicates the desired expression.

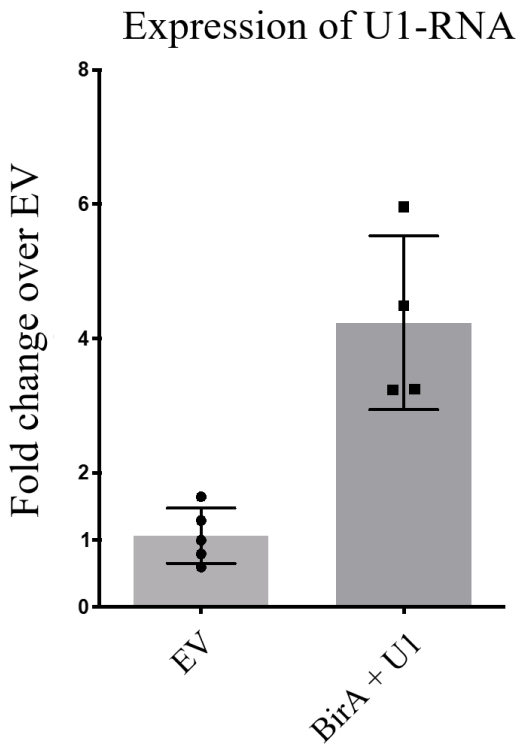

Figure 2.6 Increased expression levels of U1-RNA as an indirect marker for modified U1 expression. *qRT-PCR with primers specific for U1-RNA was performed after RNA isolation of uninfected cells and cells infected with the biotin ligase BirA and the modified U1-RNA. Infected cells showed a 4-fold change of U1 expression which hints to the expression of the modified U1-RNA. Each symbol represents an independent qPCR measurement from the same RNA isolation experiment.*

The *Bacillus subtilis* biotin ligase was marked with an HA-Tag for expression control. Also, it was designed to be solely expressed in the presence of doxycycline (Figure 2.7).

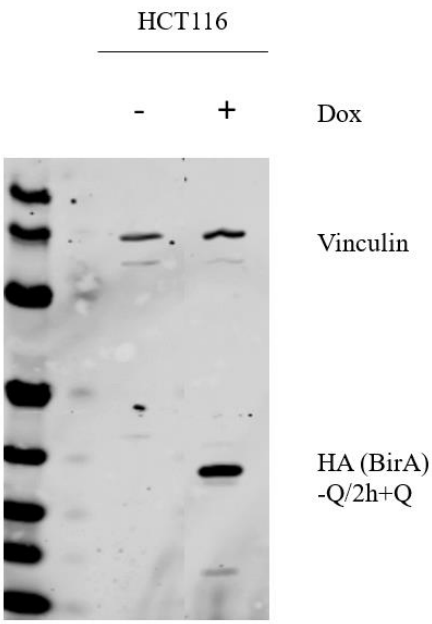

Figure 2.7: Western Blot confirmation of doxycycline dependent expression of the Bacillus subtilis biotin ligase (BirA) indirectly via an antibody against the BirA-HA-tag. *The infected HCT116 cells showed a strong and doxycycline dependent expression of the modified BirA after 24h incubation with doxycycline supplement.*

As the interaction between U1 snRNA and the spliceosomal Sm-ring structure takes place in the nucleus, the biotin ligase had to be present in the nucleus as well. This was confirmed via fluorescence microscopy. A primary antibody against the HA-Tag was used to detect the modified biotin ligase in the nucleus (Figure 2.8).

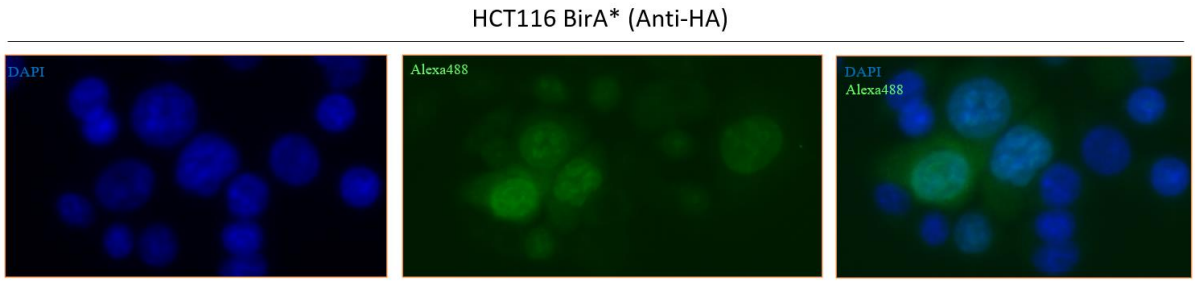

Figure 2.8: Fluorescence microscopic confirmation and localization of the modified BirA with an antibody against the HA-tag of the BirA. *After 24 h incubation of infected HCT116 cells with an anti-HA antibody and a 5 min incubation with DNA-intercalating probe DAPI to stain the nucleus, the BirA was shown to be located in the nucleus, but also to a lower extend in the cytoplasm.*

With all necessary components expressed in a HCT116 and in a LS174 cell line the RaPID-Assay could be performed in two separate colon carcinoma cell lines. Representative for the spliceosomal Sm-ring the protein SmB was chosen, as it could be easily detected by the highly specific Y12 antibody. After the streptavidin pulldown, an immunoblot was performed to mark all biotinylated proteins, which were extracted from the cell lysate. The blot membrane was stained with the antibody against SmB (Y12), which stains at 29 kDa and with an antibody against vinculin as a control staining at 117 kDa. For each cell line three independent cultures were grown. Two cultures were kept in medium with biotin supplemented and one culture without any biotin. The immunoblot showed a weak vinculin band in all three LS174 cultures, while vinculin was only visible in the two HCT116 lysates of cultures kept in biotin containing medium (Figure 2.9). The Y12 signal indicating SmB was detected in all lysates. The signal was slightly stronger in cells incubated in biotin containing medium than in biotin-less medium. Since the expressed biotinylase and the modified U1 RNA were present in all cultures, the difference between the lysates was only the presence of biotin. So, the enrichment observed in the latter lanes of the membrane shown in Figure 2.9 was fully biotin dependent. The pulldown could therefore be used to specifically enrich the interaction partners of an RNA with the BoxB stem-loops through biotinylation by the modified BirA-biotin ligase.

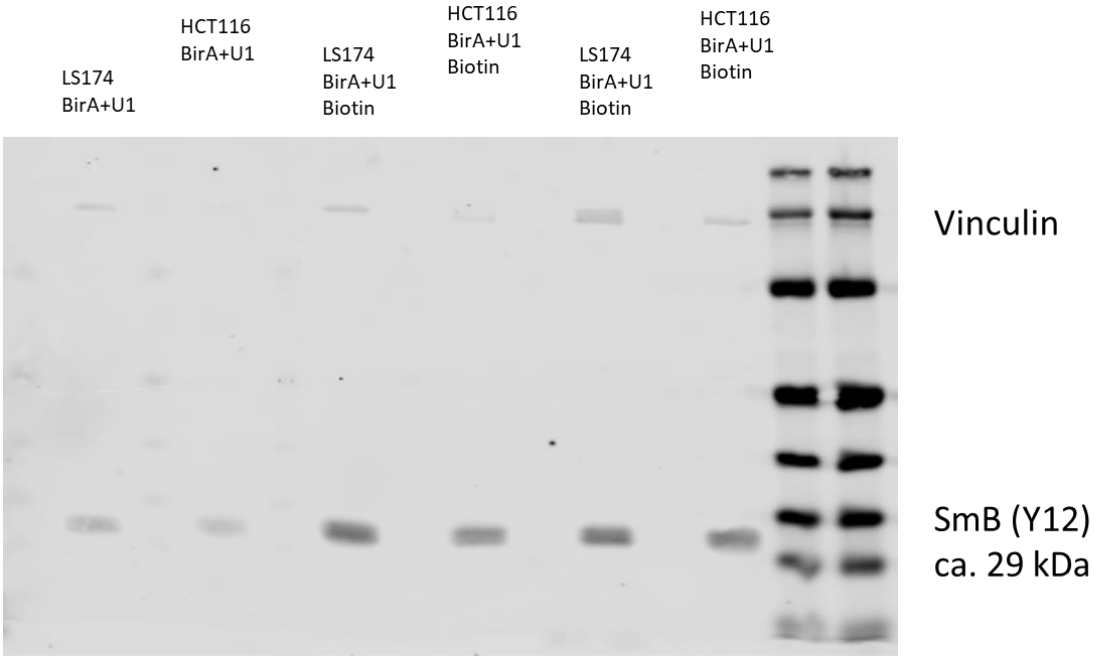

Figure 2.9: Western Blot staining to determine the efficiency of the pulldown of biotinylated proteins with BirA biotin ligase. *HCT116 and LS174 cells infected with BirA and BoxB stem-loop modified U1 snRNA were grown either in biotin-free medium (one culture) or serum- free medium with 0.2 mol/l biotin (two cultures). The biotin labelled proteins were pulled down with biotin-specific streptavidin beads. A specific smB antibody was used in an immuno-blot, which is a close interaction partner protein of the U1 snRNA.*

2.3 RNaseH1 incorporation and MYC-ER activation increases apoptosis during glutamine starvation

The c-MYC protein levels depend directly on glutamine availability in the medium in colon carcinoma cell lines as shown before (2.1.1) and in Dejure et al., 2017. As shown in that paper, the protein levels are linked to the 3'-UTR of *c-MYC* mRNA. To keep the c-MYC protein levels stable during glutamine starvation, an ectopically expressed c-MYC protein had to be introduced into a cell line. Since constant high levels of c-MYC can induce apoptosis in cells (Evan, et al., 1992), the MYC-ER system was chosen as the most viable transgene. The MYC-ER system features a *c-MYC* gene without its regulatory 3'-UTR and the transgene is inducible by hydroxytamoxifen (OHT). So, the expression of the transgene is not regulated by glutamine levels and the trans protein is only active when the cells are supplemented with OHT.

In cells starved for glutamine, transcription usually stalls due to a lack of c-MYC protein. When c-MYC levels are kept on high levels artificially by the MYC-ER system, transcriptional stress can occur in these cells in form of DNA-RNA hybrids (R-loops). These R-loops are a source of genomic instability (Aguilera, Garcia-Muse, 2012) and can lead to apoptosis under certain conditions (Dejure, Eilers, et al., 2017). The overexpression of RNaseH1, which degrades R-loops could prevent the apoptotic phenotype in these cells.

2.3.1 Introducing a stable overexpression of RNaseH1 in HCT116 cells reduced R-loop formation slightly

To test which effect a strong overexpression of RNaseH1 has on cells that form R-loops as transcription stress, an HCT116 cell line with the MYC-ER system was infected with a constitutively active transgene or RNaseH1. The RNaseH1 was designed with an HA-Tag for easier detection and localization (Figure 2.10).

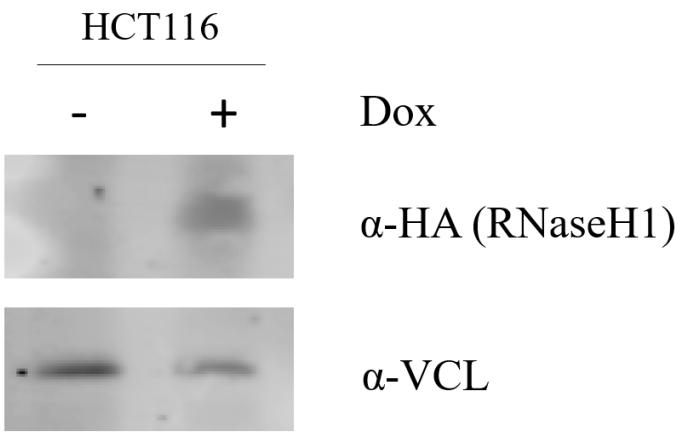

Figure 2.10: Western blot confirmation of constitutive RNaseH1 overexpression. *An anti-HA-tag antibody was used to detect the expression of ectopically introduced RNaseH1 in infected HCT116 cells.*

Since R-loops form on DNA in the nucleus, the modified RNaseH1 had to be located in the nucleus as well. An immunofluorescence staining with an antibody against the RNaseH1's HA-Tag was performed (Figure 2.11). It showed a strong expression of the RNaseH1 in the cells, mostly in the cytosol and less in the nucleus.

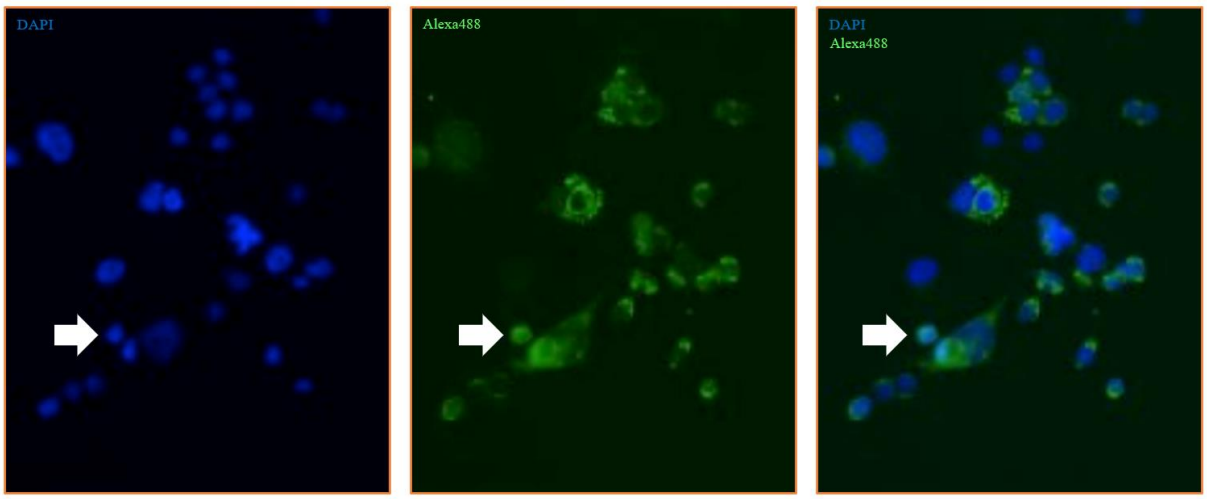

Figure 2.11: Localization of RNaseH1 expression via HA-tag staining under fluorescence microscope. *HCT116 cells were fixated paraformaldehyde and stained with an HA-tag specific antibody and DAPI for nuclear staining. The HA-tagged RNaseH1 fluorescence signal was mostly located in the cytoplasm and to a lesser extend in the nucleus.*

A DNA:RNA hybrid immunoprecipitation (DRIP) was performed to check, whether the RNaseH1 which gets into the nucleus was sufficient to show an effect on R-loop formation and degradation. One cell line containing RNaseH1 overexpression and with the MYC-ER system and another one with just the MYC-ER system and an empty vector were grown and starved for glutamine. The MYC-ER system was activated with OHT for 24 h and the cells harvested for the DRIP. The R-loop specific S9.6 antibody

was used to pull down the R-loops. The DNA was degraded, and the RNA reverse transcribed and used for a qPCR. In Hatchi, et al., 2015, the *beta-actin* gene was described as a common formation site during transcriptional stress. Specific primers for different locations in the *beta-actin* gene were used in the qPCR. The PCR showed R-loop formation took place during glutamine starvation and MYC-ER activation in the *beta-actin* gene (Figure 2.12). The weakest signals were detected by primers binding at the polymerase pause sites and the strongest signal by the primer located shortly after the transcription start site in the first exon. The qPCR performed with the DRIP of the cells expressing RNaseH1 was slightly lowered in comparison to the cells with the empty vector further in the gene body. The highest reduction of qPCR signal could be detected at the beginning and the end of the gene. Here the RNaseH1 incorporation reduced the R-loops to about 60% of the empty vector cells.

The stable expression of RNaseH1 in HCT116 cells could reduce the number of R-loops in cells suffering transcription stress due to glutamine starvation and lacking c-MYC downregulation, although only a limited fraction of modified RNaseH1 was located in the nucleus.

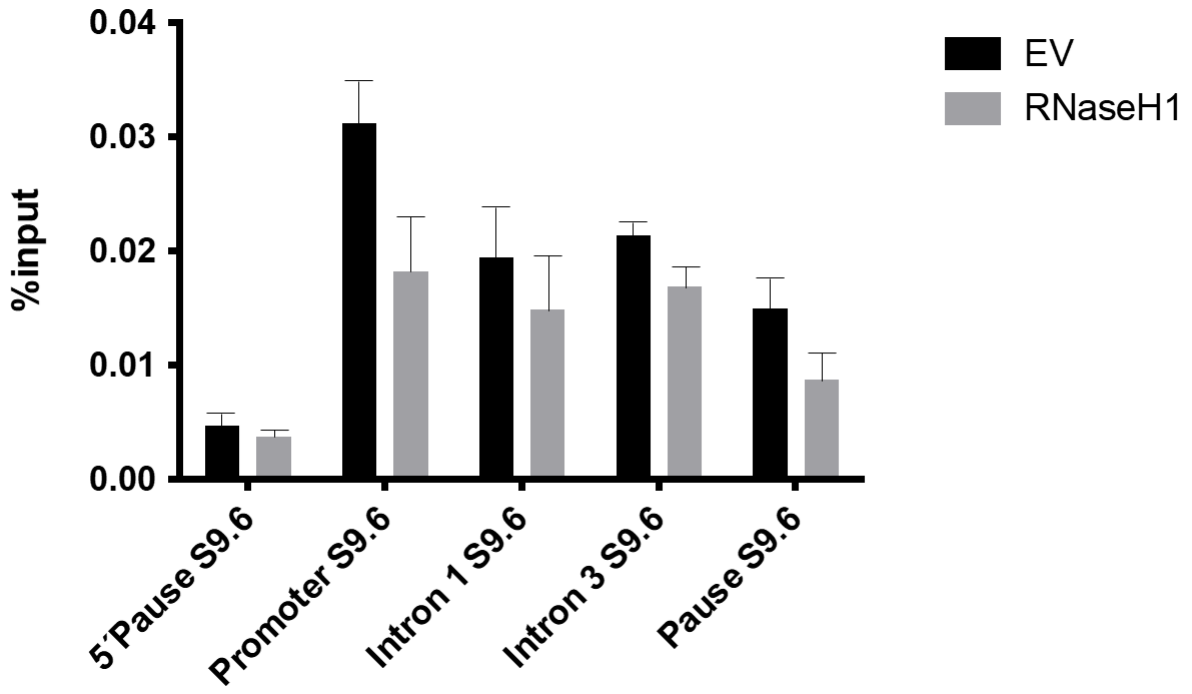

Figure 2.12: DNA:RNA hybrid immunoprecipitation (DRIP) showed slightly decreased R-loop formation in constitutively RNaseH1 overexpressing HCT116 cells. *An R-loop specific antibody (S9.6) was used in the DRIP pulldown. An RNA isolation and reverse transcription were performed, and the remaining DNA was used in a qRT-PCR. Primers for specific regions in the beta-actin gene (from Hatchi, et al.) were used to determine the distribution of R-loops throughout this gene. The highest number of R-loops was found at the transcription start site (Promoter S9.6), where also the strongest reduction of R-loops in RNaseH1 overexpressing cells could be detected.*

2.3.2 Inducible RNaseH1 transfers to the nucleus and degrades the bulk of the R-loops

Since the constitutively expressed RNaseH1 showed only little impact on R-loop formation, but seemed to slow the growth rate of cells, we created a doxycycline dependent RNaseH1 expression system using the pInducer21 plasmid. The newly created HCT116 cell line was infected with a MYC-ER system and the pInducer21 with an RNaseH1 transgene with HA-Tag and a nuclear import sequence. Whilst the endogenous c-MYC was decreased during glutamine starvation, the MYC-ER expression remained unchanged due to the lacking 3'-UTR in the transgene (Figure 2.13).

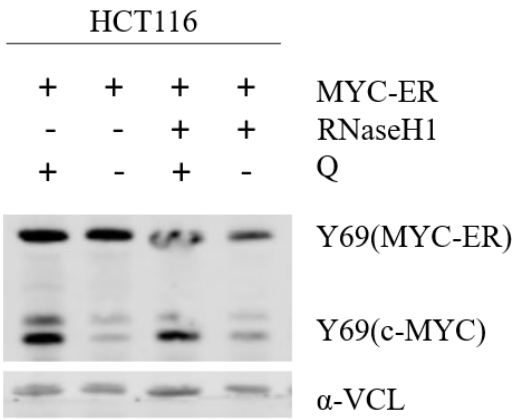

Figure 2.13: Glutamine-independent MYC-ER expression on similar levels as intrinsic c-MYC expression. *Western Blot detection with c-MYC specific Y96-antibody after glutamine starvation of 24 h in HCT116 cell lysates.*

Lysate of the afore mentioned new HCT116 cell line containing the RNaseH1 expression system showed a strong band in an HA-Tag immunoblot at the indicated 35 kDa marker after doxycycline supplement. This confirms the functionality and the high expression rate of the chosen expression system (Figure 2.14).

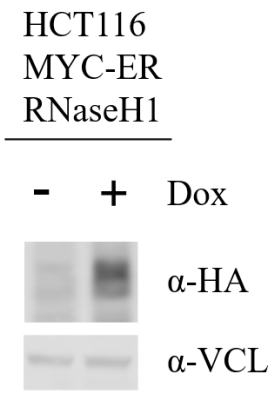

Figure 2.14: Doxycycline-dependent expression of HA-tagged RNaseH1 in HCT116 cells. *Western Blot detection with HA-tag specific antibody to determine expression levels of artificial RNaseH1 overexpression indirectly after 24 h incubation in doxycycline-containing medium (100 µg/ml).*

Since the constitutively active RNaseH1 was mostly located in the cytoplasm, the distribution of the new enzyme was also checked via immunofluorescence. This staining showed a high overlap between the HA-Tag staining of the RNaseH1 and the Hoechst fluorescence signal marking the nucleus (Figure 2.15). This indicates a high content of RNaseH1 in proximity to the DNA, where the targeted R-loops form. Although a fraction of expressed RNaseH1 was still located in the cytoplasm outside of the nucleus.

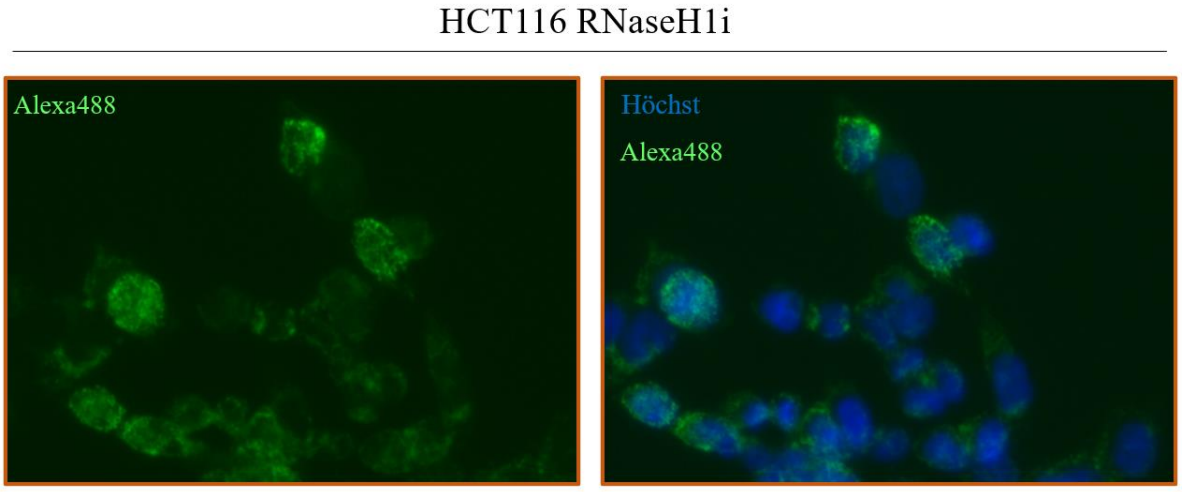

Figure 2.15: Nuclear localization of inducible RNaseH1 determined by fluorescence microscopy. *Fixation and staining of HCT116 cells with HA-tag specific antibody for RNaseH1 and Hoechst for nuclear staining after 24 h of incubation in doxycycline-containing medium (100 µg/ml).*

The cell line used in 2.3.1 showed a modest decline in cell growth of unknown reason (data not shown). To check whether the new inducible-RNaseH1 cell line shows change in growth rate when RNaseH1 is expressed, a growth curve experiment was performed. Over nine days, the cells were grown in just

glutamine containing medium (+Q), medium supplemented with doxycycline to induce RNaseH1 expression (+Q+Dox) and medium supplemented with hydroxytamoxifen (+Q+OHT) and counted every third day. The cells in +Q and +Q+Dox medium grew relatively constant and similar. The cells grown in +Q+OHT medium for a longer period of time showed a decreased growth rate (Figure 2.16). This decrease could be a result of high c-MYC levels which could not be regulated by the cell anymore due to the MYC-ER transgene. High and unregulated c-MYC levels are known to induce apoptosis in several cell types as a fail-safe mechanism (Adhikary, Eilers, 2005).

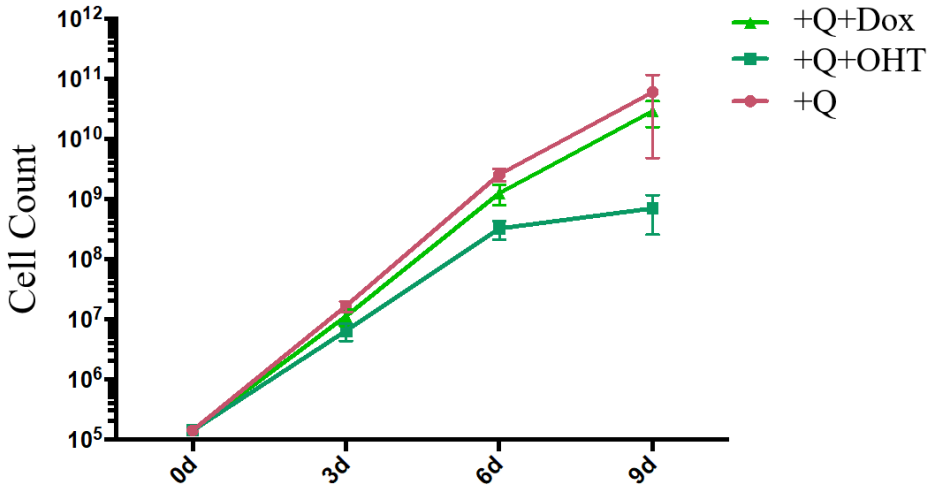

Figure 2.16: Growth curve of HCT116 cells infected with the MYC-ER system and inducible RNaseH1 showed no effect of RNaseH1 overexpression on cell growth. *3 cultures of HCT116 cells were grown in usual serum-containing growth medium, 3 in OHT-supplemented (100 nM) growth medium and 3 in doxycycline-containing (100 µg/ml) growth medium. After 3 and 6 days of growth the cells were counted and reseeded. The final cell harvest and cell counting was performed after 9 days of growth.*

The functionality of the RNaseH1 enzyme was tested via a DRIP-PCR again. 24 h before cell harvest, the growth medium was supplemented with doxycycline to induce RNaseH1 expression. Three cultures were harvested. One control cell line without RNaseH1 (EV -Dox) and two separate cultures of the RNaseH1 containing cell line cultivated with doxycycline (RNaseH1i +Dox) or without the supplement (RNaseH1i -Dox). The pull-down was performed with the S9.6 antibody against R-loops and with an unspecific IgG control antibody. The number of R-loops was determined via qPCR.

The cells grown in doxycycline supplemented medium showed a much weaker qPCR signal compared to the cells grown without doxycycline and the empty vector control cells. The qPCR was performed with primers targeting the first exon sequences of the genes *Transketolase* (*TKT*), *Nucleophosmin 1* (*NPM1*) and *Beta-Actin* (*ActB*), where the reduction of R-loops was reduced by 60-80%. In the *Nucleolin* gene (*NCL*) the reduction was even as high as 95% (Figure 2.17) compared to the control cells.

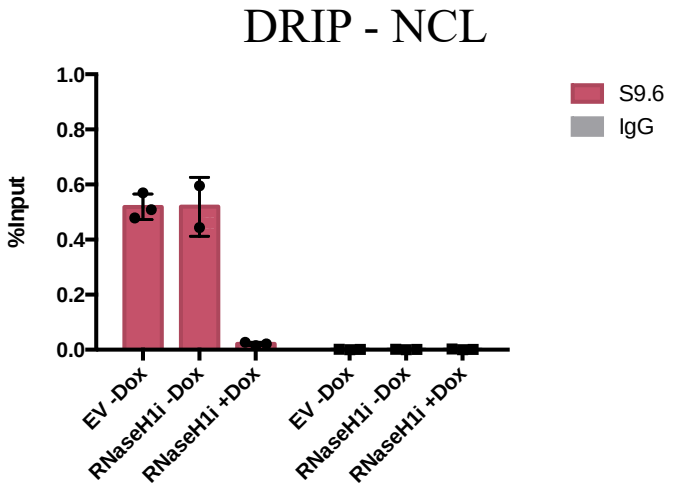

Figure 2.17: DRIP showed a strong decrease of R-loops after induced RNaseH1 overexpression. *After 24 h of incubation in doxycycline-containing medium (100 µg/ml) a DRIP was performed with R-loop specific S9.6 antibodies. A DNA digestion and RNA reverse transcription was performed, and the produced cDNA was used in a qPCR with primers for several c-MYC target genes. Representatively shown is the TSS region of NCL.*

The transport of the inducible RNaseH1 enzyme to the nucleus and the high R-loop degradation activity outperform the constitutively active variant of the transgene by far. Also, the cell growth was not impaired by the presence of the enzyme after doxycycline expression activation. In the following experiments this HCT116 with inducible RNaseH1 and MYC-ER system were used.

2.3.3 MYC-ER activation triggers increase of transcription while inducible RNaseH1 has no effect

To check whether the drop of R-loop formation was based on a decrease of overall transcription, the relative expression levels during RNaseH1 overexpression were analysed. The cultures were grown in in presence or absence of glutamine and with or without doxycycline for expression activation and hydroxytamoxifen for MYC-ER activation. After 24 h the RNA was extracted and converted into cDNA. The cDNA concentration of several genes was measured via qPCR.

The relative expression of each gene was normalized to a control group of cells grown in glutamine containing medium (Figure 2.18). The qPCR signals of cDNA from glutamine starved cells were reduced to about 50% of cDNA from the control cells, when the MYC-ER system was not activated. Glutamine starvation reduces the c-MYC protein levels significantly, which also impairs overall transcription activation (Dejure, Eilers, et al., 2017). This effect could be reduced by the addition of OHT to activate the MYC-ER system. This additional unregulated MYC protein increased relative

expression to 70-85% of control cell expression levels. The still significant drop of expression levels could be explained by the strong effect of glutamine deprivation on the cell metabolism. The lack of glutamine causes a lack of nucleotides and a halted cell cycle, which outdo the effect of MYC protein shortage (Polat, Cascante, et al., 2021). Activation of RNaseH1 overexpression showed no significant effect on overall expression levels during glutamine starvation. Also, activation of the MYC-ER system during RNaseH1 overexpression had no other effect on expression than MYC-ER activation alone.

The drop of R-loop signal in Figure 2.17 could not be explained by a reduced expression level after RNaseH1 overexpression. This strengthens the evidence that all further results are linked to the R-loop degrading activity of RNaseH1 overexpression.

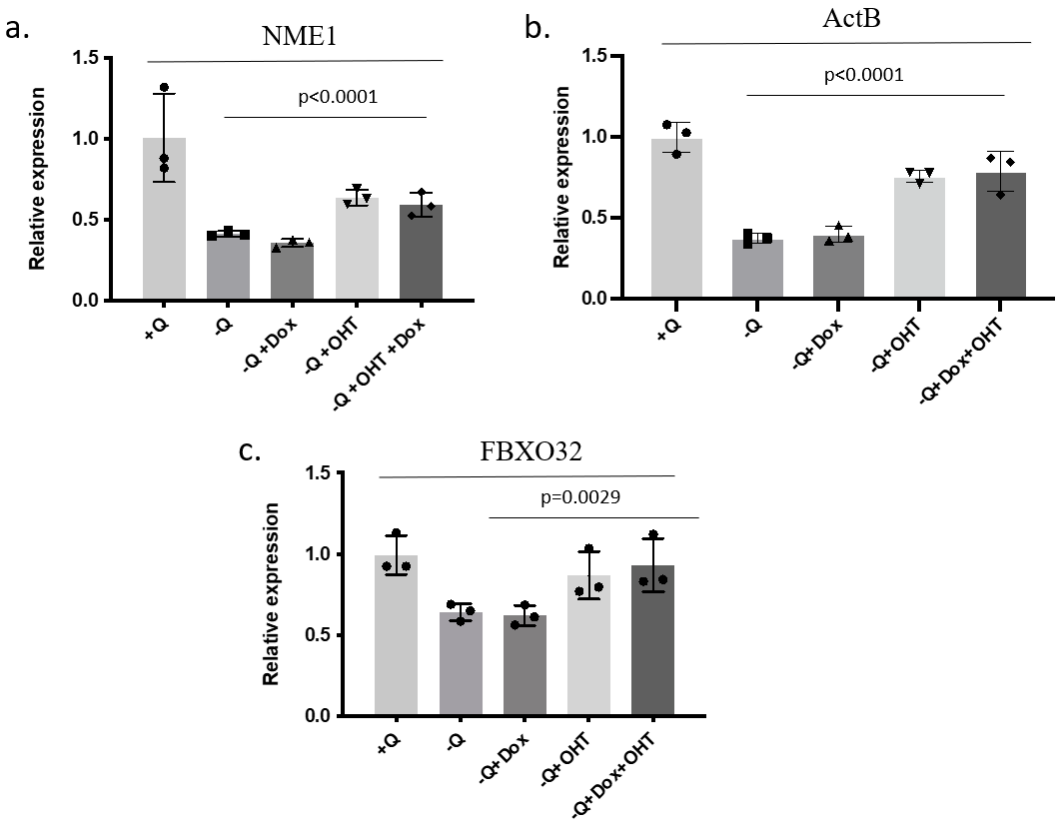

Figure 2.18: MYC-ER activation during glutamine starvation increased relative expression levels, while RNaseH1 overexpression shows no effect. *After 24 h of glutamine starvation (-Q), doxycycline supplementation (-Q+Dox), OHT supplementation (-Q+OHT), or incubation with both supplements (-Q+Dox+OHT) an RNA isolation and reversed transcription was performed from lysed HCT116 cells. The same primers for c-MYC target genes as for figure 4.17 were used in a qRT-PCR to determine relative gene expression. NME1 (a.), ActB (b.), and FBXO32 (c.) were shown as example genes. P-values were determined using a two-tailed Student's t-test.*

2.3.4 Creation of a catalytically inactive variant of inducible RNaseH1

An important negative control to most experiments to come was the creation of a catalytically inactive RNaseH1 (RNaseH1nf-HA). In Reyes, et al., 2015 a point mutation in the *RNaseH1* gene was introduced, which almost completely abolished the RNaseH1's R-loop degradation activity. This single amino acid exchange in the catalytically active region of the enzyme was introduced in our doxycycline dependent RNaseH1 overexpression system. The expression of the non-functional RNaseH1 (RNaseH1nf) could be detected via immunoblot against its HA-Tag (Figure 2.19).

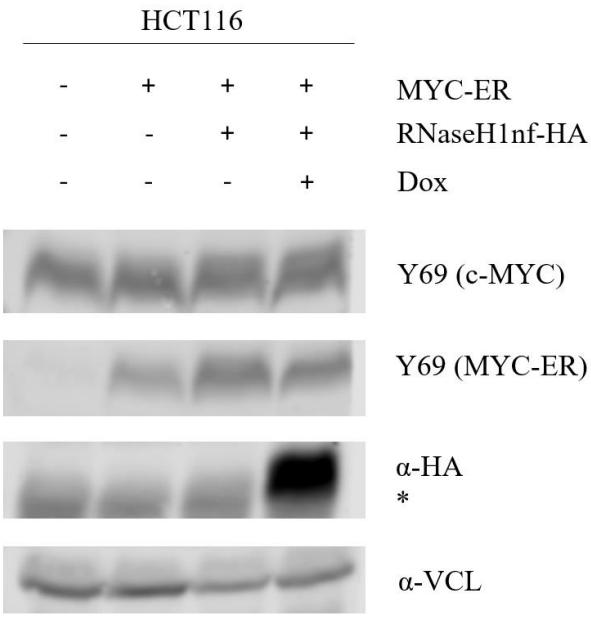

Figure 2.19: Expression control of HA-tagged catalytically inactive RNaseH1. *Inducible non-functional RNaseH1 expression was verified via HA-tag staining after isolation from HCT116 cells grown in doxycycline-containing medium (100 µg/ml).*

It was confirmed by DRIP-qPCR that indeed the R-loop degradation was impaired by the single mutation. The R-loop signal in the qPCR was only weakly reduced by RNaseH1nf overexpression (Figure 2.20).

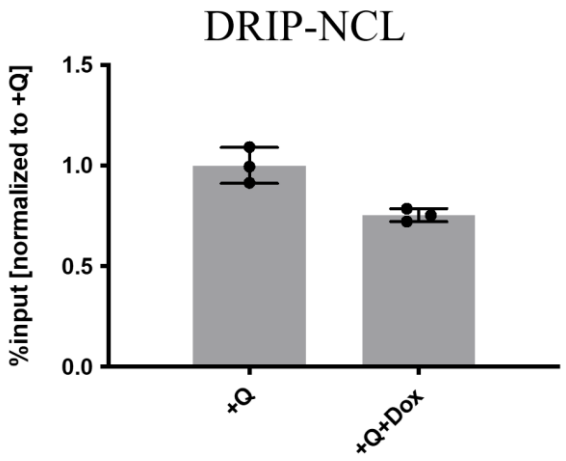

Figure 2.20: DRIP-qPCR showed only weak decrease of R-loops in cells expressing catalytically inactive RNaseH1. *After 24 h incubation of HCT116 cells with MYC-ER system and non-functional RNaseH1 overexpression system in doxycycline-containing medium (100 µg/ml) a DRIP was performed. The follow-up qPCR with the same primers as in 4.17 located in c-MYC target genes showed a slight decrease of R-loop levels in all tested genes. Representatively shown is the TSS region of NCL.*

This catalytically inactive RNaseH1 variant was used in a DRIP-sequencing experiment series to determine the main binding sites of RNaseH1. A localization of this enzyme could map main formation sites of R-loops throughout the genome. However, the sequencing experiments failed to produce reproducible results. As an alternative method, CUT&RUN profiling was performed for localization. But also, this sequencing experiment failed to produce reproducible results in two independent attempts.

2.3.5 AnnexinV/PI-FACS and Crystal violet staining indicate elevated apoptosis levels during RNaseH1 overexpression, glutamine starvation, and MYC-ER activation

It is described in several studies that MYC overexpression induces apoptosis in many cell types (Sutherland, et al., 2006; Phesse, et al., 2014) and in Dejure et al., this was also shown in colon carcinoma cells when starved for glutamine, which usually contain high levels of MYC protein. To check apoptosis rates in RNaseH1 overexpressing cells, an AnnexinV/PI-FACS experiment was performed thrice. Cells were grown in different media and harvested a few hours before measurement. The growth medium was also collected to include all dead and detached cells. All cells were stained with an antibody against Annexin V to mark cells in early apoptosis stages. Also, late apoptotic stages were stained using propidium iodide. The measurement was performed with the BD FACS Canto II device. The cells were sorted using forward and sideward scatter for cell size, a FITC (pacific blue) detector for Annexin V measurement and the PI-2A scanner for PI measurement.

HCT116 cells with inducible RNaseH1 and MYC-ER were grown in eight different conditions. One control condition was grown in glutamine medium without any supplements (+Q-OHT-Dox). This culture showed overall apoptosis rates of about 7%. This can be considered as the natural apoptosis rate of this cell culture (Figure 2.21). In the same culture supplemented with doxycycline to trigger the expression of RNaseH1 the same percentage of apoptotic cells could be measured. Expression of RNaseH1 alone had no effect on the apoptosis rate. When cells grown in glutamine abundance were supplemented with OHT to activate the MYC-ER system (+Q+OHT) no change in apoptosis rate was observed. Also, when these cells were additionally supplemented with doxycycline to trigger RNaseH1 expression (+Q+OHT+Dox), the viability of the HCT116 cells was not affected.

However, glutamine starvation had grave effects on cell viability. The apoptosis rate of cells grown in absence of glutamine was about twice as high as the natural apoptosis rate at about 15-20% apoptotic cells, even without any supplements (-Q-OHT-Dox). Also, RNaseH1 overexpression (-Q+Dox) showed no effect on viability during glutamine starvation. In Dejure et al., 2017, it was described that glutamine starvation and MYC-ER activation together dramatically increase the apoptosis rate in colon carcinoma cells. In contrast, these results could not be reproduced with the used cell lines (-Q-Dox+OHT). The apoptosis rate was at about 15% as it was in cultures grown without OHT. The combination of MYC-ER activation and RNaseH1 overexpression, however, had strong effects on cell viability. This treatment increased the proportion of apoptotic cells to 30-40% after 24 h of treatment.

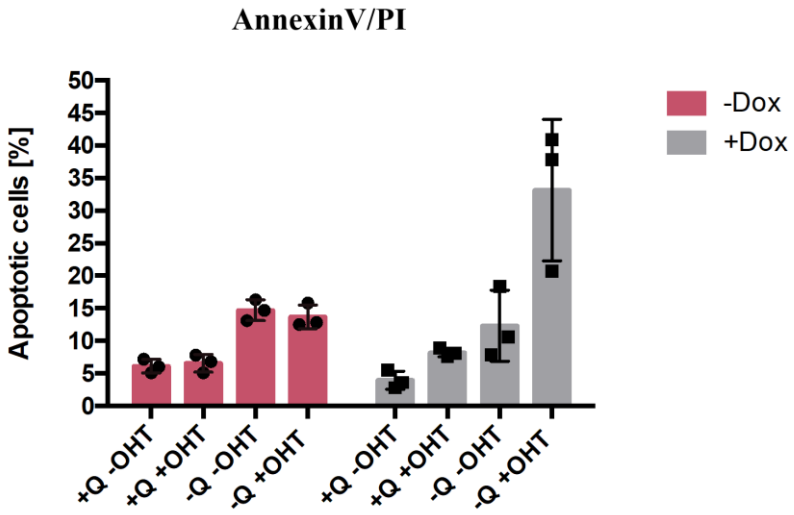

Figure 2.21: AnnexinV/PI-Assay showed strongly increased apoptosis rates in glutamine starved cells with MYC-ER activation and RNaseH1 overexpression. *HCT116 cells were grown for 24 h in growth medium. The medium was changed to glutamine deprived medium (-Q) containing OHT for MYC-ER activation (+OHT) or doxycycline for RNaseH1 overexpression (+Dox). After further 24 h the cells were harvested and stained with an Annexin V fluorescence antibody and propidium iodide. The cells were analysed with the fluorescence activated cell sorting system (FACS) FACS Canto from BD Biosciences.*

This effect could also be confirmed by a crystal violet assay (Figure 2.22). HCT116 cells (WT) and the modified HCT116 cells with the MYC-ER system and inducible RNaseH1 overexpression were grown for 72 h on 6-well plates until the cells were at about 60% confluency. The media were changed to the before described supplemented media for specific treatment. The cells were harvested, fixed and stained after 48 h of treatment. Each well was treated uniquely and had full confluency after staining. Only the modified HCT116 cells, which were treated with glutamine deprived medium supplemented with OHT and doxycycline showed non-confluent growth after the treatment. This indicated a high apoptosis rate under these conditions and supported the results from the AnnexinV/PI assay.

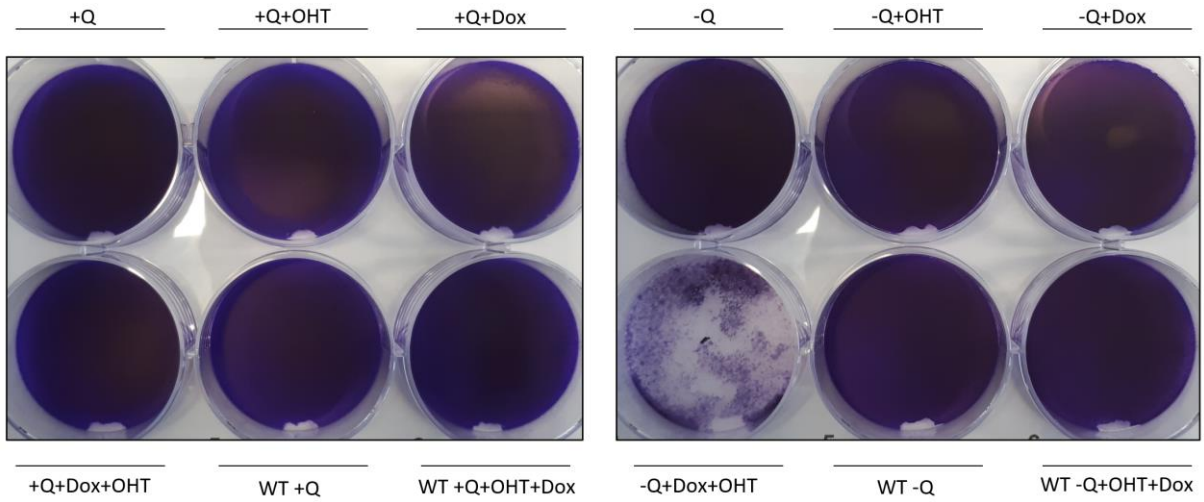

Figure 2.22: Increased apoptosis rates of glutamine starved cells with MYC-ER activation (OHT) and RNaseH1 overexpression (Dox) could also be shown by crystal violet assay. *Cells were grown for 24 h in a 6-well plate and incubated in indicated medium for 24 h before fixation and staining. WT indicates control cell cultures without incorporation of the MYC-ER and the RNaseH1 system.*

To confirm that this drastic decline in cell viability was linked specifically to the R-loop degrading activity of the overexpressed RNaseH1, a second AnnexinV/PI assay was performed with the cells containing the non-functional RNaseH1 mutant (Figure 2.23). The natural apoptosis rates of this cell line were slightly higher than the cell line used before. But most importantly, the strong increase of apoptosis during glutamine starvation could not be observed. Instead, the apoptosis rate was approximately at the same level as glutamine starved cells with MYC-ER activation alone, at about twice the natural apoptosis rate of this cell line.

This second experiment confirmed that the decrease in cell viability was in fact caused by the R-loop degradation activity of the overexpressed RNaseH1.

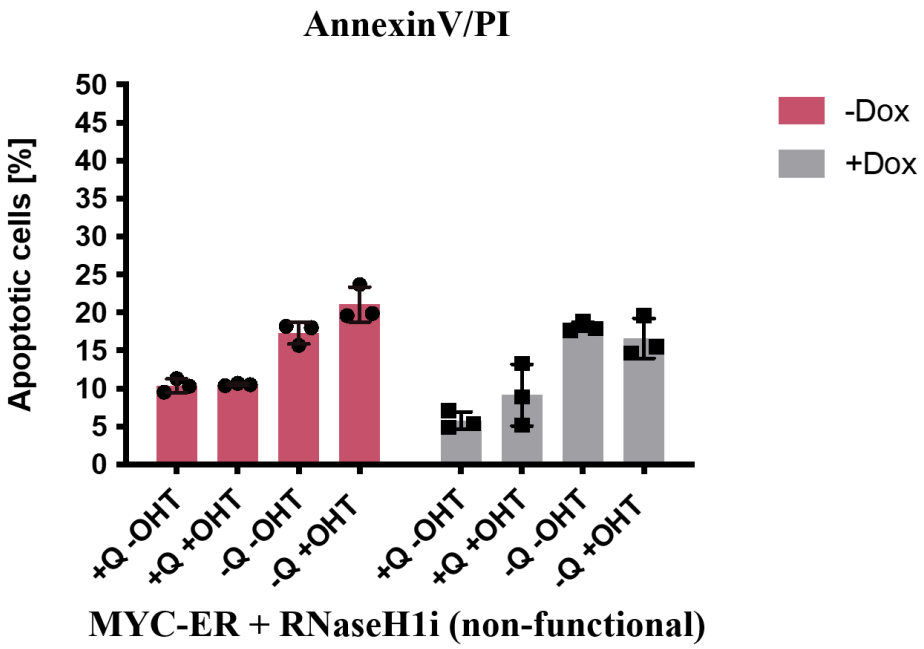

Figure 2.23: AnnexinV/PI assay of cells infected with a catalytically inactive RNaseH1 showed no increased apoptosis rates after glutamine starvation, MYC-ER activation and non-functional RNaseH1 overexpression. *HCT116 cells were grown for 24 h in growth medium. The medium was changed to glutamine deprived medium (-Q) containing OHT for MYC-ER activation (+OHT) or doxycycline for non-functional RNaseH1 overexpression (+Dox). After further 24 h the cells were harvested and stained with an Annexin V fluorescence antibody and propidium iodide. The cells were analysed with the fluorescence activated cell sorting system (FACS) FACS Canto from BD Biosciences.*

2.4 RNaseH1-dependent apoptosis was not induced by unregulated cell cycle progression during glutamine starvation

One possible explanation for the increased apoptosis rate could be the link between cell cycle progression and glutamine starvation. c-MYC is known to promote cell cycle progression by activation of cyclins and CDKs, and by inactivation of cell cycle inhibitors like p15 and p21 (Garcia-Gutierrez, et al., 2019). Furthermore, c-MYC promotes nucleotide synthesis and DNA replication by inducing expression of linked genes (Dejure, Eilers, et al., 2017). Since c-MYC protein levels are strongly decreased during glutamine starvation, the cell cycle progression should be halted in the G1-phase of the cell cycle.

A BrdU-PI-FACS experiment was performed to investigate the effect of glutamine starvation, MYC-ER activation and RNaseH1 overexpression on the cell cycle. The synthetic thymidine analogue bromodeoxyuridine (BrdU) was added to the growth medium of proliferating cells. These cells incorporate the BrdU during DNA replication. The BrdU can be detected using specific antibodies in a

FACS analysis. Propidium iodide (PI) was used to stain DNA to determine the overall amount and hence the stage of cell cycle.

When comparing cells grown in glutamine abundance with glutamine starved cells, the -Q cells showed fewer cells with high PI signal (Figure 2.24, blue square). These cells had already undergone DNA synthesis and were halted in G2/M phase ready for mitosis. Also, the BrdU signal was lower in -Q condition. The lack of cells with high PI and BrdU signals indicate a cell cycle arrest in the G1 phase before replication start.

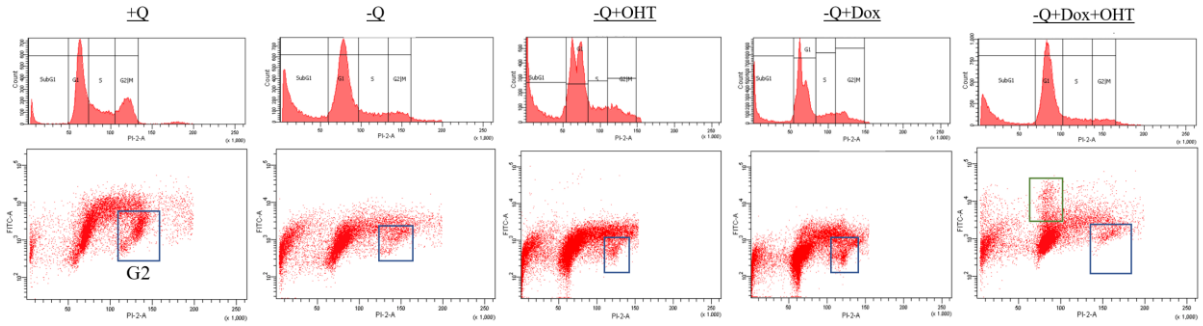

Figure 2.24: BrdU-PI-FACS showed cell cycle arrest of glutamine starved cells which continues even after MYC-ER activation and RNaseH1 overexpression. *HCT116 cells were grown for 24 h in usual growth medium (+Q), glutamine deprived medium (-Q) or glutamine deprived medium supplemented with OHT (100 nM) and Doxycycline (100 µg/ml). The media were supplemented with BrdU 1 h before measurement. The cells were stained with PI 5 min before FACS. Cells currently in G2 phase were indicated by the blue square. The green square indicates cells with high BrdU, but low PI signal.*

When treating the cells with OHT and doxycycline during glutamine starvation to activate MYC-ER and express RNaseH1, the pattern of the FACS analysis resembled the distribution of the -Q cells. This ruled out a grave effect of c-MYC and degradation of R-loops on the cell cycle during glutamine starvation. However, a small fraction of cells (Figure 2.24, green square) shows a high BrdU signal and low PI signal. In comparison with the glutamine starved cells without any supplements, the number of BrdU-positive cells was doubled. While 4-8% of the -Q cells were BrdU-positive, 10-15% of -Q+OHT+Dox cells were BrdU-positive (Figure 2.25). These are cells with low DNA content in the G1 phase, that incorporated BrdU. So, it is possible that a small fraction of cells was able to undergo mitosis even during glutamine starvation.

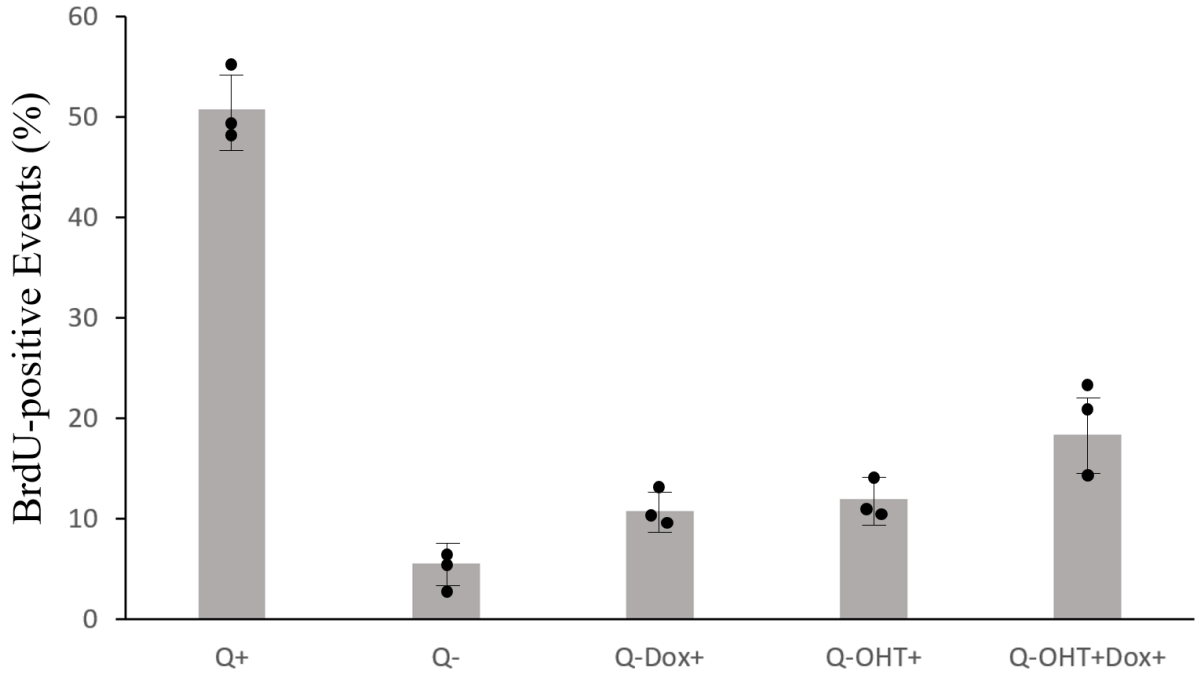

Figure 2.25: Quantification of BrdU-positive cells in G1-phase. *Glutamine starved cells with activated MYC-ER and RNaseH1 overexpression showed an increased number of BrdU-positive cells compared to just glutamine starved cells. HCT116 cells were starved for 24 h and supplemented with 100 nM OHT and 100 µg/ml doxycycline.*

2.5 Apoptosis during glutamine starvation is not induced by DNA damage response mechanisms

Glutamine starvation and MYC overexpression are both known factors to introduce DNA damage. As a combination of harmful effects glutamine starvation can stall RNA polymerase II while MYC-ER activation triggers RNA polymerase accumulation in many genes (Dejure, Eilers, et al., 2017). This transcriptional stress promotes the formation of R-loops in these genes, which in turn are a hotspot for DNA damage. To check, whether the high apoptosis rates in glutamine starved, MYC-ER activated and RNaseH1 overexpressing cells are linked to DNA damage immunofluorescence staining of DNA damage markers pKAP1 and gamma-H2AX were performed. Cells grown under different conditions were fixed and stained and analysed via Operetta high throughput microscopy.

As a positive control for DNA damage cells were treated with etoposide prior to fixation (+Q+Eto). Etoposide targets the DNA topoisomerase II activity and induces double strand breaks by inhibiting the DNA re-ligation after introducing double strand breaks for resolving DNA entanglements (Montecucco, et al., 2015). Single stranded DNA and double strand breaks trigger a DNA damage response cascade, which lead to the accumulation of gamma-H2AX at the damage site. This cascade involves the activation of the protein kinase ATM, which can phosphorylate the DNA repair protein KAP1 to pKAP1 (White, et al., 2012).

The cells treated with etoposide showed high fluorescence signals, when stained with antibodies specific for pKAP1 (about 60% positive cells) or gamma-H2AX (about 90% positive cells). The thresholds for positive cells were chosen considering the background by unstained control cultures and 95% of cells grown in non-supplemented glutamine-rich medium (Figure 2.26). Glutamine starved cells regardless of supplements showed a significantly higher fluorescence signal than cells grown in presence of glutamine. Since glutamine plays an important role in DNA repair (Hwang, Hong, et al., 2021), the lack of it results in increased DNA damage response protein recruitment. About 20-50% of glutamine starved cells were pKAP1 positive, while 10-20% were positive for gamma-H2AX. The cultures grown in absence of glutamine and presence of doxycycline and 4-hydroxytamoxifen showed fluorescence signals for the two DNA damage markers in the same level as cells with each supplement alone or with just glutamine starvation. Thus, DNA damage cannot be the sole cause of the high apoptosis rates during glutamine starvation, MYC-ER activation and RNaseH1 overexpression.

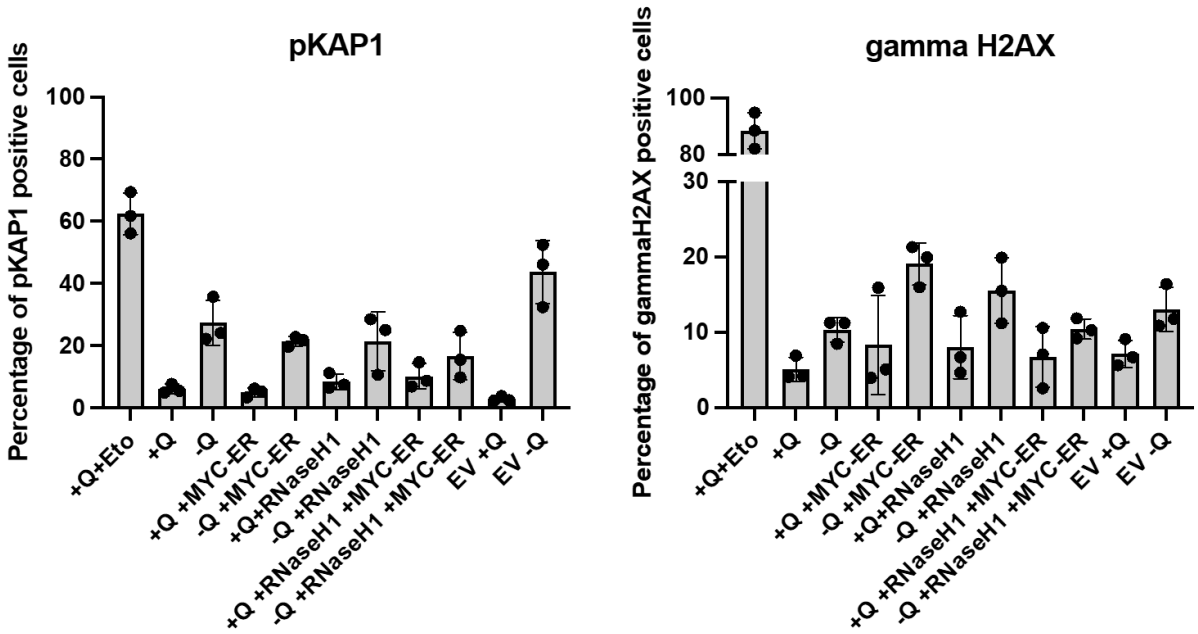

Figure 2.26: Combination of glutamine starvation, MYC-ER activation, and RNaseH1 overexpression had no effect on concentration of the DNA damage indicators pKAP1 and gamma H2AX. *HCT116 cells with MYC-ER system and inducible RNaseH1 overexpression and EV cells were grown in 96-well plates for 24 h. The media were exchanged to the indicated activation media for another 24 h before fixation and staining. Specific antibodies against pKAP1 and gamma H2AX were used, and detection was performed by the Operetta high-throughput microscopy system. Etoposide was added to one culture 2 h prior to fixation as a positive control as it induces DNA damage.*

2.6 Ribonucleotide di- and triphosphates are reduced during glutamine starvation with MYC-ER activation and RNaseH1 overexpression

Another possible cause of increased apoptosis rates in glutamine starved cells with RNaseH1 overexpression and MYC-ER activation was a deprived level of nucleotides since the nucleotide metabolism is linked tightly to the availability of glutamine. It acts not only as an energy source for the cell, but instead is the main nitrogen donor for the *de novo* synthesis of purine nucleobases via the 5-phosphoribosyl-1-pyrophosphate (PRPP) amidotransferase enzyme (Cory, et al., 2006). High levels of nucleotides act as pro survival factors for stressed cells since they inhibit the formation of the cytochrome c-initiated apoptosome and the activation of the apoptotic pathway protein caspase-9 (Chandra, et al., 2006).

First, we checked for overall nucleotide levels contained in cells under optimal growth conditions, cells grown in glutamine deprived conditions, and each of those conditions with additional doxycycline and OHT for RNaseH1 overexpression and MYC-ER activation (Figure 2.27). The mass spectrometric results were normalized to the overall nucleotide levels of the +Q condition. Cells starved for glutamine showed a 2.6-fold increase of nucleotide levels. Cells treated with Dox and OHT showed a similar pattern regarding the nucleotide levels. This indicates that RNaseH1 overexpression and MYC-ER activation have no effect on overall nucleotide concentration.

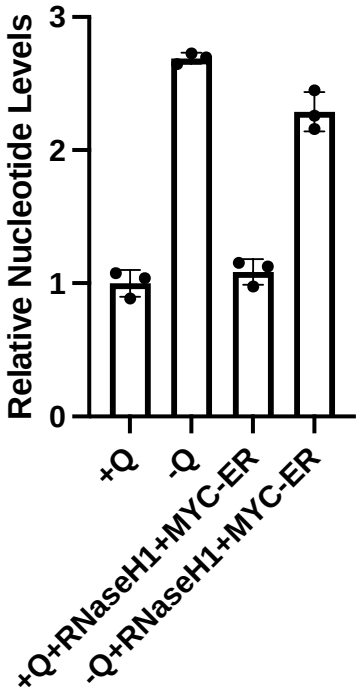

Figure 2.27: Glutamine starvation increased relative nucleotide levels. *HCT116 cells were cultivated for 24 h in media with glutamine (+Q), without glutamine (-Q), or supplemented with OHT (100 nM) and doxycycline (100 µg/ml) for MYC-ER activation and RNaseH1 overexpression (+RNaseH1+MYC-ER). The cell lysates were analysed via mass spectrometric measurement regarding the overall number of nucleotides. The graphs were integrated to calculate absolute numbers, which were then normalized to the +Q measurement for easier comparison.*

Next, the mono-, di- and triphosphates of each nucleotide under the specific growth conditions were analysed. The nucleotide levels were normalized to the glutamine rich conditions (+Q and +Q+MYC+RNaseH1) again (Figure 4.28). Uridinemonophosphate (UMP) showed the highest concentrations during glutamine deprivation at 2.4-fold increased levels without MYC-ER activation and RNaseH1 overexpression (-Q) and a 3-fold increase in the presence of doxycycline and OHT (-Q+MYC+RNaseH1). Uridinediphosphate (UDP) and Uridinetriphosphate (UTP) were 4-fold increased in -Q condition, while in the -Q+MYC+RNaseH1 condition the UDP level was only about 2-fold increased compared to the -Q+MYC+RNaseH1 condition and the UTP levels were even lower than in the respective glutamine containing condition.

Similar results could be observed for the other nucleotides AXP, CXP and GXP. While Adenosinediphosphate (ADP) and Adenosinetriphosphate (ATP) were only mildly increased during -Q condition compared to the Adenosinemonophosphate (AMP) levels, CXP and GXP showed almost identical patterns. Overall, the levels of di- and triphosphorylated nucleotides were decreased in the -Q+MYC+RNaseH1 condition compared to the respective monophosphorylated nucleotides. The strongest effect could be observed when comparing the ATP level in presence and absence of glutamine. The ATP level during glutamine deprivation, MYC-ER activation and RNaseH1 overexpression was decreased to about 50% ATP levels in similar conditions in presence of glutamine. Whereas the cells in -Q conditions without further supplements also show increased ATP levels. The decrease of NTP levels could be linked to the energy consuming process of apoptosis. As already shown, cells grown in absence of glutamine and with MYC-ER activation and RNaseH1 overexpression tend to undergo apoptosis in an increased ratio. Since apoptosis is an energy dependent cell death and the tumour cells lack the energy gained from glutamine uptake, the excess ATP could be used up in the process of apoptosis. This contrasts with the quiescent cells grown in absence of glutamine, doxycycline and OHT. These dormant cells seem to be able to maintain a high concentration of nucleotides possibly through salvage pathways and a strongly decreased protein biosynthesis caused by low c-MYC levels.

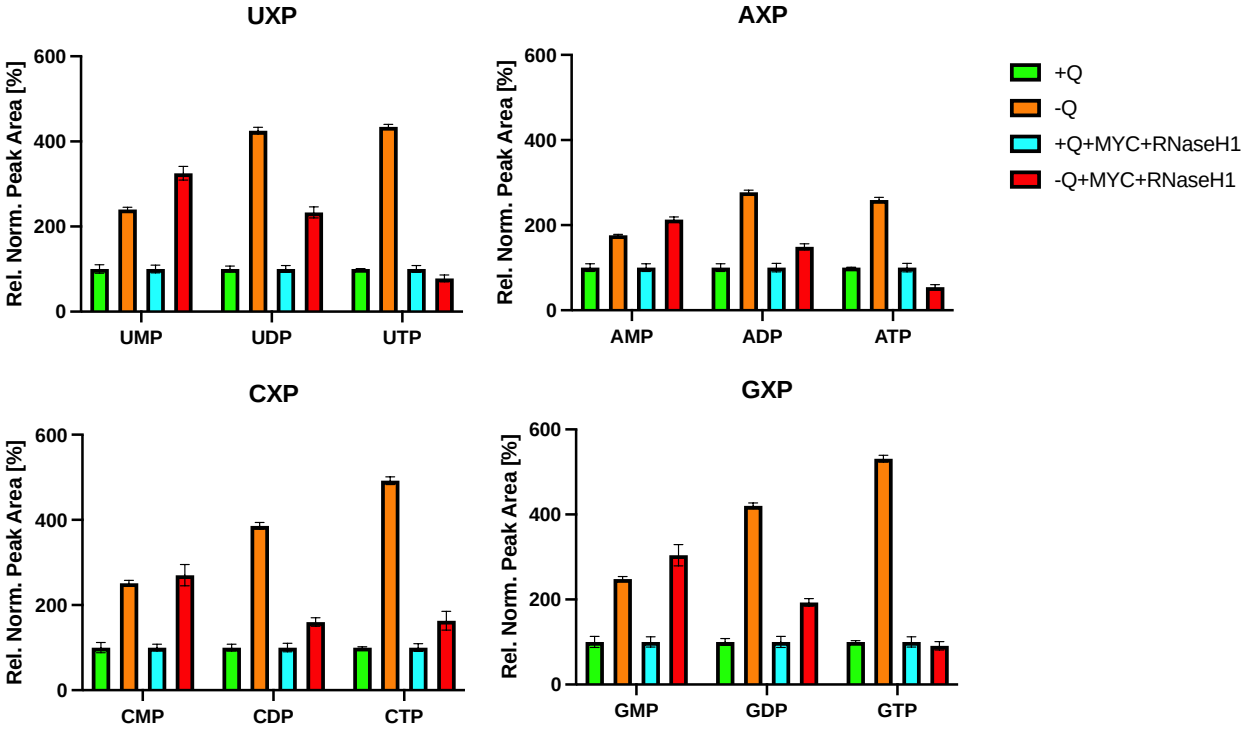

Figure 2.28: NDPs and NTPs increased during glutamine starvation but decreased with additional MYC-ER activation and RNaseH1 overexpression. *HCT116 cells were cultivated in corresponding media for 12 h prior to harvest. Mass spectrometric analysis shows the distribution of UXP, AXP, CXP, and GXP normalized to the normalized peak area of the +Q condition. 3 independent measurements are shown in this figure.*

3 Discussion

Since c-MYC expression is deregulated in many forms of cancer, especially in most colon carcinomas c-MYC would present a valuable target of cancer treatment. Unfortunately, the direct targeting of the global expression factor is difficult due to its protein structure. Although several targeting compounds could be created so far, indirect targeting remains a viable strategy to target c-MYC in cancer cells (Llombart, et al., 2021). In this study we could identify KPNB and HSPE1 as possible indirect targets to control c-MYC expression on translational level. Further studies are necessary to validate the effect of the knockdown of these two proteins in larger scale. Depleting colon carcinoma cells of RNA-Polymerase subunits also induces effects on c-MYC translation. This could have been evoked by deregulation of transcription activity and nucleotide availability.

Furthermore, we could show an effect of R-loop depletion by *in vivo* degradation with a biotechnical engineered RNaseH1-protein in glutamine starved, c-MYC overexpressing colon carcinoma cells. The absence of R-loops and glutamine combined with the presence of c-MYC increases apoptosis rates in these cells. Since Dejure et al. showed that glutamine starved colon carcinoma cells are susceptible to c-MYC overexpression, this result paves the way for further targeting glutamine dependent survival pathways in cancer cells. We could identify the transcription pathways of mitochondrial genes as critical in combination with R-loop degradation, but further results are needed for clarification and verification.

3.1 Identification of proteins with influence on c-MYC regulation

Our two-way screening approach with an *in vitro* RNA-protein interaction screening performed by the group of Stefan Kempa in Berlin and an *in vivo* knockdown screening by small interfering RNAs (siRNA) represented a viable method of interaction detection. In the first step, our partner lab could identify 70 proteins which interact with the 3'-UTR of c-MYC in either presence or absence of glutamine or both. This narrowed the number of potentially essential proteins for translation regulation down to a manageable number for an siRNA screening. In this screening we could identify all protein knockdowns with a significant effect on c-MYC translation via immunostaining and high-throughput microscopy.

3.1.1 Knockdown of RNA-Polymerase subunits deregulates c-MYC expression

Knockdown of different RNA-Polymerase subunits showed a strong effect on c-MYC protein levels in colon carcinoma cells. The most significant siRNA knockdowns in this group were shown by siRNAs against Polymerase III subunit A protein (POLR3A) and Polymerase II, I and III subunit L (POLR2L).

Since both proteins are part of the enzymatic centre of the functional RNA-Polymerases, an RNA binding activity shown in the *in vitro* pulldown was unsurprising. siRNAs against Polymerase subunit proteins showed an increase of relative c-MYC protein levels during glutamine starvation and an even stronger increase during recovery after glutamine starvation (Figure 2.4). This indicated a presumably indirect effect on c-MYC translation due to the spatial separation of the Polymerase and the translatable mRNA.

The function of RNA-Polymerase III includes the synthesis of tRNAs necessary for protein translation (Lata, et al., 2021). An inhibition of this function by knocking down the essential POLR3A could increase nucleotide availability by reducing the demand for them. Since high adenosine concentrations in the cell trigger c-MYC translation (Dejure, Eilers, et al., 2017), the missing Polymerase activity could explain the high c-MYC protein levels during glutamine starvation (Figure 2.4). Also, the inhibition of transcription generally by Polymerase protein knockdowns could affect the overall nucleotide or adenosine levels.

These indirect translation deregulations are most likely due to the fact, that Polymerase knockdowns have severe side effects on the whole cell metabolism by transcription inhibition. A specific c-MYC translation regulation mechanism is very unlikely linked to Polymerase subunits.

3.1.2 Knockdown of KPNB and HSPE1 reduces effect of glutamine starvation on c-MYC expression

In colon carcinoma cells a glutamine starvation for about 12 hours causes a c-MYC protein depletion to about half the physiological conditions (Figure 2.2). Addition of glutamine after starvation replenishes the c-MYC levels in less than 2 hours. This recovery is too rapid to be the result of a transcription activation after glutamine re-addition since activation and expression of c-MYC would take more time to produce a visible effect. Instead, the cells keep high levels of *c-MYC* mRNA during starvation to quickly synthesize the protein as soon as glutamine is available again. Furthermore, it is known that especially the presence of adenosine restores c-MYC translation through direct or indirect interaction with the 3'-UTR of *c-MYC* mRNA. In this siRNA-screening we looked for proteins which have one of the following effects on this regulation mechanism: If cells with a specific protein knocked out was unable to replenish c-MYC protein levels during the recovery phase after glutamine starvation, this protein influenced mRNA-stability and prevents mRNA degradation. On the other hand, if there was a protein knockdown, which prevents c-MYC protein levels to drop during glutamine starvation, the depleted protein might display the interaction partner of the *c-MYC* mRNA 3'-UTR to keep up the translation activity.

In this screening the knockdown of the proteins KPNB and HSPE1 strongly reduced the fluorescence signal of the c-MYC antibodies and hence indicated a depletion of c-MYC protein. Knockdown of Karyopherin/Importin Subunit Beta 1 (KPNB) reduced the effect of glutamine starvation on c-MYC protein levels significantly. The protein levels were reduced to 75% of the physiological levels without KPNB, in contrast to the usual reduction to about 40% without knockdown (Figure 2.3). KPNB is involved in the nuclear protein import, as it is part of the NLS import receptor. This receptor recognizes the nuclear localization signal (NLS) of proteins, which are destined for the active transport into the nucleus (Görlich, Kutay, 1999). KPNB is also linked to the translation pathway, since it is responsible for the import of SRP19 and several other ribosomal subunits into the nucleus, where they are assembled into the fully functional enzymes (Dean, et al., 2001). The activity of KPNB is also strongly dependent on the availability of nucleoside triphosphates (Rout, et al., 1997), which are abundant during glutamine starvation (Figure 2.28). A direct involvement in translation has not been described yet. It is also unknown how or why the protein can bind mRNA. Hence, it is unlikely that KPNB has a direct effect on c-MYC translation. Since KPNB is linked to several critical pathways, it can be assumed that the observed effect on the c-MYC protein levels was caused indirectly. For a more detailed analysis a cell culture could be depleted for KPNB for longer, to check its influence on cell cycle and proliferation. Since c-MYC is more abundant during glutamine starvation upon KPNB knockdown, an effect on cell survivability during starvation or mitosis rate might be observed.

HSPE1 knockdown also had a strong effect on c-MYC protein regulation. During glutamine starvation and HSPE1 knockdown the c-MYC levels dropped only non-significantly (Figure 2.3). The Heat Shock Protein Family E Member 1 (HSPE1) functions mainly as a chaperonin. It enhances ATP-dependent protein folding and is involved in mitochondrial protein import (Levy-Rimler, et al., 2001). HSPE1 is only loosely classified as a cancer-related gene. Its expression is slightly upregulated in colon carcinoma, but without any prognostic relevance (https://www.proteinatlas.org). A link between c-MYC and HSPE1 proteins was not described in literature yet, but the *HSPE1*-gene is a c-MYC target gene. So, transcription of HSPE1 is dependent on c-MYC activity (Stojanova, et al., 2016). HSPE1 as a stress-related protein represents the most probable candidate for a direct involvement in c-MYC translation regulation of all tested proteins. Although no such activity was described for HSPE1 yet, its involvement in several stress-related pathways could hint for a connection. Glutamine starvation imposes a major stress condition for colon carcinoma cells. The fact of a mitochondrial stress-related protein binding to the 3'-UTR of mRNA in the cytoplasm is not trivial. Further insight into the mechanism and the exact conditions of binding is needed to verify an involvement of HSPE1 in c-MYC translation regulation mechanisms.

3.1.3 Implication of further in vivo testing of identified proteins

In the list of *c-MYC* 3'-UTR binding proteins identified in *in vitro* experiments were 78 candidates for an interaction with c-MYC translation regulation pathways during glutamine starvation. Knockdown of 71 of these proteins via siRNA screening showed no effect on c-MYC protein levels during glutamine starvation and recovery phase after starvation. Several of these proteins were the most probable candidates for involvement in translational pathways, like EIF6 or ribosomal proteins RPL15, RPL19 and RPL30. Since the exact concentrations of c-MYC protein could not be measured in this scale, an overall deregulation of translation by knockdown of any of these proteins could disguise any specific effect on c-MYC translation. Increasing comparability of the protein levels under each of these specific conditions could strengthen the results of this screening, even regarding the remaining 7 proteins with an effect on c-MYC levels. These proteins (RNA-polymerase subunits, HSPE1 and KPNB) have rather weak connections to translation regulation or mRNA stability. But still, their observed effect on c-MYC protein levels during glutamine starvation were solid evidence for a transcription deregulation under these stress conditions.

This large-scale screening for protein candidates involved in c-MYC regulation could be a first step for in depth analysing of interaction and spatial proximity with this reduced number of candidates. Since other candidates like mTOR and eIF4E were already investigated and ruled out regarding their influence on c-MYC translation (Dejure, Eilers, et al. 2017), the possible pathway is narrowed down enough for future closer investigation of possibly essential interaction proteins.

3.2 RNA-Protein Interaction Detection Assay (RaPID-Assay) was unsuitable for detection of 3'-UTR interaction partners

The RNA-Protein Interaction Detection Assay is a promising new method created by Ramanathan et al. in 2017. This *in vivo* Assay uses a modified biotin ligase enzyme to biotinylate RNA-binding proteins in proximity of a marker secondary RNA structure. The RNA motif of interest is cloned between RNA sequences, which form BoxB stem loops in physiological conditions. The λN targeting structure of the modified biotin ligase binds to the BoxB stem loops close to the RNA motif of interest and labels proteins binding to this motif. Those labelled proteins can be pulled down via streptavidin capture and detected via Western blot or mass spectrometry (Ramanathan, et al., 2018).

The advantage of this assay in comparison to *in vitro* interaction detection methods lies in its high specificity of the detection. RNA binding proteins can be labelled under physiological conditions, which allows direct investigation of RNA-protein interaction without external influence like in *in vitro* experiments. Furthermore, a high flexibility during altered expression systems allows easy adaptation to different physiological conditions while maintaining the high specificity. This interaction detection assay represents an additional method to the afore mentioned *in vitro* pulldown assay to detect protein

interaction partners of the 3'-UTR of *c-MYC* mRNA. The aim was to find overlaps between the protein list from Stefan Kempa's group in table 4.1 and this *in vivo* RaPID-Assay.

To establish this new method, the U1 spliceosomal snRNA was chosen for a first analysis. The U1 snRNA is part of the RNA spliceosome and interacts directly with smB, a part of the Sm-ring, which forms the core unit of the RNA spliceosome (Nagai, et al, 2001). The *U1*-gene modified with the BoxB-sequence was transfected into colon carcinoma cells also expressing the modified biotin ligase enzyme. Since it was impossible to verify the expression of the modified U1 snRNA by qPCR with primers for the BoxB-stem loops due to its structure, an indirect detection was necessary. The engineered cell line was cultivated under the same condition as a control cell without the modified U1-RNA and the biotin ligase. Both cell lines were prepared side by side for qPCR with primers for the U1-RNA motif. In the qPCR an approximately 4-fold increase of fluorescence signal was detected in the samples prepared from modified cell culture (Figure 2.6). This indirect detection method is not ideal, as it is not guaranteed that the measured U1-RNA contains the BoxB-stem loops necessary for biotin ligase binding, but the significant increase of U1-RNA signal indicates a functional expression system.

This setup was established for the two colon carcinoma cell lines HCT116 and LS174. Both cell lines were used to perform the full protocol of the RaPID-Assay (5.12.4). The Western blot detection was performed with an antibody against the smB-protein binding directly to the U1-RNA. In the cell lines without biotin containing medium, only a weak signal of smB could be detected after the biotin-dependent pulldown. In contrast, the smB-signal of cells grown in biotin containing medium was much stronger in the Western blot (Figure 2.9). This indicates a highly specific detection of biotin-labelled proteins with only a weak leakage in the streptavidin pulldown. This leakage could impose a strong background if the detection method were changed to a mass spectrometric analysis of pulled down proteins.

After establishing the assay, RaPID should be used to detect interaction partners of *c-MYC* mRNAs 3'-UTR. Three different constructs were created containing the BoxB-stem loops and different parts of the 3'-UTR. The first sequence contained the whole UTR, the second was shortened to contain only the first two AU-rich elements of the UTR and the third was shortest and contained only the first AU-rich element. Cells infected with the transgene for the whole 3'-UTR flanked by the BoxB stem loops were cultivated as in the U1-test before. Analysis by western blot with antibodies against ARE-binding proteins like Human antigen R (HuR, Szostak, et al., 2013) and a more general Coomassie staining showed no protein staining after streptavidin pulldown (data not shown). One possible explanation is the spatial distance between the BoxB stem loops and possible protein binding sites at the 3'-UTR. The biotin ligase enzyme biotinylates only proteins in close proximity. But also, the two smaller constructs of c-MYC 3'-UTR showed the same negative result in protein detection assays. Possibly the quantity of pulled down proteins was too low to be detected via Coomassie staining. A more sensitive detection

method like a liquid chromatography would be a promising next step to test this method further in this expression system since this method proved practical in other studies (Verma, et al., 2021).

Further investigation of 3'-binding proteins is key to understand the pathway to control c-MYC translation and translation regulation during glutamine starvation. The AREs represent a valuable target for enhanced protein interaction examination. These regions play an important role in mRNA stability and degradation mechanisms (Chen, Shyu, 1995). These mechanisms include rapid mRNA turnover rates by c-*jun* proteins or by c-*fos* ARE-mediated mRNA decay. The latter can be inhibited by binding of HuR-proteins to the AREs to block RNA degradation (Peng, et al., 1998). The high stability of *c-MYC* mRNA combined with the low translation rates during glutamine starvation suggests a more complex form of regulation than ARE-mediated mRNA regulation all alone. Further protein interactions sites could induce a very complex interplay of different regulation mechanisms to cause the mRNA conservation and sustain the quick reestablishment of c-MYC translation after glutamine starvation.

3.3 R-loop depletion during glutamine starvation increases apoptosis in colon carcinoma cells

3.3.1 R-loop formation and its role in cancer proliferation and apoptosis

During glutamine starvation not only translation but also transcription is strictly regulated to secure cell survival. Both mechanisms are highly interlinked due to c-MYCs involvement in transcription regulation of many genes, especially pro-proliferation genes. During transcription c-MYC promotes elongation by recruiting the elongation factor P-TEFb which increases the overall transcriptional output of c-MYC regulated genes (Rahl, Young, 2014). Interruption of transcription elongation, for instance during glutamine starvation, causes the formation of R-loops by slowing down or stalling of RNA-polymerase II (RNAPII). Stalled RNAPII decreases the spatial distance between nascent RNA and the transcribed single-stranded DNA, which favours the R-loop formation (Costantino, Koshland, 2015). Furthermore, the induction of the MYC-ER transgene and its activation during glutamine starvation increases R-loop formation even more, which coincides with stalled RNAPII in the gene body (Dejure, Eilers, et al., 2017). R-loops can play an important role both in positive ways, like in gene expression regulation, and in negative ways, like reducing genome stability. To this day it is unknown, whether R-loop formation during glutamine starvation is cause or effect of transcription regulation. Since higher concentrations of R-loops increase the risk of detrimental effects, glutamine starvation and MYC-ER activation increase tension on colon carcinoma cells. R-loops are harmful to cells in multiple ways. The complementary DNA-strand of the part of the DNA which is bound to the nascent RNA remains single stranded and is so chemically more unstable. This can induce mutagenesis and double strand breaks in this part of the gene (Wimberly, et al., 2014). Double strand breaks can also be an effect of replication

fork collapse induced by R-loops if they are still present during DNA replication. Several evolutionary conserved mechanisms are necessary to prevent the collision between R-loops formed during transcription and replication forks like topoisomerases to relieve negative supercoiling right behind the RNAPII or RNaseH1 and 2 to degrade longer persisting R-loops throughout the genome (Gan, Guan, et al., 2011). Since c-MYC specifically amplificates the transcription of pro-proliferation genes, the R-loop-fork collisions pose an immense threat to cells accumulating R-loops in MYC-target genes during glutamine starvation. Previous studies have shown that glutamine starvation can lead to c-MYC dependent apoptosis in cancer cells. Although the exact mechanism remains unknown yet, several possible hypotheses have been proposed and some disproven. Glutamine starvation impairs the TCA cycle by a shortage of intermediates which could cause oxidative stress or damage due to an abnormally functioning respiratory chain. This could reduce p53 levels which are usually increased in high c-MYC levels and therefore cause apoptosis (Yuneva, et al., 2007). High c-MYC levels could also deregulate several metabolic pathways including mitochondrial proteins which trigger apoptosis in unusual concentrations (Morrish, et al., 2003). These expressional deregulations could be induced by R-loop formation and hence transcriptional changes.

3.3.2 Modified HCT116 cells were persistent in glutamine starvation with induced MYC-ER

For unknown reasons, the modified HCT116 colon carcinoma cell lines which were used in and created for this study, did not show the same apoptosis rates as previously described. As shown in the AnnexinV/PI-Assay (Figure 2.21), cells incubated without glutamine and with OHT to induce MYC-ER activity were not significantly driven into apoptosis after 24h. In HFF cells from Yuneva, et al., 2007, about 70% of the cells were already apoptotic. In Dejure, et al., 2017, HCT116 cells which were transformed with the same MYC-ER construct as the cells in this study, a crystal violet staining after 72h of incubation showed high levels of apoptotic cells. In Figure 2.22 there was no visible effect of MYC-ER activation during glutamine starvation on apoptosis after 72h.

There are several possible reasons for this outcome. The c-MYC levels could be lower than in the cell lines used in the former studies. A proper comparison of c-MYC levels is not possible since c-MYC protein levels were not measured precisely. Only relative concentrations were verified by immunostaining via western blot (Figure 2.13). If c-MYC or MYC-ER levels were overall lower than in other studies, the effects of glutamine starvation combined with MYC-ER activation could have been lowered and the apoptotic outcome attenuated. Furthermore, a too short incubation time of OHT activation could be a reason for reduced apoptosis. Although periods differing from described duration were tested, none increased apoptosis to similar levels as in previous studies. The right time frame might still to be determined for this cell line. A possible leakage of the RNaseH1 transgene could have

unknown side effects on cell viability. As seen in figure 2.14 a small amount of RNaseH1 could be expressed even without doxycycline induction. This feature would be hard to disprove or avoid in further studies even if it were confirmed. These biochemical side effects could include interplays with the mTOR-dependent growth and survival pathways. mTOR (mammalian target of rapamycin) is involved in several pathways activated by growth factors and amino acid and energy-sensing pathways (Tokunaga, et al., 2003). Also, the mTOR complex formation is linked to normal mitochondrial functionality (Zou, et al., 2020). As shown in figure 2.29, one main effect of RNaseH1 overexpression is the deregulation of mitochondrial protein expression. Even a small depletion of R-loops could impair mitochondrial functionality and affect the mTOR pathways. Since glutamine starvation depletes many amino acid levels and energy availability the fragile balance between proliferation and apoptosis could be tipped by a small leakage of RNaseH1.

The persistence of the modified HCT116 cells to MYC-ER activation during glutamine starvation must be kept in mind when viewing the experimental R-loop depletion results and further discussions. It could have major impacts to any implications and discussions made resulting from the experiments performed in 2.3 to 2.7.

3.3.3 RNaseH1 overexpression causes apoptosis

The specific effect of RNaseH1 overexpression on apoptosis during glutamine starvation and MYC-ER activation was verified via the creation and incorporation of a catalytically inactive variant of RNaseH1 (RNaseH1nf). The inactive mutant contained a single nucleotide exchange to interrupt its R-loop degrading activity without affinity loss to its substrate. The mutant was first described in Reyes, et al., 2015, to localize R-loops throughout the genome. In the performed apoptosis assays, both RNaseH1 and RNaseH1nf were used side by side to verify the specificity of the experiments. The effects of both proteins could be best observed in DRIP experiments shown in figures 2.17 (R-loop depletion in the gene body of the *NCL* gene) and 2.20 (R-loops persistent in *NCL* with RNaseH1nf). While RNaseH1 overexpression decreased R-loop concentration, RNaseH1nf expression showed only a slight decrease of R-loops. This remaining effect despite the impaired functionality of this protein could be caused by its binding to the R-loop site. RNaseH1 dissolves after degrading the R-loop, while RNaseH1nf remains longer on site, block further transcription and along the formation of other R-loops. The AnnexinV/PI-apoptosis assay (Figure 2.21) showed a significant increase of apoptosis upon RNaseH1 overexpression during MYC-ER activation and glutamine depletion, but no increase when overexpressing RNaseH1nf. This confirms the specific effect of R-loop depletion on cell survivability.

3.4 Apoptotic effect is not caused by deregulating c-MYC-target gene expression, cell cycle deregulation or DNA-damage

3.4.1 c-MYC target genes NME1, ActB and FBXO32 are not deregulated by RNaseH1 overexpression

As described earlier, R-loops are known to have regulatory functions during transcription in some genes under specific conditions (Wimberly, et al., 2013). R-loops can even trigger histone modifications and hence transcriptional changes in specific ways contradictory to unwanted R-loops which form during transcriptional stress and are able to suppress transcription (Niehrs, Luke, 2020). Several c-MYC target genes were tested via qPCR for their relative expression upon RNaseH1 overexpression. The three important c-MYC target genes *NME1*, *ActB* and *FBXO32* were shown exemplary in figure 2.18. Due to low c-MYC levels during glutamine starvation, the relative expression of the genes was strongly reduced compared to high glutamine conditions. The activation of RNaseH1 overexpression had no significant effect on their transcription, whereas the increase of c-MYC levels by activating the MYC-ER system rescued the decreased expression at least partially. Both RNaseH1 overexpression and MYC-ER activation during glutamine starvation did not significantly change expression. Thus, suppressed transcription due to R-loop formation can be ruled out as a main regulation mechanism of c-MYC target genes. Since c-MYC acts as a transcriptional amplifier for its target genes by targeting their promoter and enhancer regions as part of the MYC-MAX complex, the gene transcription regulation during glutamine starvation takes place on an elongational level (Sabo, Kress, et al., 2014). The hypothesis that persistent R-loops block the gene for RNAPII and the elongating transcription renders untrue since dissolving these R-loops by RNaseH1 shows no impact on the expression of the c-MYC target genes.

3.4.2 R-loop depletion does not affect cell cycle progression during c-MYC-dependent cell cycle arrest

R-loop formation differs greatly throughout the cell cycle in highly proliferative cells. High levels of harmful R-loops were found in cells arrested in the G1-phase and after entering the S-phase due to high levels of transcription and RNA processing. Since R-loops are not detected by any cell cycle checkpoint mechanisms, no evidence has been shown that high levels of R-loops prevent cell cycle progression (San Martin-Alonso, Aguilera, et al., 2021). However, glutamine starvation can trigger a cell cycle arrest in colon carcinoma cells (Figure 2.24). Re-addition of glutamine or activating MYC-ER to increase c-MYC levels quickly restores cell cycle progression (Dejure, Eilers, et al., 2017). A combination treatment of RNaseH1 overexpression and MYC-ER activation showed, that the G1-cycle arrest was persistent during glutamine starvation. Only a small fraction of cells could be detected in the G2-phase

in a BrdU-PI-FACS assay. Some cells showed high levels of BrdU-signal alongside a weak PI-signal (Figure 2.24 green rectangle). This indicates that cells stuck in S-phase during glutamine starvation could have restored cell cycle progression and underwent mitosis since a reduced number of cells could be detected in G2-phase. The high levels of R-loops could impair DNA-synthesis by transcription-replication conflicts. A degradation of these R-loops by RNaseH1 could resolve these conflicts and promote further replication as this group of cells was not observed in non-supplemented glutamine starved cells. Since the ratio of cells in G1-phase to cells in G2/M-phase compared to -Q-cells with a great number of cells in G1 and a small number in G2/M-phase, a further cell cycle arrest in G1-phase could be constated. One explanation could be the lack of nucleotides caused by glutamine starvation. But since only a small fraction of cells differed from known cell cycle patterns, this most likely rules out cell cycle impairments as a cause for high apoptosis rates.

3.4.3 RNaseH1 overexpression and MYC-ER activation during glutamine starvation do not increase accumulated DNA-damage

Formation of R-loops throughout the genome can be a sincere source of DNA damage and genome instability. Replication stress and prolonged periods of open chromatin can cause single and double strand breaks in regions with accumulated R-loop forming (Rinaldi, Pizzul, et al., 2021). In non-cycling cells or cells in G0/G1-phase nucleases, genotoxics or reactive oxygen species (ROS) can harm the single stranded DNA component of an R-loop structure, while in proliferating cells mainly suffer transcription replication conflicts by head-on collision of the replication fork and the RNAPII or an R-loop stabilization causing a replication fork collapse in a co-directional conflict. Both incidents lead to DNA damage, while transcription replication conflicts can cause double strand DNA breakage by replication fork collapse (Garcia-Muse, Aguilera, 2019). Transcriptional stress by glutamine starvation and MYC-ER activation are also known origins for DNA damage (Dejure, Eilers, et al., 2017).

RNaseH1 activity prevents the accumulation of harmful R-loops under physiological conditions. Overexpression of RNaseH1 degrades not only harmful but also regulatory R-loops. Degradation of these could be a possible cause for DNA damage and the high apoptosis rates observed earlier. In fact, RNaseH1 overexpression did not increase the activation of the DNA damage indicator pKAP1 during glutamine starvation and MYC-ER overexpression. It even reduced the gamma H2AX signal compared to signal levels caused by MYC-ER activation during glutamine starvation by half. MYC-ER activation in combination with glutamine starvation increases transcription elongation while nucleotide levels are low, which leads to stalled RNAPII throughout c-MYC target genes. This stalled RNAPII could be released by degradation of stable R-loops in combination with transcription termination afterwards. The reason for the high apoptosis rates seems to be independent of DNA damage but might be linked to the degradation of regulatory R-loops in combination with low nucleotide levels.

3.5 Ratio of polyphosphorylated nucleotides changes significantly during RNaseH1 overexpression

High proliferation rates of cancer cells induce a glutamine dependence as an oxygen independent energy source and as a resource for anaplerotic reactions to replenish used up intermediates of the TCA cycle. These reactions are essential for the synthesis of proteins, lipids and nucleic acids (Chen, Cui, 2015). In Dejure, et al., 2017 it was shown that nucleotide levels were decreased after 15 h of glutamine starvation. However, in the nucleotide analysis shown in this study, nucleotide levels in cells starved for glutamine for 12 h showed increased nucleotide levels. Mono-, di- and triphosphates were all significantly higher than in the control cells grown in the presence of glutamine. Since we discussed a clear difference between HCT116 cells used in the previous study and the cells used here in 3.3.2 this result could be affected by the metabolic differences, too.

One possible explanation for the high levels of nucleotides shown in Figure 2.28 could be an altered balance of salvaging mechanisms and strongly decreased transcription rates. Nucleotide salvaging pathways are activated during nutrient scarcity to maintain nucleotide levels that prevent cell starvation and apoptosis. These mechanisms enable cells to recycle nucleotides without an external nitrogen source like glutamine. Recycled bases can be used to rebuild nucleotides needed for cell survival or to produce lacking intermediates (Jeannotte, 2014). Since glutamine starvation poses an imminent malnutrition for cells these recycling pathways should be active in the investigated cells. Glutamine scarcity might also explain high salvage rates for nucleotides compared to salvaged intermediates. These intermediates need a functioning TCA cycle to be replenished, but glutamine starvation restrains the TCA cycle from anaplerotic reactions. This could open a greater part of salvaged resources for nucleotide synthesis. Concurrently, transcription rates are significantly reduced due to c-MYC depletion during glutamine starvation as well as DNA synthesis is stopped during cell cycle arrest. Consumption of deoxyribonucleotides and replenishment of the necessary pool of deoxyribonucleotides can use up free nucleotides as well. As DNA synthesis is impaired, no ribonucleotides must be used for dNTP synthesis. RNA transcription consumes large amounts of nucleotides as well. A lack of c-MYC reduces overall transcription rate and hence the consumption of free nucleotides. Combined, these conditions could explain high levels of free nucleotides in glutamine starved cells. The fact that these nucleotides are energy rich triphosphates could be explained by the high availability of glucose in the growing medium. Since the cells still can use up this energy source, synthesis of triphosphates is still possible under glutamine starving conditions.

In contrast to these results are the nucleotide measurements of cells starved for glutamine while activating MYC-ER and overexpressing RNaseH1. These cells show slightly increased levels of nucleotide monophosphates compared to glutamine starvation cultures, but strongly decreased levels of

diphosphates and even more depleted triphosphates. While the overall levels of nucleotides are similar in glutamine rich or glutamine depleted medium with MYC-ER activation and RNaseH1 overexpression (Figure 2.27), the distribution of differently phosphorylated nucleotides is not. The lack of triphosphorylated nucleotides indicates an increased energy consumption or higher consumption of nucleotide triphosphates. When viewing transcription rate measurements (Figure 2.18) side by side with nucleotide measurements, the low levels of triphosphates can be explained. Transcription of c-MYC target genes is increased during MYC-ER activation and RNaseH1 overexpression even during glutamine starvation. This transcription activity uses up large amounts of nucleotides and available energy sources during the process. This consumption of scarce energy resources could terminally trigger apoptosis in these cells.

3.6 Proposed model for lethal feedback loop in glutamine starved cells with MYC-ER activation and RNaseH1 overexpression

Increased apoptosis rates observed in glutamine starved cells with ectopically introduced c-MYC by MYC-ER activation and overexpression of R-loop degrading RNaseH1 in HCT116 cells could have been explained by several hypothesis. We ruled out an involvement of DNA-damage in this pathway. DNA-damage indicators like gamma H2AX and pKAP1 showed no exceptionally high activity during the apoptotic condition. Also, R-loop degradation does not affect the expression pattern of important c-MYC target genes like NME1 as confirmed by expression analysis. Cell cycle analysis showed no significant changes in the cells by this treatment. Vast alteration of available nucleotides, especially triphospho-nucleotides, could be observed in pre-apoptotic cells.

In conclusion, these findings support our proposed model to explain the high apoptosis rates under glutamine starving conditions (Figure 3.1). In glutamine starved cells (-Q) RNAPII fails to transcribe genes entirely, caused by reduced c-MYC levels and energy scarcity. RNAPII stalls in the gene body, which causes the formation of R-loops by spatial proximity of the nascent RNA strand and the unwound and single stranded DNA-template strand. The R-loop stabilizes stalling RNAPII and prevents further transcription until glutamine is available again and the R-loop is degraded by RNaseH1. When overexpressing RNaseH1 in glutamine starving cells (-Q+RNaseH1), stalled RNAPII also forms R-loops, which are degraded rapidly by abundant RNaseH1. Further transcription is then quickly terminated by XRN2 and torpedo termination as soon as a free 5'-end of nascent RNA created by R-loop degradation (Eaton, Francis, et al., 2019). Transcription is halted afterwards by the lack of c-MYC protein for transcription elongation.

MYC-ER activation and RNaseH1 overexpression during glutamine starvation (-Q+MYC+RNaseH1) circumvents this regulatory mechanism. RNAPII stalls in the gene body and an R-loop is formed. This R-loop is rapidly degraded by the abundant RNaseH1, and transcription is terminated. Due to MYC-ER

activation and high c-MYC activity, transcription elongation starts over, RNAPII stalls and an R-loops forms again. This recurrent loop uses up many of the cell's scarce resources like ATP and other triphosphates (see Figure 2.28) and starves the cell into apoptosis.

This model could provide another mechanism of regulating R-loops during transcription. Since uncontrollable loops pose an imminent risk to cells, even under non-stressful conditions, identifying such regulation mechanisms might bear a chance to find new targets for drug strategies. Since some results shown here are disputable and controversial to other studies, further verification of perfect physiological conditions is necessary. To further validate the essence of the model, investigations and quantifications about transcription and termination seem to be the first best step as follow up experiments. In depth screening might also uncover essential genes for this mechanism and important accumulation points for R-loops.

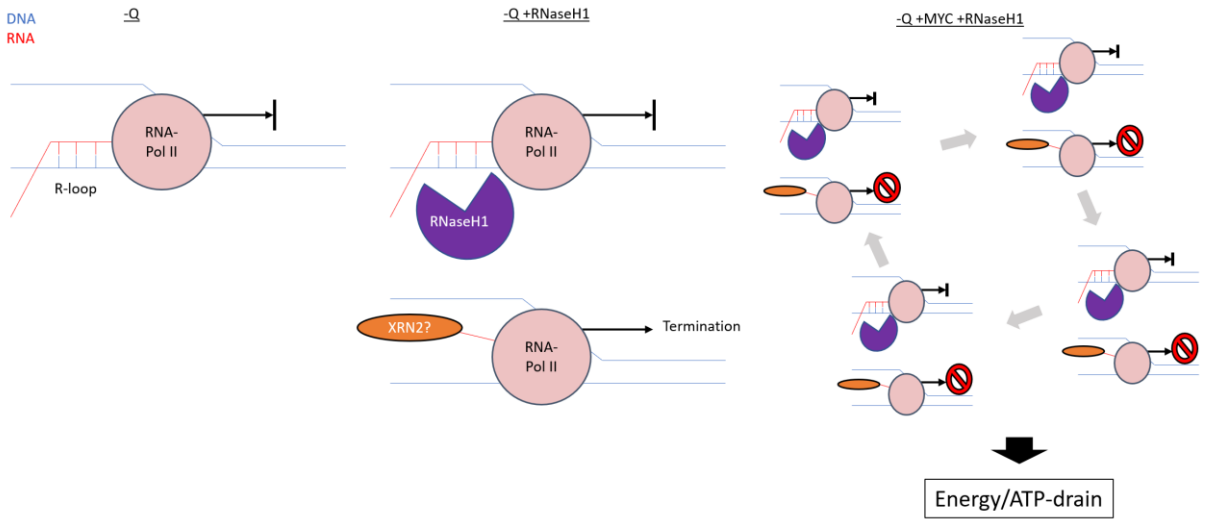

Figure 3.1: Proposed model *describes a faulty loop of transcription initiation, elongation and termination, which cumulates to a lethal energy drain in glutamine starved cells due to unregulated c-MYC activity and R-loop degradation. During glutamine starvation, RNAPII stalls as transcription elongation is halted by limited nucleotide availability while R-loops are forming. RNaseH1 degrades the R-loops and RNAPII gets terminated. Transcription starts over again and stalls during transcription again. Energy and nucleotides are drained unregulated, which leads to cells undergoing apoptosis.*

4 Materials

4.1 Human cell lines

Cell line	Source
HEK293T	Human embryonic kidney cell line (ATCC)
HCT116	Human colon carcinoma cell line (ATCC)
U-2 OS-W11	Human osteosarcoma cell line + inducible MYC-construct
LS174T	Human colorectal adenocarcinoma cell line (ATCC)

4.2 Culture media and supplements

4.2.1 Cell culture media

Name	Use	Supplements
DMEM D6429 (Thermo Fisher Scientific)	Cell transfection	2% Fetal Bovine Serum Advanced (Capricorn Scientific GmbH, heat inactivated at 56°C for 30 min before use)
DMEM D6429 (Thermo Fisher Scientific)	Cell cultivation, infection (HCT116, HEK293T)	10% Fetal Bovine Serum Advanced (Capricorn Scientific GmbH, heat inactivated at 56°C for 30 min before use) 1% Penicillin/Streptomycin (Sigma)
DMEM D5030 (Thermo Fisher Scientific) dissolved in ddH_2O	Glutamine recovery experiments	3,7 g/l Sodium Bicarbonate (Roth) 10% dialyzed FBS (Sigma, heat inactivated at 56°C for 30 min before use) 1% Penicillin/Streptomycin (Sigma)

		2.5 g/l D-glucose (Sigma) 2 mM glutamine (Sigma)
DMEM D5030 (Thermo Fisher Scientific) dissolved in ddH20	Glutamine starvation experiments	3,7 g/l Sodium Bicarbonate (Roth) 10% dialyzed FBS (Sigma, heat inactivated at 56°C for 30 min before use) 1% Penicillin/Streptomycin (Sigma) 2.5 g/l D-glucose (Sigma)
Opti-MEM I Reduced Serum Media (Thermo Fisher Scientific)	siRNA transfection	
RPMI-1640 Medium, with L-Glutamine (Thermo Fisher Scientific)	Cell cultivation (LS174T, U2OS-W11)	10% Fetal Bovine Serum Advanced (Capricorn Scientific GmbH, heat inactivated at 56°C for 30 min before use)
Gibco™ Trypsin-EDTA (0,25%, Thermo Fisher Scientific)	Cell passaging	

4.2.2 Supplements

Name	**Stock concentration**	**Final concentration**
4-hydroxytamoxyfen (OHT)	10 mM in ethanol	100 nM
Doxycycline (Dox)	1 mg/ml in ethanol	100 µg/ml
Polyethylenimin (PEI, Merck)		
Puromycin (InvivoGen)	10 mg/ml	2 µg/ml
Hygromycin B Gold (InvivoGen)	100 mg/ml	200µg/ml

4.3 Bacteria strains

Strain	Description
DH5α	Escherichia coli, genotype F- Φ80lacZΔM15 Δ (lacZYA-argF) U169 recA1 endA1 hsdR17 8rK-,mK+) phoA supE44 λ-thi-1 gyrA96 relA1 Bacteria used for plasmid amplification
XL1 blue	Escherichia coli, genotype recA1 endA1 gyrA96 thi-1hsdR17 supE44 relA1 lac [F´ proAB lacIqZΔM15 Tn10 (Tetr)] Bacteria used for plasmid amplification

4.4 Bacteria culture media and supplements

Name	Composition
LB medium	10% (w/v) Bacto tryptone (Roth) 0,5% (w/v) Yeast extract (Roth) 1% (w/v) NaCl (Roth) Autoclaved after preparation
LB Agar	LB-medium with 1.2% (w/v) Agar-agar (Roth) Autoclaved, heated in microwave oven, cooled down to 50°C; Addition of antibiotics, poured into 10 cm dishes afterwards

4.5 Solutions and buffers

Buffer	Components
TAE (x50)	2 M Tris, pH 8.0 5,7% acetic acid 50 mM EDTA
DRIP lysis buffer	TE-buffer, pH 8.0 0.5% SDS 5 µl Proteinase K
DRIP binding buffer	TE-buffer 10 mM Sodium phosphate 140 mM Sodium chloride 0.05% Triton X-100 (Sigma-Aldrich)
DRIP wash buffer 1	TE-buffer 20 mM Tris HCl pH 8.0

	150 mM Sodium chloride 2 mM EDTA 0.1% SDS 1% Triton X-100
DRIP wash buffer 2	TE-buffer 20 mM Tris HCl pH 8.0 500 mM Sodium chloride 2 mM EDTA 0.1% SDS 1% Triton X-100
DRIP wash buffer 3	TE-buffer 10 mM Tris HCl pH 8.0 250 mM Lithium chloride 1 mM EDTA 1% NP40 (Sigma-Aldrich)
DRIP elution buffer	TE-buffer 1% SDS 50 mM Sodium hydrogen carbonate
Phenol/Chloroform/Isoamylalcohol	Mixing ratio 12:12:1
CR wash buffer	H_2O 20 mM HEPES 150 mM NaCl 0.5 mM Spermidine
CR Dig-wash buffer	CR wash buffer 0.05% Digitonin
CR antibody buffer	CR Dig-wash buffer 2 mM EDTA
CR binding buffer	H_2O 20 mM HEPES 10 mM KCl 1 mM $CaCl_2$ 1 mM $MnCl_2$
CR low-salt rinse buffer	H_2O 20 mM HEPES 0.5 mM Spermidine 0.05% Digitonin
CR incubation buffer	H_2O

	3.5 mM HEPES
	10 mM$CaCl_2$
	0.05% Digitonin
CR STOP buffer	H_2O
	170 mM NaCl
	20 mM EGTA
	0.05% Digitonin
	50 µg/ml RNaseA
	25 µg/ml Glycogen
AnnexinV binding buffer	H_2O
	10 mM HEPES (pH7.4)
	140 mM NaCl
	2.5 mM $CaCl_2$
RaPID Wash buffer 1	100 ml PBS
	2 mg SDS
RaPID Wash buffer 2	80 ml PBS
	10 ml 5 M NaCl solution
	5 ml 1 M HEPES
	5 ml 20 % Triton X-100
	2 µl 0.05 M EDTA
	0.1 mg Na-Doc
RaPID Wash buffer 3	99 ml PBS
	1 ml Tris
	1.05 mg LiCl
	0.5 mg NP-40
	0.5 mg Na-Doc
	10 µl 0.05 M EDTA
RaPID Wash buffer 4	95 ml PBS
	5 ml Tris
RaPID Lysis buffer	5 ml 5 M NaCl
	0.1 g SDS
	0.75 mg DTT
	2.5 ml Tris HCl
RaPID Biotin labelling solution 20x	50 ml serum-free medium
	50 g biotin

4.6 Enzymes and kits

Kit	Company
GeneJET Gel Extraction Kit	Thermo Scientific
QIAquick Gel Extraction Kit	Qiagen
QIAquick PCR Purification Kit	Qiagen
MiniElute PCR Purification Kit	Qiagen
RNeasy MiniKit	Qiagen
miRNeasy MiniKit	Qiagen
RNeasy MinElute Cleanup	Qiagen
M-MLV Reverse Transcriptase Kit	Promega
NEBNext Ultra II Directional RNA Library Prep Kit for Illumina	NEB
NEBNext rRNA Depletion Kit	NEB
NEB Next ChiP-Seq Library Prep Master Mix Set for Illumina	NEB
NEB Next Multiplex Oligos for Illumina (Dual Index Primers Set I)	NEB
NEB Next Small RNA Library Prep Set for Illumina	NEB
NEB Next Ultra II RNA Library Prep Kit for Illumina	NEB
NEB Next Ultra II DNALibrary Prep Kit for Illumina	NEB
peqGOLD TriFast	Peqlab
Gateway Cloning Kit	Life Technologies
Immobilon Western HRP Substrate	Millipore
Quant-iT PicoGreen dsDNA Assay Kit	Life Technologies

4.7 Oligonucleotides, Gene Blocks and plasmids

All Primers were ordered from and synthesized by Sigma.

All following oligos were synthesized at 0.025 µmole scale and purified by desalting.

The Primers were ordered in a concentration of 100 µM and were diluted to 10 µM as final concentration. They were stored at -20°C.

The gene blocks (gBlocks) were synthesized by IDT and diluted to a final concentration of 10 nM for cloning.

a. Primer

Name	Sequence
KH01_Left end primer (BamH1)	GCGGGATCCGTCGAAATGCTTCCCGGTG
KH02_Right end primer (EcoR1)	GGCTCAAGTTCTCCCAAGGACTTAAGGCG
KH03_Internal left primer	CTGGTTCTGTATACAAACAG
KH04_Internal right primer	GACCAAGACATATGTTTGTC
KH05_left_Fwd (BamH1)	GCGGGATCCGTATGAGCTGGCTTCTCTTG
KH06_left_internal_Rev	ACATATGTTTGTCATACAAATGCT
KH07_right_internal_Fwd	TGTATACAAACAGTATGTTTACGATAACT
KH08_right_Rev (EcoR1)	TCAGTCTTCCGATTGTTTAGCCTTAAGATT
KH09_BGH_Rev (EcoR1)	TAGAAGGCACAGTCGAGGTTAAGATT
KH10_right_Rev_EcoR1	CTTAAGTCAGTCTTCCGATTGTTTAGC
KH11_BGH_Rev_EcoR1	CTTAAGTAGAAGGCACAGTCGAGG
KH16_BirA2.1_Rev_Seq	TGCCTTAAGCGTAATCT
KH17_RNaseH1_Rev_Seq	TTGGCTCAAGCGTAATCT
KH18_Box_B-Stem-loop-Verifizierungsprimer_fwd	CCATCGCGGGACTTTTTCCCG
KH19_Box_B-Stem-loop-Verifizierungsprimer_rev	TTTGCCCTTTTTCAGGGC
KH20_pLeGO_Rev-Seq	GCGGAATTTACGTAGCGGC
KH21_RNaseH1_Fwd	ATGAGCTGGCTTCTGTTCCT
KH22_NCL_fwd	CCACTTGTCCGCTTCACA
KH23_NCL_rev	TCTTGGGGTCACCTTGATTT
KH24_NPM1_fwd	GGAGGTGGTAGCAAGGTTCC
KH25_NPM1_rev	TTCACTGGCGCTTTTTCTTCA
KH26_NME1_fwd	CGTGGAGACTTCTGCATACAAG
KH27_NME1_rev	GATGATCTCGCCCACCAG
KH28_CAMKV_fwd	ACTTCCTCCCTGTGACCAAC
KH29_CAMKV_rev	TTCTTCTTGTCGCCCAGAGT
KH30_CAMKV_fwd FL	TGATTTGGGACAGGTCATCA
KH31_CAMKV_rev FL	TGGAACTTCTTGCAGGTGTG
KH32_BoxB_Fwd	CCA TCG CGG GAC TTT TTC CCG
KH33_BoxB_Rev	AGA AAA CGG GAA AAA GTC CCG AAT
KH34_b2MG_Fwd	TTCTGGCCTGGAGGCTATC
KH35_b2MG_Rev	TCAGGAAATTTGACTTTCCATTC
KH36_TKT_TSS_Fwd	AGCCGCTATCTCTGTGTGTC
KH37_TKT_TSS_Rev	GTTGGCCGTGTCCTTCAAG

KH38_TKT_GB_Fwd	TTCCCTGTTCACAACCCCTT
KH39_TKT_GB_Rev	TTCGAGACTAGGGACAAGGC
KH40_TKT_TES_Fwd	GATTCCAGAAACCGACGCTC
KH41_TKT_TES_Rev	ATGTTCTGCTGTGCTGTTCC
KH42_BoxB_Fwd_MkII	ACCGGTAGCGCCCTGAAAAA
KH43_BoxB_Rev_MkII	CTAGTGAATTCTTTGCCCTTTTTC
KH44_ACTB_Prom_fw	GAGGGGAGAGGGGGTAAA
KH45_ACTB_Prom_rev	AGCCATAAAAGGCAACTTTCG
KH46_ACTB_5´pause_fw	TTACCCAGAGTGCAGGTGTG
KH47_ACTB_5´pause_rev	CCCCAATAAGCAGGAACAGA
KH48_ACTB_pause_fw	GGGACTATTTGGGGGTGTCT
KH49_ACTB_pause_rev	TCCCATAGGTGAAGGCAAAG
KH50_U1_fw	TATGAATGGACCGTCCCCTCTA
KH51_U1_rev	CAGGGGAAAGCGCGAACGCAGT
KH52_K1_fw	CCTTTTCATTCCTTTTGCTAAGGAAGA
KH53_K_rev	TTAAGATTTGGCTCAATGATATATTTGCC
KH54_K2_fw	GTTACAAAGAGACATTTATAACGGTAA
KH56_K3_fw	TCAACTAAAAAAAGATAACAAAAATCTTTTTTA
KH57_BoxB_BsmBI_fw	AAGCTTGGAGACGACCGGTAGCGCCCTGAAAAAGGGC
KH58_BoxB_BsmBI_rev	AAGAGCTAGAGACGTCTTTTGCCCTTTTTCAGGGC
KH59_RNA_motif_cloning_K1_oligofwd_fwd	GCTT GGAAAAGTAAGGAAAACGATTCCTTCT
KH60_RNA_motif_cloning_K1_oligofwd_rev	TTAAGATTTGGCTCAATGATATATTTGCC
KH61_RNA_motif_cloning_K1_oligorev_fwd	GGAAAAGTAAGGAAAACGATTCCTTCT
KH62_RNA_motif_cloning_K1_oligorev_rev	AGCT TTAAGATTTGGCTCAATGATATATTTGCC
KH63_RNA_motif_cloning_U1_oligofwd_fwd	GCTT ATACTTACCTGGCAGGGGAGA
KH64_RNA_motif_cloning_U1_oligofwd_rev	CAGGGGAAAGCGCGAACGCA
KH65_RNA_motif_cloning_U1_oligorev_fwd	ATACTTACCTGGCAGGGGAGA
KH66_RNA_motif_cloning_U1_oligorev_rev	AGCT CAGGGGAAAGCGCGAACGCA
KH67_RNaseH1_Fwd	CGGGATGTTCTATGCCGTGA

KH68_RNaseH1_Rev	ACATCGTATGGGTAGTCTTCCG
KH69_Luci_K1_fwd	ATGGCGCTCTAGAGTAAGGAAAAGTAAGGAAAACGATTCCTT
KH70_Luci_K123_rev	GCGATTTACGGATCCTTAAGATTTGGCTCAATGATATATTTGCCAG
KH71_Luci_K2_fwd	ATGGCGCTCTAGATACACAATGTTTCTCTGTAAATATTGCCATT
KH72_Luci_K3_fwd	ATGGCGCTCTAGATTAAAGTTGATTTTTTTCTATTGTTTTTAGAA
KH73_Luci_GRR_rev	GCGATTTACGGAACTTTAAAAAGCAAAATGTACTTAAATAAAA
Konstrukt1_Seq_Fwd	GGTAGCGCCCTGAAA
Konstrukt1_Seq_Rev	ACTTTTTCCCGTTTT
BirA-Lambda_Seq_Fwd	TGACCGCTACGATGA
KW-SFFV_Seq	CTTCTGCTTCCCGAGCTCTA
Fwd. attB1_RNaseH1_HA	GGGGACAAGTTTGTACAAAAAAGCAGGCTTCACCATGAGCTGGCT TCTGTTCCT
Rev. attB2_RNaseH1_HA	GGGGACCACTTTGTACAAGAAAGCTGGGTTTCAAGCGTAATCTGG AACATCG

b. Gene Blocks

Name	**Sequence**
U1-boxB-Stemloops	ACGTCAGCAG GATCCACCGG TAGCGCCCTG AAAAAGGGCA TACTTACCTG GCAGGGGAGA TACCATGATC ACGAAGGTGG TTTTCCCAGG GCGAGGCTTA TCCATTGCAC TCCGGATGTG CTGACCCCTG CGATTTCCCC AAATGTGGGA AACTCGACTG CATAATTTGT GGTAGTGGGG GACTGCGTTC GCGCTTTCCC CTGGCCCTGA AAAAGGGCAA AGAATTCACT AGTGCACGAC TGCAATCATA
Bacillus subtilis Biotin-ligase + LambdaN-Sequence at N-Terminus	GCATTTAAAT GGCTGGATCC ACCGGTGACC GCTACGATGA ACGCGCGCAC CCGCCGCCGC GAACGCCGCG CGGAAAAACA GGCGCAGTGG AAAGCGGCGA ACATGCGGTC AACATTAAGA AAAGACCTTA TTGAATTATT TTCTCAGGCC GGCAATGAAT AAGGACATCG CGACAAGCCT CAGCCAAGCT GCTGGGGAAA AAATTGATCG GGCCGGCGTC ATCCAGCATA TTTTACTATG CTTTGAGAAA CGGTACCGGG ATTATATGAC GCACGGATTT ACGCCGATTA AGCTTTTATG GGAAAGCTAT GCGCTCGGTA TTGGCACTAA TATGAGAGCC AGAACGTTAA ACGGAACCTT TTACGGTAAG GCGTTAGGTA TAGATGATGA AGGCGTTCTG CTTTTAGAAA CGAACGAAGG CATTAAAAAA ATCTATTCTG CCGATATCGA ATTGGGCTAC CCATACGATG TTCCAGATTA CGCTTAAGGC ACGCGTGAAT TCAGTCGACC GGATCCCGAT TTATTTCCGG CCAAAAAATC AGTGATGCTC TCGGCTGTTC AAGAACTGCT GTGTGGAAGC ATATTGAAGA GCTTCGGAAA GAGGGTTATG AAGTAGAAGC CGTTAGAAGA AAAGGATATC GGCTCATCAA AAAACCCGGA AAACTCAGTG AAAGCGAAAT TCGTTTTGGA TTAAAAACGG AAGTGATGGG CCAGCATCTT ATTTACCATG ACGTTCTTTC AAGCACGCAA AAAACGGCTC ATGAGCTCGC GAATAATAAC GCACCGGAAG GCACCCTTGT GGTGGCTGAC AAACAAACAG CCGGAAGGGG CCGAATGTCT

	AGGGTATGGC ATTCTCAAGA AGGAAACGGT GTTTGGATGA GCCTGATTTT GCGGCCTGAC ATTCCGCTCC AAAAAACACC GCAGCTGACT CTGCTTGCTG CAGTAGCTGT TGTGCAGGGA ATAGAAGAGG CAGCAGGCAT CCAAACGGAT ATTAAATGGC CAAATGATAT TTTGATTAAC GGAAAAAAAA CAGTCGGTAT CCTAACGGAA ATGCAGGCTG AAGAAGACCG CGTACGTTCA GTGATCATTG GGATCGGCAT TAACGTTAAC CAGCAGCCTA ATGATTTTCC AGATGAATTG
RNaseH1-NLS	GGGGACAACA AGTTTGTACA AAAAAGCAGG CTTTAAACAA CTAGTGACCG GTTTAATTAA GGAGTGAGCG ATGAGCTGGC TTCTGTTCCT GGCCCACAGA GTCGCCTTGG CCGCCTTGCC CTGCCGCCGC GGCTCTCGCG GGTTCGGGAT GTTCTATGCC GTGAGGAGGG GCCGCAAGAC CGGGGTCTTT CTGACCTGGA ATGAGTGCAG AGCACAGGTG GACCGGTTTC CTGCTGCCAG ATTTAAGAAG TTTGCCACAG AGGATGAGGC CTGGGCCTTT GTCAGGAAAT CTGCAAGCCC GGAAGTTTCA GAAGGGCATG AAAATCAACA TGGACAAGAA TCGGAGGCGA AAGCCAGCAA GCGACTCCGT GAGCCACTGG ATGGAGATGG ACATGAAAGC GCAGAGCCGT ATGCAAAGCA CATGAAGCCG AGCGTGGAGC CGGCGCCTCC AGTTAGCAGA GACACGTTTT CCTACATGGG AGACTTCGTC GTCGTCTACA CTGATGGCTG CTGCTCCAGT AATGGGCGTA GAAGGCCGCG AGCAGGAATC GGCGTTTACT GGGGGCCAGG CCATCCTTTA AATGTAGGCA TTAGACTTCC TGGGCGGCAG ACAAACCAAA GAGCGGAAAT TCATGCAGCC TGCAAAGCCA TTGAACAAGC AAAGACTCAA AACATCAATA AACTGGTTCT GTATACAGAC AGTATGTTTA CGATAAATGG TATAACTAAC TGGGTTCAAG GTTGGAAGAA AAATGGGTGG AAGACAAGTG CAGGGAAAGA GGTGATCAAC AAAGAGGACT TTGTGGCACT GGAGAGGCTT ACCCAGGGGA TGGACATTCA GTGGATGCAT GTTCCTGGTC ATTCGGGATT TATAGGCAAT GAAGAAGCTG ACAGATTAGC CAGAGAAGGA GCTAAACAAT CGGAAGACTA CCCATACGAT GTTCCAGATT ACGCTTGAGC CAACGCGTTG TCGACGTGAC TAGTGGCCAC CCAGCTTTCT TGTACAAAGT GGTCCCC
RNaseH1- catalytically inactive (Reyes, et al. 2015)	ATCTGAGTAC GAATTCATCT GTCAGGATCC ATGAGCTGGC TTCTGTTCCT GGCCCACAGA GTCGCCTTGG CCGCCTTGCC CTGCCGCCGC GGCTCTCGCG GGTTCGGGAT GTTCTATGCC GTGAGGAGGG GCCGCAAGAC CGGGGTCTTT CTGACCTGGA ATGAGTGCAG AGCACAGGTG GACCGGTTTC CTGCTGCCAG ATTTAAGAAG TTTGCCACAG AGGATGAGGC CTGGGCCTTT GTCAGGAAAT CTGCAAGCCC GGAAGTTTCA GAAGGGCATG AAAATCAACA TGGACAAGAA TCGGAGGCGA AAGCCAGCAA GCGACTCCGT GAGCCACTGG ATGGAGATGG ACATGAAAGC GCAGAGCCGT ATGCAAAGCA CATGAAGCCG AGCGTGGAGC CGGCGCCTCC AGTTAGCAGA GACACGTTTT CCTACATGGG AGACTTCGTC GTCGTCTACA CTGATGGCTG CTGCTCCAGT AATGGGCGTA GAAGGCCGCG AGCAGGAATC GGCGTTTACT GGGGGCCAGG CCATCCTTTA AATGTAGGCA TTAGACTTCC TGGGCGGCAG ACAAACCAAA GAGCGGAAAT TCATGCAGCC

	TGCAAAGCCA TTGAACAAGC AAAGACTCAA AACATCAATA AACTGGTTCT GTATACAAAC AGTATGTTTA CGATAAATGG TATAACTAAC TGGGTTCAAG GTTGGAAGAA AAATGGGTGG AAGACAAGTG CAGGGAAAGA GGTGATCAAC AAAGAGGACT TTGTGGCACT GGAGAGGCTT ACCCAGGGGA TGGACATTCA GTGGATGCAT GTTCCTGGTC ATTCGGGATT TATAGGCAAT GAAGAAGCTG ACAGATTAGC CAGAGAAGGA GCTAAACAAT CGGAAGACTA CCCATACGAT GTTCCAGATT ACGCTTGAAC AGGCCTACTC GCGGCCGCAT CGCAGAATTC ATCGTACGTA
Konstrukt-1 MYC 3’UTR	ACGTCAGCAGGATCCACCGGTAGCGCCCTG AAAAAGGGCGGAAAAGTAAGGAAAACGATT CCTTCTAACAGAAATGTCCTGAGCAATCAC CTATGAACTTGTTTCAAATGCATGATCAAA TGCAACCTCACAACCTTGGCTGAGTCTTGA GACTGAAAGATTTAGCCATAATGTAAACTG CCTCAAATTGGACTTTGGGCATAAAAGAAC TTTTTTATGCTTACCATCTTTTTTTTTTCT TTAACAGATTTGTATTTAAGAATTGTTTTT AAAAAATTTTAAGATTTACACAATGTTTCT CTGTAAATATTGCCATTAAATGTAAATAAC TTTAATAAAACGTTTATAGCAGTTACACAG AATTTCAATCCTAGTATATAGTACCTAGTA TTATAGGTACTATAAACCCTAATTTTTTTT ATTTAAGTACATTTTGCTTTTTAAAGTTGA TTTTTTTCTATTGTTTTTAGAAAAAATAAA ATAACTGGCAAATATATCATTGAGCCAAAT CTTAAGCCCTGAAAAAGGGCAAAAGAATTC ACTAGTGCCGACTGCATCATA
Konstrukt-2 MYC-3’UTR	ACGTCAGCAGGATCCACCGGTAGCGCCCTG AAAAAGGGCCAATGTTTCTCTGTAAATATT GCCATTAAATGTAAATAACTTTAATAAAAC GTTTATAGCAGTTACACAGAATTTCAATCC TAGTATATAGTACCTAGTATTATAGGTACT ATAAACCCTAATTTTTTTTATTTAAGTACA TTTTGCTTTTTAAAGTTGATTTTTTTCTAT TGTTTTTAGAAAAAATAAAATAACTGGCAA ATATATCATTGAGCCAAATCTTAAGCCCTG AAAAAGGGCAAAGAATTCACTAGTGCACGA CTGCAATCATA
Konstrukt-3 MYC-3’UTR	ACGTCAGCAGGATCCACCGGTAGCGCCCTG AAAAAGGGCAGTTGATTTTTTTCTATTGTT TTTAGAAAAAATAAAATAACTGGCAAATAT ATCATTGAGCCAAATCTTAAGCCCTGAAAA AGGGCAAAAGAATTCACTAGTGCCGACTGC AATCATA

c. Plasmids

Template plasmids

Name	Description
pDONR221	Vector for generating entry clones for Gateway Cloning
pInducer21	Vector for expressing proteins doxycycline dependent; IRES-GFP labelled (Meerbrey et al., 2011)
pRRL-SFFV-IRES-puro	Lentiviral expression vector with SFFV-promoter and puromycin resistance (Wiese et al, 2015)
pRRL-SFFV-IRES-hygro	Lentiviral expression vector with SFFV-promoter and hygromycin resistance (Wiese et al, 2015)
pMD2.G	Plasmid encoding for virion envelope
psPAX.2	Plasmid encoding for virion packaging system
pJET	Plasmid for cloning; Insert-amplification (Thermo Fisher)

Newly designed and cloned plasmids

Name	Description
pJET Konstrukt 1	Plasmid for amplification and restriction of shortened c-MYC 3'UTR (construct 1)
pJET Konstrukt 2	Plasmid for amplification and restriction of shortened c-MYC 3'UTR (construct 2)
pJET Konstrukt 3	Plasmid for amplification and restriction of shortened c-MYC 3'UTR (construct 3)
pJET U1-Konstrukt	Plasmid for amplification and restriction of U1 spliceosomal RNA flanked by Box B stem-loops as target for biotin ligase BirA*
pJET BirA	Plasmid for amplification and restriction of *Bacillus subtilis* biotin ligase BirA with N-terminal λ bacteriophage peptide (BirA*)

pICE-RNaseH1-D10R-E48-NLS-mCherry puro CMV-tet	Plasmid for expression of catalytically inactive RNaseH1 of *Escherichia coli* with mCherry fluorophore tag (Dobbelstein lab)
pICE-RNase-NLS-mCherry puro CMV-tet	Plasmid for expression of *Escherichia coli* RNaseH1 with mCherry fluorophore tag (Dobbelstein lab)
pRRL-SFFV-IRES-puro RNaseH1-HA	Plasmid for stable expression of human RNaseH1 with HA-tag; puromycin resistance
pRRL-SFFV-IRES-puro RNaseH1-nf-HA	Plasmid for stable expression of catalytically inactive human RNaseH1 with HA-tag; puromycin resistance
pRRL-SFFV-IRES-hygro RNaseH1-HA	Plasmid for stable expression of human RNaseH1 with HA-tag; puromycin resistance
pRRL-SFFV-IRES-hygro RNaseH1-nf-HA	Plasmid for stable expression of catalytically inactive human RNaseH1 with HA-tag; puromycin resistance
pInducer 21 RNaseH1 GFP	Plasmid for doxycycline dependent expression of human RNaseH1 with HA-tag; plasmid containing stable GFP expression for FACS
pInducer 21 RNaseH1-nf GFP	Plasmid for doxycycline dependent expression of catalytically inactive human RNaseH1 with HA-tag; plasmid containing stable GFP expression for FACS
pInducer 21 BirA* GFP	Plasmid for doxycycline dependent expression of *Bacillus subtilis* biotin ligase with N-terminal λ bacteriophage peptide; plasmid containing stable GFP expression for FACS

4.8 Antibodies

Target	**Company**	**Order number**	**Use**
Vinculin	Sigma-Aldrich	V9131	IB
c-Myc (Y69)	Abcam	Ab32072	IB/IF/IP
HA-Tag	Santa Cruz	Sc-805 (Y-11)	IB/IF
RNA-DNA hybrids (S9.6)	Merck	MABE1095	IP

SNRPB	Thermo Fisher	MA5-13449	IB/IP
phospho-Histone H2A.X (Ser139)	Cell Signaling	2577	IB/IF
RNA Pol2 phospho-Ser2	Abcam	Ab5095	IB/IP
KAP1	Thermo Fisher	A300-274A	IB/IF
pKAP1 (phospho S824)	Abcam	Ab70369	IB/IF
RNA Pol2 phospho-Ser5	Cosmo Bio USA	MABI0603 (CMA602)	IB/IP
HA-Tag	Cell Signaling	3724S	IB/IF/IP
RPA32	Santa Cruz	Sc-53496	IB/IF
phospho RPA32	Thermo Fisher	A300-246A	IB/IF
Histone 2B	Abcam	Ab1790	IB
RNaseH1	Santa Cruz	Sc-136343	IB/IF

4.9 Consumables

The consumables cover disposable plastic vessels like reaction tubes, cell and bacteria culture dishes, cuvettes, syringes, cryotubes and pipette tips and were purchased from the companies Eppendorf, Greiner, Nunc, Sarstedt and VWR.

4.10 Equipment and utilities

Device	**Use**
Avanti J-26 XP (Beckman Coulter)	Centrifuge
BD FACS Canto II (BD Biosciences)	Flow cytometer
BD FACS Aria III (BD Biosciences)	Flow cytometer
LAS-4000 mini (Fujifilm)	Chemiluminescence imaging
BBD 6220 (Heraeus)	Cell culture incubator
Countess automated cell counter (Thermo Fisher Scientific)	Automated cell counting
NextSeq 500 (Illumina)	Next-Generation-Sequencing
Dry Bath System (Starlab)	Heating block
Axiovert 40CFL (Zeiss)	Microscopic imaging
TCS SP5 (Leica)	Microscopic imaging
Operetta high-content analysis system (Perkin-Elmer)	High-throughput microscopic imaging

C1000 Thermal cycler (Bio-Rad)	PCR thermal cycling
Multiscan Ascent (Thermo Labsystems)	Photometric measurement
Spectrofluorometer NanoDrop 1000 (Thermo Fisher Scientific)	Photometric DNA-concentration measurement
NanoDrop One (Thermo Fisher Scientific)	Photometric DNA-concentration measurement
UltrospecTM 3100 pro UV/Visible (Amersham Biosciences)	Photometric measurement
Immobilon-P transfer membrane (Millipore)	Membrane for Western Blotting
StepOne plus (Applied Biosystems)	Quantitative RT-PCR cycling
Minigel (Bio-Rad)	SDS-PAGE
HeraSafe (Heraeus)	Sterile cell culture bench
Digital Sonifier W-250 D (Branson)	Ultrasonification
M220 Focused-ultrasonicator (Covaris)	Ultrasonification
UV fluorescent table (Peqlab)	UV irradiation
Vortex genie 2 (Scientific Industries)	Mixing
Julabo ED-5M (Julabo)	Water Bath
Gel Blotting Paper (Schleicher and Schuell)	Whatman filter paper for Western Blotting

4.11 Software

Program	**Source**
ApE plasmid editor	M. Wayne Davis
BD FACSDiva v6.1.2	BD Biosciences
EndNote X7	Clarivate Analytics
FlowJo v10.8	FlowJo, LLC
Image J	Wayne Rasband
Integrated Genome Browser	Nicol et al, 2009
Mac OS Big Sur 11.6	Apple Inc.
Multi Gauge	Fujifilm
Office 2016 Mac	Microsoft Inc.
Prism9	GraphPad Software Inc.
Stepone software v2.3	Applied Biosystems
UCSC Genome Bioinformatics	http://genome.ucsc.edu
Harmony High-content imaging and analysis Software v4.9	Perkin Elmer
Affinity Photo v1.9.1	Serif
Affinity Designer v1.9.1	Serif

Serial Cloner 2.6	Serial Basics
Sequel Pro	Sequel Pro Developers
Ensembl Genome Browser	EMBL-EBI
BLAST	NCBI
Primer3 v4.1.0	Whitehead Institute for Biomedical Research

5 Methods

5.1 Molecular biological methods

5.1.1 Cloning of gBlocks and oligonucleotides into plasmids

The designed gBlocks and oligonucleotides are diluted to a concentration of 10 ng/µl. The restricted constructs must be ligated into the pJET-vector for amplification. The constructs were heated to 50°C for 20 min and shortly mixed and centrifuged. The following 10 µl ligation mix was prepared for each construct:

0.5 µl T4 DNA ligase

0.5 µl pJET vector (10 ng/µl)

1 µl 10x T4 Buffer

ad µl H_2O

x µl DNA construct (0.15 pmol)

The ligation mix was incubated for 10 min at RT and transformed into competent *E. coli* bacteria. Amplified construct containing plasmids had to be restricted for cloning into target vectors. Each restriction mix had to be specific for each construct and its restriction sites.

The restriction enzymes were manufactured by New England Biolabs or Thermo Fisher Scientific and were used as described in the manufacturer's manual for each enzyme. The optimal mix was determined using the DoubleDigest Calculator by Thermo Fisher Scientific. For the truncated MYC-5'-UTR constructs, as well as the *Bacillus subtilis* biotin-ligase enzyme and the U1-boxB-target sequence the following mix was prepared:

5 µl Tango buffer (x10)

20 µl Plasmid solution (1 µg/µl)

1.5 µl BamH1 RE

1.5 µl Spe1 RE

For RNaseH1-HA and RNaseH1-catalytically-inactive-HA another mix was used:

5 µl Tango buffer (x10)

20 µl Plasmid solution (1 µg/µl)

3 µl Hind III RE

3 µl Not1 RE

The restriction mixes were incubated for 2 h at 37°C. The quality of restriction was checked via agarose gel separation.

5.1.2 Agarose gel separation (AGS) and extraction of DNA

To optimize the size separation the agarose gels were prepared according to the sizes of the different restricted DNA fragments. The agarose powder was diluted by boiling in TAE buffer and briefly cooled down. While the gel was still liquid 0.4 µg/ml ethidium bromide was added, briefly mixed and poured into gel chambers with combs according to the needed well size. The DNA samples were mixed with a loading dye buffer and loaded into the wells as well as a matching DNA ladder. The separation was performed at 150 V for 30 min for a 1% agarose gel and at 180 V for 40 min for a 2% agarose gel. The DNA was visualized on a UV transilluminator, and the pictures were edited with the ImageJ software.

For the isolation of DNA from the agarose gel, the desired DNA bands had to be cut out of the gel while illuminating the DNA via UV radiation. The DNA was cut carefully using a scalpel and transferred into reaction tubes. The gel pieces were covered with 400 µl Binding buffer and melted at 80°C for approximately 10 min. 100 µl isopropanol was added to the solution as soon as the gel melted completely. After a few inversions the mix was transferred to a GeneJet purification column and centrifuged for 1 min at 12.000 rpm. The flowthrough was discarded and 700 µl were added to the column. The centrifugation was repeated, and the flowthrough discarded again. The centrifugation was performed once more, and the column was placed on a fresh reaction tube afterwards. 20 µl elution buffer were added carefully to the membrane of the column. Column and tube were centrifuged for 1 min at 12.000 rpm. The concentration of DNA contained in the flowthrough was determined using the NanoDrop device.

5.1.3 Gateway cloning (Life Technologies)

The vector pInducer21 was used for doxycycline-inducible protein expression. Cloning into this vector was performed by Gateway cloning from Life Technologies. The attB1 and attB2 sequences, which are necessary for the cloning process had to be introduced into the desired construct in a way, that they flank both sides of the gene sequence. The attB1 and attB2 sequences were inserted via PCR amplification (5.3) with special primers. The PCR product was then cloned into the pDORN221 vector by using the BP clonase enzyme. This vector was transformed into competent *E. coli* bacteria, amplified and analyzed via Mini-Prep and sequencing. The verified vector was afterwards ligated into pInducer21 with the LR clonase enzyme from the Gateway cloning kit.

5.2 Transformation of competent *E. coli* with plasmid-DNA and amplification of plasmids

XL-1 blue competent *E. coli* cultures (stored at -80°C) were thawed on ice. For each ligation mix 50 µl bacteria solution was used. The ligation mix was added to the bacteria and gently mixed. The solution was incubated on ice for 30 min, put into a 42°C water bath for 45 sec and chilled on ice for additional 3 min. 500 µl freshly prepared LB-Medium was added to the bacteria. After gently mixing the solution was incubated at 37°C for 45 min. The bacteria were centrifuged for 2 min at 3000 rpm and the supernatant discarded except for approximately 100 µl. The pellet was resuspended, and the mix plated on a carbenicillin containing LB agar plate. The plates were incubated overnight at 37°C.

5.2.1 Analytical preparation of transformed plasmids from bacteria (Mini-Prep-Kit, Invitrogen)

The colonies grown on the LB agar plate were used to inoculate several 15 ml tubes containing 5 ml LB medium. The tubes were incubated at 37°C on a shaker moving at 216 rpm overnight. 500 µl of the culture was stored for later use. The leftover overnight cultures were centrifuged for 10 min at 4000 g and the supernatant was removed. The pellet was resuspended in 400 µl miniprep resuspension buffer (R3) and mixed with 400 µl miniprep lysis buffer (L7). The tubes were inverted several times and incubated for 5 min at RT. 400 µl miniprep neutralization buffer (N3) was added and inverted several times again, followed by 10 min centrifugation at 12.000 g. The supernatant of each lysis solution was transferred to reaction tubes and mixed with 500 µl ice-cold isopropanol. The tubes were incubated at -20°C for 30 min. Afterwards, the tubes were centrifuged for 5 min at 4°C and 14.000 g. The supernatant was carefully removed, and the pellet washed with 70% EtOH, followed by another centrifugation for 5 min at 8.000 g. The supernatant was removed again, and the centrifugation was repeated. After removal of the supernatant the pellet was air-dried and resuspended in 30 µl H_2O. The diluted DNA was used in a restriction digestion to check for the correct insert size and afterwards sequenced.

5.2.2 Preparative isolation of transformed plasmids from bacteria (Maxi-Prep, Invitrogen)

The stored overnight cultures grown for the Mini-Prep were used to inoculate 200 ml LB medium containing 200 µl ampicillin (1mg/ml). The cultures were incubated overnight at 37°C on a shaker at 120 rpm. The bacteria solution was transferred into tubes suitable for centrifugation in a high-performance cooling centrifuge (Beckman-Coulter) and sedimented for 10 min at 4°C and 4000 rpm. The supernatant was removed, and the pellet resuspended in 10

ml maxiprep resuspension buffer (R3) containing RNase A. 10 ml maxiprep lysis buffer (L3) was added and mixed by inversion. The lysis mix was incubated at RT for 5 min. 10 ml maxiprep precipitation buffer (N3) was added and mixed again by inversion. The mix was then centrifuged for 25 min at 8000 g and RT. During centrifugation, the filtering columns could be prepared by adding 30 ml maxiprep equilibration buffer (EQ1) to each column. The supernatant of the centrifuged precipitation mix was transferred to the calibrated columns via a pleated filter. 60 ml maxiprep washing buffer (W8) were added to the columns and the flowthrough was discarded. Centrifugation tubes were taped to the columns and the DNA was eluted from the columns by adding 15 ml maxiprep elution buffer (E1) and the columns were discarded. 10.5 ml ice-cold isopropanol was added to the eluted DNA solution and incubated at 4°C for 30 min. Afterwards, the solution was centrifuged for 30 min at 4°C and 12.000 g. The supernatant was discarded, and the pellet washed with 5 ml 70% EtOH. The centrifugation was repeated, and the pellet air-dried. The pellet was resuspended in 300 µl H_2O. The DNA concentration was determined by NanoDrop measurement and diluted to 1mg/ml.

5.3 PCR amplification of DNA inserts from plasmids

The DNA inserts had to be checked for the right length and sequence. They were amplified using a specific Polymerase Chain Reaction (PCR) for each insert. The primers used for each reaction are listed in 2.7. The PCR-Mix was prepared after the following scheme:

10 µl Phusion Buffer (5x)

2.5 µl Reverse Primer

2.5 µl Forward Primer

5 µl Template Plasmid DNA (1 mg/ml)

1 µl Phusion Polymerase

2 µl Deoxyribonucleotide triphosphate (dNTP) solution (20 ng/ µl of each dXTP)

27 µl H_2O

The mixes were incubated in a thermo cycler. The annealing temperature was changed according to the melting temperature of each primer pair.

Temperature	Duration	Cycle repeats
98°C	30 sec	
98°C	5 sec	x30
59-65°C	15 sec	
72°C	15 sec	
72°C	10 min	
4°C	hold	

The PCR products were loaded to 2% agarose gels to check for the correct sequence length. Afterwards the PCR products and the matching primers were sent to LGC Genomics for sequencing and checked for the right DNA sequence via BLAST analysis.

5.4 Lentivirus production in HEK293T cells

Cultivated HEK 293T cells were used to produce lentivirus containing desired DNA plasmids for cell infection. The HEK293 were transfected with DNA plasmids using the polyethyleneimine (PEI) transfection method. 11 µg template plasmid, 2.8 µg psPAX2 and 1.4 µg pMD2G were mixed into 700 µl Opti-MEM medium. psPAX2 and pMD2G contain the genes for the packaging proteins of the lentivirus. In another reaction tube 700 µl Opti-MEM medium was mixed with 30 µl PEI solution and both mixes were incubated at RT for 5 min. The plasmid mix was transferred to the PEI solution dropwise and incubated for another 20 min. the PEI plasmid mix was added to 10 ml DMEM medium containing 2% FCS and no antibiotics. The HEK293T cells were incubated in this medium in an incubator overnight. On the next day the infection medium was replaced by DMEM cultivation medium containing 10% FCS and 1% Penicillin-Streptomycin and incubated overnight again. The medium was collected and replaced by fresh medium. After 7 h the medium was harvested again, and the cells were discarded. The collected medium was filtered through a 0.45 µm filter and stored at -80°C till infection.

5.5 RNA isolation from whole cells and cDNA synthesis

HCT116 MYC-ER cells and HCT116 MYC-ER+RNaseH1 cells were treated with Hydroxytamoxifen (1 µmol/ml) overnight to activate the MYC-ER system. After incubation, the medium was discarded and 1 ml TriFast solution was added to the plate under a fume hood. The cells were scraped and collected in a 1.5 ml reaction tube and incubated for 5 min. 200 µl Chloroform were added and the tube was mixed for 15 sec on a vortex mixer. The tube was incubated at RT for approximately 10 min and afterwards centrifuged for 5 min at 14.000 rpm and 4°C. The aqueous phase was transferred to a fresh reaction tube and mixed with 500 µl ice cold isopropanol. The solution was mixed and incubated for 15 min at -20°C.

The tube was centrifuged for 10 min at 14.000 rpm and 4°C and the supernatant was discarded. The RNA pellet was washed carefully with 70% EtOH twice and centrifuged again. The pellet was air-dried and solved in 25 µl ddH_2O. The RNA concentration was determined via NanoDrop measurement.

The M-MLV Reverse Transcriptase Kit by Promega was used for cDNA synthesis. 2 µg of RNA were diluted into 10 µl ddH_2O. The following Master Mix was added to the RNA solution:

10 µl	First Strand Buffer (5x)
1.25 µl	dNTPs (20 mM)
2 µl	Random Primers
0.2 µl	Ribolock
1 µl	M-MLV reverse transcriptase
22.5 µl	H_2O

The mix was incubated for 10 min at RT followed by 50 min at 37°C and 15 min at 70°C. The cDNA was stored at -20°C till further use.

5.6 Quantitative Real-Time Polymerase Chain Reaction (qRT-PCR)

qRT-PCR was used to check for the presence of desired cDNA or to measure the amount of DNA precipitated by DNA:RNA-Immunoprecipitation. Each reaction was performed in triplicates and with water instead of DNA-mix as negative control and *β2-Microglobulin* (*b2MG*) as normalization.

The following master mixes were prepared for the reactions (x3 each):

<u>DNA-mix:</u>

1 µl	cDNA (1 µg/µl)
9 µl	H_2O

<u>SYBR-green-mix:</u>

5 µl	SYBR-green
1 µl	Primer Mix (10 µM forward primer and 10 µM reverse primer)
4 µl	H_2O

The master mixes were combined in every single well of a 96-well plate. The plate was sealed, mixed, and centrifuged for 3 min at 800 rpm.

qRT-PCR was performed in a StepOne plus RT-PCR thermocycler (Applied Biosystems) using the following setup:

Temperature	**Duration**	**Cycle repeats**
50°C	2 min	
95°C	2 min	
95°C	5 sec	x40
60°C	15 sec	

The thermocycler data were expressed as the Ct (Cycle threshold) value, which indicates the cycle repeat in which the fluorescence of the PCR product exceeds the background fluorescence.

The Ct value of the performed reactions were analyzed by normalization to the Ct value of the positive control (*b2MG*). The standard deviation (SD) of each target gene triplicate was calculated as well as the SD of *b2MG* triplicates. The ΔCt value of each target gene was calculated by subtracting the average of *b2MG* Ct from each Ct value. The difference of ΔCt (ΔΔCt) values was calculated by comparing the ΔCt of a control condition and treated condition (i.e., Doxycycline, Tamoxifen, etc.): $\Delta Ct_{treated} - \Delta Ct_{control}$

To calculate the relative expression of the target gene the following formula was used:

Relative expression = $2^{-\Delta\Delta Ct}$

For the DRIP data the Percent-input-method was used to quantify the precipitated DNA. 1% of the chromatin was used as input sample (just as the control condition mentioned before).

Again, the average Ct values were calculated and subtracted. This value was used to calculate the percentage of input:

$\%_{input} = 0.5\text{^}Ct_{precipitation}$ - average Ct_{input}

5.7 Next Generation Sequencing

5.7.1 DRIP-sequencing

The following protocol is adapted from Weber et al. (2005) and Ginno et al. (2012).

Harvest

Six 15 cm culture dishes were seeded for each condition with HCT116 cells containing the MYC-ER system and a doxycycline-inducible RNaseH1 system. At the day of harvest, the plates were washed two times with ice-cold PBS. 2 ml of PBS were left on the plate for scraping the cells carefully. The cells of all six dishes were collected in a 50 ml tube. The cells were sedimented in a centrifuge at 250 rpm for 5 min. The supernatant was discarded, and the cell pellet was resuspended in 2 ml DRIP lysis buffer with freshly added Proteinase K. The tubes were incubated on a mixing wheel over night at 37°C.

Phenol-chloroform extraction

The samples were divided equally to two 2 ml reaction tubes. 1 ml Phenol/Chloroform was added to each reaction tube and mixed well on a vortex shaker. The mix was incubated for 3 min at room temperature and centrifuged at 4°C for 5 min with 14.000 rpm. The supernatant of each tube was split into two 1.5 ml reaction tubes. 1 ml 100% EtOH and 50 µl 3M sodium acetate were added to each tube, mixed well on a vortex mixer, and incubated at -20°C for 30 min. Afterwards, the tubes were centrifuged for 30 min at 4°C and 14.000 rpm. The supernatant was discarded, and the pellets were washed with 1 ml 70% EtOH. The samples were centrifuged for 10 min at 4°C and 14.000 rpm, the supernatant was discarded, and the pellets were allowed to air-dry for about 10 min to evaporate all remaining EtOH. The pellets were resuspended in 125 µl TE buffer and combined to a total of 500 µl per condition.

Genomic DNA restriction

50 µl 10x NEB 2.1 buffer was added to each sample. For the restriction reaction the following enzyme mix was prepared and added to each tube:

Restriction enzyme (NEB)	**Volume**
Bsr GI	6 µl
EcoRI	3 µl
HindIII	0.6 µl
SSpI	2.4 µl
XbaI	0.6 µl

An additional 50 µl 10x RNaseH buffer and 12 µl RNaseH enzyme were added to the negative control sample. The tubes were incubated on a mixing wheel over night at 37°C.

Restriction efficiency test

500 µl Phenol/Chloroform were added to each sample. They were mixed thoroughly on a vortex mixer, incubated at RT for 3 min, and centrifuged for 5 min at 4°C and 14.000 rpm. The aqueous phase was divided into two 1.5 ml reaction tubes. 1 ml 100% EtOH and 50 µl sodium acetate were added to each sample, mixed well, and incubated for 30 min at -20°C. The samples were then centrifuged for 30 min at 4°C and 14.000 rpm. The supernatant was discarded, and the pellet washed with 1 ml 70% EtOH. The samples were centrifuged again for 10 min at 14.000 rpm and 4°C. The supernatant was discarded again, and the pellet was air-dried for 5 min. The pellet was resuspended in 1 ml DRIP binding buffer. 10 µl of the samples were separated on a 2% agarose gel to check the restriction efficiency. The restriction was successful when the smear of the DNA bands is at 1 kb and below. Another 10 µl was stored at -20°C as input sample for later normalization.

Antibody-beads coupling and pull-down

60 µl A protein dynabeads and 60 µl G protein dynabeads were mixed for each sample. The beads were washed thrice with 0.5% BSA/PBS solution. Half of the dynabead mixes was incubated over night with 8 µl IgG mouse antibody as negative control. The remaining beads were mixed with 8 µl S9.6 anti-DNA:RNA hybrid antibody solution. The beads were incubated over night at 4°C on a mixing wheel.

The beads were washed again three times with 0.5% BSA/PBS solution and resuspended in 30 µl 0.5% BSA/PBS. The beads were added to the samples and incubated on a mixing wheel over night at 4°C.

The beads were washed three times with DRIP wash buffer I, then three times with DRIP wash buffer II and three times with DRIP wash buffer III. Each washing step was about 5 min. The beads were washed one final time with TE buffer and transferred into new reaction tubes. From this step on the input samples were treated in the same way as the pull-down samples again. 150 µl DRIP elution buffer were added to the beads and the input samples. The tubes were incubated on a mixing wheel for 15 min to elute the DNA from the beads. The supernatant was collected in a separate tube and the elution was repeated. The eluates were combined and mixed with 2 µl Proteinase K. The tubes were incubated on a thermo shaker at 45°C for 2 h. 300 µl Phenol/Chloroform were added to each sample and mixed thoroughly. After 3 min incubation at RT and 5 min centrifugation at 4°C and 14.000 rpm, 1 ml 100% EtOH and 50 µl 3M sodium acetate were added to the aqueous phase of each sample. The tubes were incubated at -20°C for 30 min and centrifuged for 30 min at 4°C and 14.000 rpm. The supernatant was discarded, and the pellet washed in 70% EtOH. After another 10 min centrifugation at 14.000 rpm and 4°C, the supernatant was discarded, and the pellet air-dried. The pellet was resuspended in 300 µl TE buffer.

To check whether the pull-down was successful a qRT-PCR was performed (5.1.8).

Library preparation

The NEBNext Ultra II DNALibrary Prep Kit for Illumina was used for the library preparation.

For NEB End Prep the following mix was prepared on ice in a nuclease-free reaction tube for each sample:

25 µl purified DNA (about 6 ng DNA)

1.5 µl NEBNext Ultra II End Prep Enzyme Mix

3.5 µl NEBNExt Ultra II End Prep Reaction buffer

After careful mixing and spinning down remains of the mix at the sides of the tube, the mix was placed in a thermocycler with the heated lid set to 60°C. The following program was run:

Time	**Temperature**
30 min	20°C
60 min	50°C
Hold	4°C

The samples were next prepared for adaptor ligation. The NEBNext Adaptor was diluted to 0.5 µM in 0.1% TE buffer. With this Adaptor dilution the following mix was prepared:

30 µl End Prep DNA mix

15 µl NEBNext Ultra II Ligation Master Mix

0.5 µl NEBNext Ligation Enhancer

1.25 µl NEBNext Adaptor for Illumina (0.5 µM)

The samples were mixed thoroughly and incubated at 20°C for 15 min. 1.5 µl USER enzyme was added to the ligation mixture and mixed well. The samples were incubated at 37°C for 15 min.

To clean up the Adaptor-ligated DNA SPRIselect beads were used. 80 µl (1.75x) SPRIselect beads were added to the ligation mixture and mixed well. After 5 min incubation at RT the tubes were placed on a magnetic stand to separate the beads from the supernatant. The supernatant was carefully removed and discarded. 200 µl 80% EtOH was added to each tube, incubated for 30 sec and carefully removed as well. This washing step was repeated and all remaining EtOH was removed carefully, and the beads were air-dried for several minutes. The DNA was eluted using 15 µl 0.1% TE buffer by incubating for

at least 5 min at RT. The beads were placed on a magnetic stand again and the supernatant was collected and transferred into a fresh PCR tube.

For DNA amplification the following mix was prepared for each sample:

13 µl Adaptor-ligated Fragments

15 µl NEBNext Ultra II Q5 Master Mix

1 µl i7 index primer

1 µl i5 index primer

The index primers were chosen for each sample individually to create distinguishable PCR products for the Illumina Sequencer. The amplification mixes were put in a thermocycler with the following program running:

Cycle step	**Temperature**	**Time**	**Cycles**
Initial Denaturation	98°C	30 sec	1
Denaturation	98°C	10 sec	12-15
Annealing/Extension	65°C	10 sec	
Final Extension	65°C	5 min	1
Hold	4°C	-	-

The amount of Denaturation/Annealing cycles was determined by the mass of DNA library used for amplification. At less than 20 ng DNA more than 12 cycles were needed to ensure a proper amplification of DNA for sequencing.

The amplified DNA was cleaned up with SPRIselect beads again (x1.1 volume) and eluted in 15 µl 0.1% TE buffer.

The quality of the DNA library was checked using the Fragment Analyzer. The size of the DNA fragments should be at about 160-350 base pairs. Afterwards a pair-end sequencing was performed.

5.7.2 CUT&RUN profiling

Harvest

HCT116 cells were seeded in 10 cm dishes to a total amount of about 500.000 cells per dish the cells were treated with either doxycycline or hydroxytamoxifen for appropriate times before harvest. At the day of harvest, the medium was washed away and 1 ml of accutase solution was put into the dishes, which were then incubated for 5 minutes at 37°C. The loose cells in the accutase solution were transferred into 2 ml reaction tubes and centrifuged for 3 min at 600 g. The supernatant was replaced, and the cell pellet was washed thrice with 1.5 ml CR wash buffer. The centrifugation was repeated, and the cells resuspended gently in 1 ml CR wash buffer. 10 µl ConA-coated magnetic beads were mixed to each cell solution and put in a tube rotator for 10 min.

Permeabilization and binding of primary antibodies

The bead-bound cells were mixed into a homogenous suspension and divided into two 1.5 ml low-binding reaction tubes per sample. The tubes were placed on a magnetic stand to clear the solution. The supernatant was removed and 150 µl of antibody buffer was added to each sample. The beads were carefully resuspended by slow mixing on a vortex mixer. The different primary antibodies were mixed to the beads with appropriate concentrations for immunofluorescence. The tubes were placed on a tube shaker set to 800 rpm over night at 4°C.

Binding of Protein-A/G-MNase fusion protein and chromatin digestion

The tubes were placed on a magnetic stand to clear and pull off the liquid. 1 ml CR Dig-wash buffer was added to the beads to resuspend them carefully. This Dig-wash step was repeated to a total of two washing steps. The tubes were placed on a magnetic stand again and all the liquid was removed. 150 µl of Protein-A/G-MNase fusion protein at 700 ng/ml in CR Dig-wash buffer were added to the beads. The tubes were placed on a tube shaker at 800 rpm for 1 h at 4°C.

The liquid was removed completely from the sides of the tube by a quick pulse in a micro-centrifuge. The tubes were placed on a magnetic stand and the supernatant was discarded. 1 ml CR Dig-wash buffer was added and mixed by inversion. This washing step was repeated once. The tubes were put back to the magnetic stand and the liquid was removed. 1 ml CR low-salt rinse buffer was added to the beads and mixed by inversion. The tubes were placed again on a magnetic stand and the supernatant was removed. 200 µl CR incubation buffer were added to each sample and incubated for 15 min at 0°C. The tubes were put on a magnetic stand and the liquid was discarded. 200 µl CR STOP buffer were mixed with the beads. These steps were critical to the experiment and had to be performed very quickly, because the MNase enzyme can cleave at unspecific sites when incubated at higher temperatures or for longer incubation times. This could lead to unacceptable background signals.

The beads in the STOP buffer were incubated for 30 min at 37°C to release the CUT&RUN fragments from the nuclear chromatin. The tubes were placed on a magnetic stand and the supernatant containing the wanted DNA fragments was transferred into a fresh 1.5 ml microcentrifuge tube.

Phenol chloroform extraction

To extract and purify the DNA from the buffer, a phenol chloroform extraction was performed for each sample-antibody combination. 2 µl 10% SDS and 5 µl Proteinase K (10 mg/ml) were added to each sample. The mixture was incubated at 50°C for 1 h. An equal volume of phenol chloroform was added to each sample and mixed thoroughly on a vortex mixer. The samples were then transferred to a Qiagen MaXtract phase-lock tube and centrifuged for 5 min at 16.000 rpm and RT. An equivalent volume of chloroform to the initial sample volume was added and mixed by inverting the tube 10 times. The centrifugation was repeated, and the top liquid phase was transferred into a fresh tube already containing 2 µl 3 mg/ml Glycoblue. 500 µl 100% EtOH were added and mixed thoroughly. The mixture was incubated on ice for 10 min and centrifuged for 10 min at 4°C at 16.000 g. The supernatant was discarded and drain completely on a paper towel. The pellet was rinsed in 1 ml 100% EtOH and centrifuged at 4°C and 16.000 g for 1 min. The liquid was drained again, and the pellet was air-dried. As soon as the ethanol has completely evaporated, the pellet was resuspended in 30 µl 1mM Tris-HCL pH 8 0.1 mM EDTA and transferred to a new 0.6 ml low-binding microcentrifuge tube.

Library preparation

For the library preparation the NEBNext Ultra II DNALibrary Prep Kit for Illumina was used. The following end preparation mix was prepared in a sterile nuclease-free tube:

Reagent	**Volume**
CUT&RUN DNA (6 ng)	25 µl
NEBNext Ultra II End Prep Enzyme Mix	1.5 µl
NEBNext Ultra II End Prep Reaction Buffer	3.5 µl

The reagents were mixed thoroughly and placed in a thermocycler with the heated lid set to 60°C and the following program was run:

Time	**Temperature**
30 min	20°C
60 min	50°C
Hold	4°C

The adaptor stock was diluted to 0.5 µM and the following reagents were pipetted to the samples:

Reagent	Volume
NEBNext Ultra II Ligation Master Mix	15 µl
NEBNext Ligation Enhancer	0.5 µl
NEBNext Adaptor For Illumina	1.25 µl

The reagents were mixed thoroughly by pipetting up and down several times and incubated in a thermocycler at 20°C for 15 min. 1.5 µl USER enzyme was added to the ligation mixture. The samples were then incubated in a thermocycler for 15 min at 37°C.

The adaptor-ligated DNA was purified using SPRIselect beads. 80 µl (1.75x) of the beads were added to the samples and incubated at RT for 5 min. The tubes were placed on a magnetic rack until the solution is clear. The supernatant was discarded and the beads containing the adaptor-ligated DNA were washed twice with 200 µl 80% EtOH. After the second washing step all traces of EtOH were removed and the beads were air-dried. The tubes were removed from the magnetic rack and the DNA was eluted from the beads using 15 µl 0.1% TE buffer. The beads were incubated at RT for 2 min with the buffer and placed on a magnetic rack again. 13 µl of the supernatant containing the adaptor-ligated DNA were transferred to a fresh PCR tube for the following PCR amplification.

For PCR enrichment of the adaptor ligated DNA, the following reaction mix was prepared for each sample individually according to the desired i5/i7-sequencing-primer combination:

Reagent	Volume
Adaptor Ligated Fragments	13 µl
NEBNext Ultra II Q5 Master Mix	15 µl
Index Primer i5	1 µl
Index Primer i7	1 µl

The mixture was put in a thermocycler using the following program:

Cycle Step	Temperature	Time	Cycles
Initial Denaturation	98°C	30 sec	1
Denaturation	98°C	10 sec	12-14
Annealing/Extension	65°C	10 sec	
Final Extension	65°C	5 min	1
Hold	4°C	-	-

The number of cycles depended on the initially used DNA. If less than 6 ng DNA were available, the number of cycles had to be increased to 13 or 14.

The PCR product was cleaned up using SPRIselect beads again. 33 µl (1.1x) of the beads were mixed with the amplified DNA. The mix was incubated at RT for 5 min and placed on a magnetic rack afterwards. The supernatant was discarded, and the beads washed twice with 200 µl 80% EtOH. After the second washing step, all remaining EtOH was discarded, and the beads were air-dried for 5 min. The tubes were removed from the magnetic rack and the DNA was eluted using 15 µl of 0.1% TE buffer. The tubes were placed on the magnetic rack again and 13 µl of the DNA-containing supernatant were transferred to a fresh PCR tube.

To check the quality of the DNA library, 1 µl of the DNA was used for a fragment analyzer analysis. The distribution of fragments had to be between 160 bp and 350 bp to ensure high quality fragments for the following next-generation sequencing.

The sequencing was performed by Carsten Ade on an Illumina NextSeq 500 sequencer using pair-end sequencing.

5.8 Cell biology methods

5.8.1 Cultivation of eukaryotic cell lines

The cells of all cell lines were cultivated in incubators by Heraeus at 37°C, 5% CO_2 and a relative humidity of 95%. HCT116 cells and HEK293T cells were incubated in DMEM D6429 medium containing 10% FCS and 1% Penicillin-Streptomycin. U2OS and LS174T cells were incubated in RPMI-1640 containing the same supplements.

The cells were passaged twice a week to prevent confluency. The cultivation medium was removed, and the cells were washed with PBS. The medium was replaced by Trypsin to detach the cells from the plate. The plates were incubated 5-15 min in the incubator at 37°C. As soon as the cells were detached, the cell culture media were added to the plate. The cells were transferred to a 15 ml tube and centrifuged for 3 min at 1500 rpm. The supernatant was removed, and the cell pellet was resuspended in the culture medium. The cell suspension was diluted to the desired cell number and plated to a new cell culture dish.

Cell freezing and thawing

To keep stocks of cells for long time at -80°C cells were grown on a 10 cm plate to about 70% confluency in usual culture medium. The cells were detached with trypsin as described earlier and harvested. After centrifugation, the pellet was resuspended in 2 ml freezing medium, which consists of 50% cultivation medium, 40% FCS and 10% DMSO. The cells in freezing medium were transferred to cryotubes and

placed at -20°C for 0.5 h. The tubes were then put into a freezing container and placed overnight at -80°C. The cells were put into storage boxes at -80°C or liquid nitrogen on the next day.

To thaw stored cells for cultivation again, the cryotubes with the cell stocks were put into a 37°C water bath. The cell suspension was transferred to a 15 ml tube and mixed with 5 ml fresh cultivation medium. The tube was centrifuged for 3 min at 1500 rpm and the supernatant was removed. The cell pellet was resuspended in culture medium and transferred to a fresh culture dish. The cells were passaged at least 2 times before using them in experiments.

5.8.2 Cell transfection

Lentiviral production was performed using the Polyethyleneimine (PEI) transfection method. HEK293T cells were cultured on 10 cm dishes for 24 h. The transfection solutions were prepared for each desired plasmid:

Solution 1	**Solution 2**
11 µg desired plasmid	30 µl PEI
2.8 µg psPAX2	700 µl Optimem
1.4 µg pMD2G	
700 µl Optimem	

Solutions 1 and 2 were incubated for 5 min and solution 2 was then transferred dropwise into solution 1. The mixture was incubated for further 20 min. The cultivation medium was removed from the HEK293T cells and replaced by DMEM medium with 2% FCS and without antibiotics. The infection solution was transferred to the cells and mixed by gentle swaying. From now on the cells had to be incubated in a biosafety level 2 incubator (S2), as the produced virus was possibly infectious.

After 24 hours of incubation the infection medium was replaced by standard DMEM medium again. The virus containing supernatant was harvested 24 h later and replaced by standard medium again. After 12 h the harvest was repeated and the virus producing cells were discarded. The collected virus medium was filtered through a 0.44 µm syringe-filter and stored in cryotubes at -80°C until cell infection.

5.8.3 siRNA transfection

For siRNA transfection the RNAi MAX method was performed. 3500 cells were seeded into each well of a 96-well plate and incubated for 24 h. The siRNAs were transferred into another 96-well plate and mixed with 7.5 µl OptiMEM medium. The mixture was incubated for 5 min at RT. Meanwhile the RNAi

MAX solution was prepared. For each siRNA 9.8 µl OptiMEM were mixed with 0.2 µl RNAi MAX. The 10 µl OptiMEM RNAi MAX mix was transferred to each siRNA, mixed well and incubated for 20 min at RT. 80 µl DMEM with 10% FCS and without any antibiotics were added to each siRNA. The growth medium was removed from the cells and replaced by 100 µl of the transfection solution. The cells were incubated overnight until siRNA screening.

5.8.4 Cell infection

About 1.000.000 cells were seeded in 10 cm dishes and grown for 24 h. All actions involving infectious virus containing medium were performed under S2 conditions. The growth medium on the cells was discarded, and replaced by filtered virus medium mixed with polybrene to a final concentration of 6 µg/ml. The cells were incubated with the virus medium for 24 h. The virus medium was discarded, and the cells detached and collected in a 15 ml tube. The cells were centrifuged for 4 min at 1000 rpm.

Selection with Hygromycin

For plasmids containing Hygromycin resistance as selection factor medium with 800 µg/ml Hygromycin (InvivoGen) was prepared. The cell pellet of infected cells was resuspended in 10 ml of selection medium and seeded to two 10 cm dishes. One control plate with cells not infected with Hygromycin resistance plasmids was treated equally. After 3 days incubation, the medium was discarded, and replaced by fresh selection medium. As soon as all control cells were dead, usually after one week, the selection was completed, and the surviving cells were cultivated in usual cultivation medium. The expression of the infected plasmid was afterwards checked by Western Blot.

Selection with Puromycin

For plasmids containing Puromycin resistance as selection factor medium with 2 µg/ml Puromycin (InvivoGen) was prepared. The cell pellet of infected cells was resuspended in 10 ml of selection medium and seeded to two 10 cm dishes. One control plate with cells not infected with Puromycin resistance plasmids was treated equally. After 3 days incubation or as soon as all control cells were dead, the selection was completed, and the surviving cells were cultivated in usual cultivation medium. The expression of the infected plasmid was afterwards checked by Western Blot.

Selection via fluorescence

For plasmids containing GFP and no antibiotics resistances the infected cells were seeded on two 10 cm dishes in usual growth medium. After 48 h the cells were detached from the plate and sorted via FACS. The cells were centrifuged for 4 min at 1000 rpm. The supernatant was discarded, and the pellet was resuspended in 1 ml PBS with 5% FCS. For cell pools the top 2000 cells with the strongest GFP signal were seeded in a 5 cm dish with usual growth medium. As soon as the cells were about 70% confluent,

they were detached and transferred in 10 cm dishes for further cultivation. The expression of the infected plasmid was afterwards checked by Western Blot. For single cell clones a 96 well plate was prepared with 100 µl cultivation medium in each well. The FACS device sorted one cell with strong GFP signal into each well. The plate was incubated until the cells grew confluent. The plate was screened via Western Blot for the cell clone with the strongest expression of the desired protein.

5.8.5 siRNA screening

The transfection medium was discarded the next day and replaced by starvation medium or cultivation medium in the control wells. The cells were incubated in starvation medium for 18 h. The starvation medium in wells marked for recovery was discarded 2 h before fixation and replaced by 100 µl recovery medium (starvation medium with 2 mM glutamine).

During incubation 3.7% paraformaldehyde was diluted with PBS from 37% stock solution. The medium was discarded, and the cells washed twice with 100 µl PBS. 100 µl 3.7% PFA were transferred to each well and incubated for 10 min at RT. The PFA was discarded and replaced by 100 µl PBS. The 96-well plate was stored at 4°C until immunofluorescence staining.

The cells were permeabilized with Triton X-100 solution. The PBS in each well was replaced carefully by 100 µl Triton solution and incubated for 10 min at RT. The Triton solution was discarded, and the cells washed once with PBS. The primary antibody solution was prepared while the cells were blocked with 5% BSA solution for 30 min. The BSA solution was replaced by the primary antibody solution and the cells incubated at 4°C overnight.

The primary antibody solution was taken off the cells and the cells were washed twice with 100 µl PBS. The secondary antibody solution was prepared. 50 µl solution was prepared for each well. 4 µl Alexa 488 Goat Anti-Rabbit antibody were diluted in 1.6 ml 3% BSA solution (1:400 dilution). This secondary antibody solution was transferred to each well and incubated for 1 h in the dark. During incubation, a 1:2000 dilution of Höchst 33342 in PBS was prepared. After the incubation, the secondary antibody solution was replaced by 50 µl of the Höchst dilution and incubated for 5 min in the dark. The cells were then washed twice with PBS. 100 µl PBS were left on the cells and the 96-well plate was packed in tinfoil and stored at 4°C until high throughput microscopy at the Operetta microscopy system. The microscopy was performed by Dr. Ursula Eilers at the microscopy core unit at the biocentre.

5.9 FACS analysis

For the following FACS experiments the FACSCanto II and all necessary consumables from BD Biosciences were used.

5.9.1 AnnexinV/PI staining

500.000 cells were grown in 10 cm dishes for the starvation conditions and 250.000 cells for the control conditions. Each condition was cultivated in triplicates on three different dishes for 24 h. For RNaseH1 expression 100 µg/ml Doxycycline was added to these dishes. All cultures were cultivated for another 24 h. The medium on cells designated for starvation was discarded and replaced by glutamine-deprived cultivation medium with 100 µg/ml Doxycycline for RNaseH1 expression and/or 100 nM 4-Hydroxytamoxifen (OHT) for cMYC activation.

At the time of harvest the medium containing dead cells was collected in a 50 ml tube. The cells were washed twice with ice cold PBS. The PBS was also collected and transferred to the tube. The cells were detached with trypsin, the trypsin was quenched with 5 ml glutamine-deprived medium with 10 % FCS and the whole mix transferred to the tube. The cell suspension was centrifuged at 250 g and 4°C for 5 min. The supernatant was discarded, and the pellet washed once with 10 ml ice cold PBS. The centrifugation was repeated, and the supernatant discarded. The pellet was resuspended in 100 µl Annexin binding buffer and mixed carefully on a vortex mixer. 20 µl of AnnexinV were added and the cells incubated in the dark for 15 min on ice. 400 µl Annexin binding buffer were added and the whole cell suspension was transferred into the designated FACS tubes, which were prepared with 5 µl PI solution.
The tubes were stored in the dark and on ice until measurement at the FACS device. The measurement involved the parameters PI-2A (PI), Pacific blue (AnnexinV), SSC-A and FSC-A (size of the cells).

5.9.2 PI staining

The cells were treated and harvested in the same way as for the AnnexinV/ PI staining. After the centrifugation, the pellets were resuspended in 1 ml ice cold PBS. The suspension was transferred dropwise into 15 ml polystyrene tubes containing 4 ml ice cold EtOH (100%). The tubes were stored overnight at -20°C. The fixated cells were centrifuged at 250 g and 4°C for 10 min. The supernatant was discarded, and the pellets washed in ice cold PBS. The cells were resuspended in 38 mM sodium citrate solution with 54 µM PI and 24 µg RNase A. The tubes were incubated for 30 min in the dark at 37°C. The suspension was transferred into FACS tubes and kept on ice in the dark until measurement. The measurement involved the parameters PI-2A, PI-2W, SSC-A and FSC-A.

5.9.3 BrdU/PI staining

The cells were labelled with 10 µM BrdU for 60 min. Afterwards they were treated, harvested, and fixated in the same way as for the PI staining. About 3 h before the FACS measurement, the suspension was centrifuged at 400 g and 4°C for 10 min. The supernatant was discarded, and the cells washed with 5 ml ice cold PBS. The centrifugation was repeated, and the pellet resuspended in 1 ml of 2 M HCl/ 0.5% Triton X-100. The suspension was incubated for 30 min at RT and mixed gently every 10 min. The centrifugation was repeated, and the pellet resuspended in 1 ml 0.1 M Sodium borate (pH 8.5). The cells were counted, and 1 million cells were transferred into a reaction tube. The tubes were centrifuged again for 5 min at 400 g and the pellet resuspended in 100 µl PBS with 0.5 % Tween-20, 1 % BSA and 10 µl BrdU-FITC antibody. The suspension was incubated for 30 min at RT in the dark. The cells were centrifuged again and washed once with 1 % BSA in PBS-T. The pellet was then resuspended in 400 µl PBS with 54 µM PI and 24 µg RNase A. The cells were incubated for 30 min at 37°C in the dark and transferred into FACS tubes. The measurement involved the parameters FL2-A lin (PI), FL1-H log (BrdU), SSC-A and FSC-A.

5.10 Crystal Violet staining

HCT116 cells seeded in 10 cm dishes or 6 well plates and grown to a confluency of about 50%. The treatment starts 24 h before harvest. Cells were either treated with glutamine-deprived medium alone or with this medium and supplements to induce RNaseH1 expression (Doxycycline) and/or activate the MYC-ER system (4-Hydroxytamoxifen). Each condition and the control cells in usual growth medium were grown in triplicates. On the day of harvest the medium on the cells was discarded and the cells were washed twice with PBS. The cells were fixed for 10 min with 4 ml 3.7% PFA solution on 10 cm dishes and 1 ml 3.7% PFA solution per well in a 6 well plate. The PFA was discarded, and the cells washed once with ddH_2O. 4 ml Crystal Violet solution (ddH_2O + 20% EtOH + 0.1% Crystal Violet) were put on the cells in the 10 cm dish and 1 ml on each well in the 6 well plate for 30 min. The Crystal Violet solution was discarded, and the plates washed carefully in a water bath. The plates were dried overnight. The plates were photographed before quantification.

The cells on the 10 cm dishes were used for quantification of the colour intensity. 4 ml of 10% acetic acid solution were pipetted on the stained cells. The cells were de-stained by gentle swaying of the plate. 200 µl of the acetic acid solution were diluted in 800 µl H_2O in a 1 ml cuvette. The absorbance at 550 nm were measured at a photometer. The measured absorbance depended directly on the colour intensity and the number of stained cells.

5.11 Cumulative growth curve

10^5 HCT116 cells were seeded on each 10 cm dish. The cells were grown in triplicates for three days in the medium suited for each condition. For MYC-ER activation DMEM medium with 100 nM OHT and for RNaseH1 expression medium with 100 µg/ml Doxycycline was used as growth medium. After three days the medium was discarded, and the cells detached with trypsin. The cells were counted, diluted, and seeded again. This process was repeated after 6 days and after 9 days. Finally, the cell growth was estimated regarding the dilution factors and the total counts on each harvest day.

5.12 Protein biochemical methods

5.12.1 Creation of cell lysates and protein concentration measurement via BCA-assay

10^6 cells were seeded 48 h before harvest. 24 h after seeding the desired treatment started according to the conditions. On the day of harvest, the medium was discarded, and the cells washed once with PBS. 500 µl RIPA buffer was mixed with 1.5 µl PMSF and 1 µl proteinase inhibitor per 10 cm dish. The prepared RIPA buffer was pipetted onto each plate and cells were collected with a cell scraper. The lysate was transferred to a 2 ml reaction tube and incubated on ice for 20 min. After the incubation, the cells were centrifuged for 20 min at 4°C and 14.000 rpm. The supernatant was then transferred to a new 1.5 ml reaction tube.

To determine the protein concentration a BCA assay was performed for each lysate. To create a standard curve several BSA standards with defined concentrations were prepared (0, 0.5, 1, 2, 4, 6, 8 mg/ml). 4 µl of the standards and the lysates were transferred in duplicates to a 96 well plate. 150 µl of BCA solution were prepared per well. 147 µl of bicinchoninacid solution and 3 µl copper sulfate solution were mixed for 150 µl BCA solution. The samples were mixed with 150 µl BCA solution and incubated for 15 min at RT. The colour intensity was measured with a photometer (Multiscan Ascent) and the extinction analyzed with the Ascension software. The extinctions of the BSA standards were used to create a standard curve to determine the protein concentrations of the samples.

5.12.2 SDS-Polyacrylamide-Gel electrophoresis (SDS-PAGE)

For each 10 samples, one polyacrylamide gel was prepared as written in the following table:

Substance	**Collecting gel**	**Parting gel**
H2O	5.81 ml	14.4 ml
BisTris	2.86 ml	9.1 ml
Acrylamide	1.33 ml	8.5 ml
TEMED	10 µl	21 µl
APS	50 µl	107 µl

The samples were mixed 1:6 with 6x Lämmli buffer and boiled for 15 min at 95°C. The first pocket was filled with 4 µl PageRuler protein ladder. 20 µl of each sample with an equal protein concentration were filled into the other pockets. The electrophoresis chamber was filled up with 1x MOPS running buffer and a voltage of 120 V was applied. The separation was completed as soon as the running buffer front ran out of the gel after about 90 min.

5.12.3 Western Blot and immuno-staining

As soon as the separation was complete, the gel was taken from the electrophoresis chamber and the Western Blot was assembled. A Immobilon-P transfer membrane was activated in 100% methanol for 2 min and then transferred to 1x NuPAGE transfer buffer. Meanwhile, the Whatman filter papers were soaked in transfer buffer as well as the two sponges. The activated membrane and the gel were fixed between two layers of soaked Whatman papers and the sponges. It is important to place the gel on the black side of the cassette, which is the anode, and the membrane on the red side of the cassette, which is the cathode. The Western Blot was put into a Western Blot chamber and filled up with 1x NuPAGE transfer buffer. An electric current of 350 mA was applied to the chamber and placed in a 4°C room for about 2.5 h.

After the transfer the Blot was disassembled, the gel discarded, and the membrane containing the proteins was blocked for 30 min in 20% Odyssee blocking solution/ TBST on a swaying plate. The membrane was cut into pieces and incubated in primary antibodies in blocking solution overnight at 4°C. The membranes were washed thrice in TBST. The membranes were transferred to specific secondary antibody solutions for 1 h in the dark. The membranes were washed three times with TBST again. For the detection of the protein-bound antibodies the membranes were detected in a Odyssee fluorescence detector.

5.12.4 RNA-Protein interaction detection (RaPID-Assay)

The RaPID-Assay based on the Nature Methods paper from Ramanathan et al. (2017). For this method, an RNA sequence of interest was cloned between two BoxB stem loops as the motif construct. These BoxB stem loops work as a target for a modified biotin ligase of *Bacillus subtilis*, which was fused to a λN targeting peptide that binds to the stem loops. When an RNA binding protein binds to the RNA motif, it comes near the biotin ligase, which can biotinylate the protein. The biotinylated protein can then be pulled down via streptavidin assay and analyzed with mass spectrometry or Western blot (Figure 5.1)

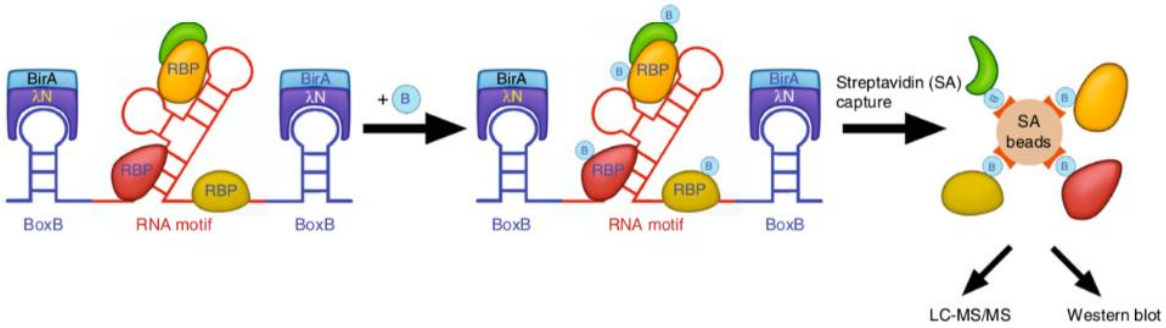

Figure 5.1: Depiction of the biochemical principle of the RaPID-Assay (Ramanathan, et al., 2017)

In this experiment the 3'-UTR of cMYC was used as RNA motif. Different lengths of the UTR based on the work of Dejure et al. were cloned between two BoxB stem loops. As a control motif with known interaction proteins the U1 spliceosomal RNA was cloned as well.

HCT116 cells were infected with a plasmid for the inducible expression of the biotin ligase and another plasmid containing one of the RNA motifs with the BoxB stem loops. The cells were grown to a confluency of 50 % on a 10 cm dish and the biotin ligase expression was induced 24 h before biotin labelling. The 20x biotin labelling solution was diluted to 1x and used to replace the growing medium. The labelling takes 24 h.

On the day of harvest, fresh lysis buffer was prepared. The labelling medium was discarded, and the cells washed with cold PBS. 500 µl PBS were pipetted to each dish and the cells were scraped and transferred to a 1.5 ml reaction tube. The cells were spun down at 500 g and 4°C for 1 min. The supernatant was discarded, and 200 µl lysis buffer were transferred to each reaction tube. 20 µl 25 % Triton X-100 were mixed to the lysis buffer and the pellet was resuspended. 220 µl cold Wash buffer 4 were pipetted to the lysis solution. The cells were sonicated at 10 % intensity for 10 sec or until the lysate was clear. The lysate was then centrifuged at 15.000 g and 4°C for 10 min. The supernatant was

transferred to a 3K MWCO filter tube and centrifuged at 1.500 g and 4°C for 1 h. The higher concentrated leftover of the protein solution was then transferred to a fresh 1.5 ml reaction tube. 20 µl of the sample were taken off and stored away at -20°C as the input sample. 50 µl MyOne C1 streptavidin beads per sample were washed twice with wash buffer 4 and then mixed with the remaining protein solution. The beads and the protein solution were placed on a spinning wheel at 4°C overnight.

The tubes were placed on a magnetic stand and the lysate was discarded. Each of the following washing steps was performed for 5 min and on a spinning wheel. The beads were washed twice with 1 ml washing buffer 1. Then once with 1 ml of washing buffer 2, washing buffer 3 and washing buffer 4. 40 µl of 1x Lämmli buffer with 6 mM biotin were transferred to each sample and the tubes heated for 98°C to detach the biotinylated protein from the beads. The supernatant was used to perform a Western blot and immunostaining to detect the proteins.

5.12.5 Mass spectrometric quantification of whole cell lysates

The mass spectrometric quantification preparation and measurement was performed by Dr. Werner Schmitz.

HCT116 cells were seeded on 10 cm dishes. 1 million cells were counted for each condition including a glutamine starvation step and 500.000 cells for each plate without glutamine starvation. This ensured relatively similar cell counts at the time of harvest. The cells were grown to about 50 % confluency before glutamine starvation and treatment with OHT to activate the MYC-ER system or Doxycycline for RNaseH1 expression. At the day of harvest the cells were washed with PBS and scraped into 2 ml reaction tubes. The suspension was centrifuged at 250 g for 4 min and the supernatant was discarded. The mass of the cell pellets was measured and equalized by resuspending in PBS. The cells were pelleted again, and the pellets were stored at -20°C until measurement.

6. Bibliography

Adhikary S, Eilers M. Transcriptional regulation and transformation by Myc proteins. Nat Rev Mol Cell Biol. 2005 Aug;6(8):635-45. doi: 10.1038/nrm1703. PMID: 16064138.

Aguilera A, García-Muse T. R loops: from transcription byproducts to threats to genome stability. Mol Cell. 2012 Apr 27;46(2):115-24. doi: 10.1016/j.molcel.2012.04.009. PMID: 22541554.

Chandra D, Bratton SB, Person MD, Tian Y, Martin AG, Ayres M, Fearnhead HO, Gandhi V, Tang DG. Intracellular nucleotides act as critical prosurvival factors by binding to cytochrome C and inhibiting apoptosome. Cell. 2006 Jun 30;125(7):1333-46. doi: 10.1016/j.cell.2006.05.026. PMID: 16814719.

Chen CY, Shyu AB. AU-rich elements: characterization and importance in mRNA degradation. Trends Biochem Sci. 1995 Nov;20(11):465-70. doi: 10.1016/s0968-0004(00)89102-1. PMID: 8578590.

Chen L, Cui H. Targeting Glutamine Induces Apoptosis: A Cancer Therapy Approach. Int J Mol Sci. 2015 Sep 22;16(9):22830-55. doi: 10.3390/ijms160922830. PMID: 26402672; PMCID: PMC4613338.

Cory JG, Cory AH. Critical roles of glutamine as nitrogen donors in purine and pyrimidine nucleotide synthesis: asparaginase treatment in childhood acute lymphoblastic leukemia. In Vivo. 2006 Sep-Oct;20(5):587-9. PMID: 17091764.

Costantino L, Koshland D. The Yin and Yang of R-loop biology. Curr Opin Cell Biol. 2015 Jun;34:39-45. doi: 10.1016/j.ceb.2015.04.008. Epub 2015 May 15. PMID: 25938907; PMCID: PMC4522345.

Dean KA, von Ahsen O, Görlich D, Fried HM. Signal recognition particle protein 19 is imported into the nucleus by importin 8 (RanBP8) and transportin. J Cell Sci. 2001 Oct;114(Pt 19):3479-85. doi: 10.1242/jcs.114.19.3479. PMID: 11682607.

Dejure FR, Royla N, Herold S, Kalb J, Walz S, Ade CP, Mastrobuoni G, Vanselow JT, Schlosser A, Wolf E, Kempa S, Eilers M. The *MYC* mRNA 3'-UTR couples RNA polymerase II function to glutamine and ribonucleotide levels. EMBO J. 2017 Jul 3;36(13):1854-1868. doi: 10.15252/embj.201796662. Epub 2017 Apr 13. PMID: 28408437; PMCID: PMC5494468.

Eaton JD, Francis L, Davidson L, West S. A unified allosteric/torpedo mechanism for transcriptional termination on human protein-coding genes. Genes Dev. 2020 Jan 1;34(1-2):132-145. doi: 10.1101/gad.332833.119. Epub 2019 Dec 5. PMID: 31805520; PMCID: PMC6938672.

Evan GI, Wyllie AH, Gilbert CS, Littlewood TD, Land H, Brooks M, Waters CM, Penn LZ, Hancock DC. Induction of apoptosis in fibroblasts by c-myc protein. Cell. 1992 Apr 3;69(1):119-28. doi: 10.1016/0092-8674(92)90123-t. PMID: 1555236.

Gan W, Guan Z, Liu J, Gui T, Shen K, Manley JL, Li X. R-loop-mediated genomic instability is caused by impairment of replication fork progression. Genes Dev. 2011 Oct 1;25(19):2041-56. doi: 10.1101/gad.17010011. PMID: 21979917; PMCID: PMC3197203.

García-Gutiérrez L, Delgado MD, León J. MYC Oncogene Contributions to Release of Cell Cycle Brakes. Genes (Basel). 2019 Mar 22;10(3):244. doi: 10.3390/genes10030244. PMID: 30909496; PMCID: PMC6470592.

García-Muse T, Aguilera A. R Loops: From Physiological to Pathological Roles. Cell. 2019 Oct 17;179(3):604-618. doi: 10.1016/j.cell.2019.08.055. Epub 2019 Oct 10. PMID: 31607512.

Garibaldi A, Carranza F, Hertel KJ. Isolation of Newly Transcribed RNA Using the Metabolic Label 4-Thiouridine. Methods Mol Biol. 2017;1648:169-176. doi: 10.1007/978-1-4939-7204-3_13. PMID: 28766297; PMCID: PMC5783291.

Görlich D, Kutay U. Transport between the cell nucleus and the cytoplasm. Annu Rev Cell Dev Biol. 1999;15:607-60. doi: 10.1146/annurev.cellbio.15.1.607. PMID: 10611974.

Hatchi E, Skourti-Stathaki K, Ventz S, Pinello L, Yen A, Kamieniarz-Gdula K, Dimitrov S, Pathania S, McKinney KM, Eaton ML, Kellis M, Hill SJ, Parmigiani G, Proudfoot NJ, Livingston DM. BRCA1 recruitment to transcriptional pause sites is required for R-loop-driven DNA damage repair. Mol Cell. 2015 Feb 19;57(4):636-647. doi: 10.1016/j.molcel.2015.01.011. PMID: 25699710; PMCID: PMC4351672.

Herold S, Kalb J, Büchel G, Ade CP, Baluapuri A, Xu J, Koster J, Solvie D, Carstensen A, Klotz C, Rodewald S, Schülein-Völk C, Dobbelstein M, Wolf E, Molenaar J, Versteeg R, Walz S, Eilers M. Recruitment of BRCA1 limits MYCN-driven accumulation of stalled RNA polymerase. Nature. 2019 Mar;567(7749):545-549. doi: 10.1038/s41586-019-1030-9. Epub 2019 Mar 20. PMID: 30894746; PMCID: PMC7611299.

Hwang S, Yang S, Kim M, Hong Y, Kim B, Lee EK, Jeong SM. Mitochondrial glutamine metabolism regulates sensitivity of cancer cells after chemotherapy via amphiregulin. Cell Death Discov. 2021 Dec 20;7(1):395. doi: 10.1038/s41420-021-00792-7. PMID: 34924566; PMCID: PMC8685276.

Jeannotte R., METABOLIC PATHWAYS | Nitrogen Metabolism, Editor(s): Carl A. Batt, Mary Lou Tortorello, Encyclopedia of Food Microbiology (Second Edition), Academic Press, 2014, Pages 544-560, ISBN 9780123847331, https://doi.org/10.1016/B978-0-12-384730-0.00199-3.

Lata E., Teichmann M., et al., *RNA Polymerase II Subunit Mutations in Genetic Diseases*, Front. Mol. Biosci., Sec. RNA Networks and Biology, https://doi.org/10.3389/fmolb.2021.696438 (2021)

Levy-Rimler G, Viitanen P, Weiss C, Sharkia R, Greenberg A, Niv A, Lustig A, Delarea Y, Azem A. The effect of nucleotides and mitochondrial chaperonin 10 on the structure and chaperone activity of mitochondrial chaperonin 60. Eur J Biochem. 2001 Jun;268(12):3465-72. doi: 10.1046/j.1432-1327.2001.02243.x. PMID: 11422376.

Llombart V, Mansour MR. Therapeutic targeting of "undruggable" MYC. EBioMedicine. 2022 Jan;75:103756. doi: 10.1016/j.ebiom.2021.103756. Epub 2021 Dec 20. PMID: 34942444; PMCID: PMC8713111.

Montecucco A, Zanetta F, Biamonti G. Molecular mechanisms of etoposide. EXCLI J. 2015 Jan 19;14:95-108. doi: 10.17179/excli2015-561. PMID: 26600742; PMCID: PMC4652635.

Morrish F, Giedt C, Hockenbery D. c-MYC apoptotic function is mediated by NRF-1 target genes. Genes Dev. 2003 Jan 15;17(2):240-55. doi: 10.1101/gad.1032503. PMID: 12533512; PMCID: PMC195978.

Nagai K, Muto Y, Pomeranz Krummel DA, Kambach C, Ignjatovic T, Walke S, Kuglstatter A. Structure and assembly of the spliceosomal snRNPs. Novartis Medal Lecture. Biochem Soc Trans. 2001 May;29(Pt 2):15-26. doi: 10.1042/0300-5127:0290015. PMID: 11356120.

Niehrs C, Luke B. Regulatory R-loops as facilitators of gene expression and genome stability. Nat Rev Mol Cell Biol. 2020 Mar;21(3):167-178. doi: 10.1038/s41580-019-0206-3. Epub 2020 Jan 31. PMID: 32005969; PMCID: PMC7116639.

Peng SS, Chen CY, Xu N, Shyu AB. RNA stabilization by the AU-rich element binding protein, HuR, an ELAV protein. EMBO J. 1998 Jun 15;17(12):3461-70. doi: 10.1093/emboj/17.12.3461. PMID: 9628881; PMCID: PMC1170682.

Phesse TJ, Myant KB, Cole AM, Ridgway RA, Pearson H, Muncan V, van den Brink GR, Vousden KH, Sears R, Vassilev LT, Clarke AR, Sansom OJ. Endogenous c-Myc is essential for p53-induced apoptosis in response to DNA damage in vivo. Cell Death Differ.

2014 Jun;21(6):956-66. doi: 10.1038/cdd.2014.15. Epub 2014 Feb 28. PMID: 24583641; PMCID: PMC4013513.

Polat IH, Tarrado-Castellarnau M, Benito A, Hernandez-Carro C, Centelles J, Marin S, Cascante M. Glutamine Modulates Expression and Function of Glucose 6-Phosphate Dehydrogenase via NRF2 in Colon Cancer Cells. Antioxidants (Basel). 2021 Aug 25;10(9):1349. doi: 10.3390/antiox10091349. PMID: 34572981; PMCID: PMC8472416.

Rahl PB, Young RA. MYC and transcription elongation. Cold Spring Harb Perspect Med. 2014 Jan 1;4(1):a020990. doi: 10.1101/cshperspect.a020990. PMID: 24384817; PMCID: PMC3869279.

Ramanathan M, Majzoub K, Rao DS, Neela PH, Zarnegar BJ, Mondal S, Roth JG, Gai H, Kovalski JR, Siprashvili Z, Palmer TD, Carette JE, Khavari PA. RNA-protein interaction detection in living cells. Nat Methods. 2018 Mar;15(3):207-212. doi: 10.1038/nmeth.4601. Epub 2018 Feb 5. PMID: 29400715; PMCID: PMC5886736.

Reyes A, Melchionda L, Nasca A, Carrara F, Lamantea E, Zanolini A, Lamperti C, Fang M, Zhang J, Ronchi D, Bonato S, Fagiolari G, Moggio M, Ghezzi D, Zeviani M. RNASEH1 Mutations Impair mtDNA Replication and Cause Adult-Onset Mitochondrial Encephalomyopathy. Am J Hum Genet. 2015 Jul 2;97(1):186-93. doi: 10.1016/j.ajhg.2015.05.013. Epub 2015 Jun 18. PMID: 26094573; PMCID: PMC4572567.

Reyes A, Rusecka J, Tońska K, Zeviani M. RNase H1 Regulates Mitochondrial Transcription and Translation *via* the Degradation of 7S RNA. Front Genet. 2020 Jan 31;10:1393. doi: 10.3389/fgene.2019.01393. PMID: 32082360; PMCID: PMC7006045.

Rinaldi C, Pizzul P, Longhese MP, Bonetti D. Sensing R-Loop-Associated DNA Damage to Safeguard Genome Stability. Front Cell Dev Biol. 2021 Jan 11;8:618157. doi: 10.3389/fcell.2020.618157. PMID: 33505970; PMCID: PMC7829580.

Rout MP, Blobel G, Aitchison JD. A distinct nuclear import pathway used by ribosomal proteins. Cell. 1997 May 30;89(5):715-25. doi: 10.1016/s0092-8674(00)80254-8. PMID: 9182759.

Sabò A, Kress TR, Pelizzola M, de Pretis S, Gorski MM, Tesi A, Morelli MJ, Bora P, Doni M, Verrecchia A, Tonelli C, Fagà G, Bianchi V, Ronchi A, Low D, Müller H, Guccione E, Campaner S, Amati B. Selective transcriptional regulation by Myc in cellular growth control and lymphomagenesis. Nature. 2014 Jul 24;511(7510):488-492. doi:10.1038/nature13537. Epub 2014 Jul 9. PMID: 25043028; PMCID: PMC4110711.

San Martin-Alonso M, Soler-Oliva ME, García-Rubio M, García-Muse T, Aguilera A. Harmful R-loops are prevented via different cell cycle-specific mechanisms. Nat Commun. 2021 Jul 22;12(1):4451. doi: 10.1038/s41467-021-24737-x. PMID: 34294712; PMCID: PMC8298424.

Shanware NP, Bray K, Eng CH, Wang F, Follettie M, Myers J, Fantin VR, Abraham RT. Glutamine deprivation stimulates mTOR-JNK-dependent chemokine secretion. Nat Commun. 2014 Sep 25;5:4900. doi: 10.1038/ncomms5900. PMID: 25254627; PMCID: PMC4200525.

Stojanova A, Tu WB, Ponzielli R, Kotlyar M, Chan PK, Boutros PC, Khosravi F, Jurisica I, Raught B, Penn LZ. MYC interaction with the tumor suppressive SWI/SNF complex member INI1 regulates transcription and cellular transformation. Cell Cycle. 2016 Jul 2;15(13):1693-705. doi: 10.1080/15384101.2016.1146836. Epub 2016 Jun 7. PMID: 27267444; PMCID: PMC4957596.

Sutherland KD, Vaillant F, Alexander WS, Wintermantel TM, Forrest NC, Holroyd SL, McManus EJ, Schutz G, Watson CJ, Chodosh LA, Lindeman GJ, Visvader JE. c-myc as a mediator of accelerated apoptosis and involution in mammary glands lacking Socs3. EMBO

J. 2006 Dec 13;25(24):5805-15. doi: 10.1038/sj.emboj.7601455. Epub 2006 Nov 30. PMID: 17139252; PMCID: PMC1698901.

Szostak E, Gebauer F. Translational control by 3'-UTR-binding proteins. Brief Funct Genomics. 2013 Jan;12(1):58-65. doi: 10.1093/bfgp/els056. Epub 2012 Nov 28. PMID: 23196851; PMCID: PMC3548161.

Tokunaga C, Yoshino K, Yonezawa K. mTOR integrates amino acid- and energy-sensing pathways. Biochem Biophys Res Commun. 2004 Jan 9;313(2):443-6. doi: 10.1016/j.bbrc.2003.07.019. PMID: 14684182.

Verma R, Saha S, Kumar S, Mani S, Maiti TK, Surjit M. RNA-Protein Interaction Analysis of SARS-CoV-2 5' and 3' Untranslated Regions Reveals a Role of Lysosome-Associated Membrane Protein-2a during Viral Infection. mSystems. 2021 Aug 31;6(4):e0064321. doi: 10.1128/mSystems.00643-21. Epub 2021 Jul 13. PMID: 34254825; PMCID: PMC8407388.

White D, Rafalska-Metcalf IU, Ivanov AV, et al. The ATM substrate KAP1 controls DNA repair in heterochromatin: regulation by HP1 proteins and serine 473/824 phosphorylation. *Mol Cancer Res*. 2012;10(3):401-414. doi:10.1158/1541-7786.MCR-11-0134

Will CL, Lührmann R. Spliceosome structure and function. Cold Spring Harb Perspect Biol. 2011 Jul 1;3(7):a003707. doi: 10.1101/cshperspect.a003707. PMID: 21441581; PMCID: PMC3119917.

Wimberly H, Shee C, Thornton PC, Sivaramakrishnan P, Rosenberg SM, Hastings PJ. R-loops and nicks initiate DNA breakage and genome instability in non-growing Escherichia coli. Nat Commun. 2013;4:2115. doi: 10.1038/ncomms3115. Erratum in: Nat Commun. 2014;5:2762. PMID: 23828459; PMCID: PMC3715873.

Yuneva M, Zamboni N, Oefner P, Sachidanandam R, Lazebnik Y. Deficiency in glutamine but not glucose induces MYC-dependent apoptosis in human cells. J Cell Biol. 2007 Jul 2;178(1):93-105. doi: 10.1083/jcb.200703099. PMID: 17606868; PMCID: PMC2064426.

Zou Z, Tao T, Li H, Zhu X. mTOR signaling pathway and mTOR inhibitors in cancer: progress and challenges. Cell Biosci. 2020 Mar 10;10:31. doi: 10.1186/s13578-020-00396-1. PMID: 32175074; PMCID: PMC7063815.

7 Appendix

7.1 Abbreviations

Abbreviation	
A	Adenosine
AGS	Agarose Gel Separation
ADP	Adenosine Diphosphate
AMP	Adenosine Monophosphate
ATP	Adenosine Triphosphate
BLAST	Basic Local Alignment Search Tool
BrdU	Bromodeoxyuridine
BSA	Bovine Serum Albumin
C	Cytosine
cDNA	Complementary DNA
CRC	Colorectal Cancer
CV	Crystal Violet
CpG	Cytosine-Phosphate-Guanosine
DNA	Deoxyribonucleic acid
dNTP	Deoxyribonucleotide Triphosphate
DMEM	Dulbecco´s Modified Eagle`s Medium
Dox	Doxycycline
DRIP	DNA:RNA immunoprecipitation
EDTA	Ethylenediaminetetraacetic Acid
EtOH	Ethanol
EV	Empty Vector
FACS	Fluorescence Assisted Cell Sorting
FCS	Fetal Calf Serum
G	Guanosine
g	Gramm
GDP	Guanosine Diphosphate
GMP	Guanosine Monophosphate
GTP	Guanosine Triphosphate
i	Inducible
IF	Immunofluorescence
IMP	Inosine 5`-Monophosphate
m	Milli
M	Molar
µ	Micro
miRNA	Micro RNA
n	Nano
nf	Non-Functional/Catalytically Inactive
OHT	4-Hydroxytamoxifen
PBS	Phosphate Buffered Saline
PCR	Polymerase Chain Reaction
PEI	Polyethylenimine
PI	Propidium iodide
PRPP	5`-Phosphoribosylpyrophosphate

Q	Glutamine
qRT-PCR	Quantitative Real-Time Polymerase Chain Reaction
RaPID	RNA-Protein Interaction Detection
RNA	Ribonucleic acid
RNA-Pol2/RNAPII	RNA Polymerase II
RT	Room Temperature
ROS	Reactive Oxygen Species
SDS-PAGE	Sodium Dodecyl Sulfate-Polyacrylamide Gel Electrophoresis
siRNA	Small interfering RNA
T	Thymidine
UDP	Uridine Diphosphate
UMP	Uridine Monophosphate
UTR	Untranslated Region
UTP	Uridine Triphosphate

7.2 Eidesstattliche Erklärung und Affidavit

Eidesstattliche Erklärungen nach §7 Abs. 2 Satz 3, 4, 5

der Promotionsordnung der Fakultät für Biologie

Eidesstattliche Erklärung

Hiermit erkläre ich an Eides statt, die Dissertation: „**Regulierungsmechanismen von c-MYC in Darmkrebszellen unter Glutaminmangelbedingungen**“, eigenständig, d. h. insbesondere selbständig und ohne Hilfe eines kommerziellen Promotionsberaters, angefertigt und keine anderen, als die von mir angegebenen Quellen und Hilfsmittel verwendet zu haben.

Ich erkläre außerdem, dass die Dissertation weder in gleicher noch in ähnlicher Form bereits in einem anderen Prüfungsverfahren vorgelegen hat.

Weiterhin erkläre ich, dass bei allen Abbildungen und Texten bei denen die Verwertungsrechte (Copyright) nicht bei mir liegen, diese von den Rechtsinhabern eingeholt wurden und die Textstellen bzw. Abbildungen entsprechend den rechtlichen Vorgaben gekennzeichnet sind sowie bei Abbbildungen, die dem Internet entnommen wurden, der entsprechende Hypertextlink angegeben wurde.

Affidavit

I hereby declare that my thesis entitled: „ **Regulation pathways of c-MYC under glutamine-starving conditions in colon carcinoma cells**” is the result of my own work. I did not receive any help or support from commercial consultants. All sources and / or materials applied are listed and specified in the thesis.

Furthermore I verify that the thesis has not been submitted as part of another examination process neither in identical nor in similar form.

Besides I declare that if I do not hold the copyright for figures and paragraphs, I obtained it from the rights holder and that paragraphs and figures have been marked according to law or for figures taken from the internet the hyperlink has been added accordingly.

Heidelberg, den_____

_____

Signature PhD-student